6. SITE 760[1]

Shipboard Scientific Party[2]

HOLE 760A

Date occupied: 11 July 1988

Date departed: 14 July 1988

Time on hole: 2 days, 13 hr, 45 min

Position: 16°55.32′S, 115°32.48′E

Bottom felt (rig floor; m, drill pipe measurement): 1981.1

Distance between rig floor and sea level (m): 11.4

Water depth (drill pipe measurement from sea level, m): 1969.7

Total depth (rig floor; m): 2266.00

Penetration (m): 284.90

Number of cores (including cores with no recovery): 38

Total length of cored section (m): 284.90

Total core recovered (m): 196.38

Core recovery (%): 68

Oldest sediment cored:
Depth (mbsf): 284.90
Nature: carbonate-cemented quartz sandstone
Age: Norian
Measured velocity (km/s): 5.134

HOLE 760B

Date occupied: 14 July 1988

Date departed: 19 July 1988

Time on hole: 4.5 days

Position: 16°55.32′S, 115°32.48′E

Bottom felt (rig floor; m, drill pipe measurement): 1981.1

Distance between rig floor and sea level (m): 11.4

Water depth (drill pipe measurement from sea level, m): 1969.7

Total depth (rig floor; m): 2487.10

Penetration (m): 506.00

Number of cores (including cores with no recovery): 29

Total length of cored section (m): 506.00

Total core recovered (m): 123.02

Core recovery (%): 24

Oldest sediment cored:
Depth (mbsf): 506.00
Nature: silty claystone, clayey siltstone, and sandy siltstone
Age: Carnian
Measured velocity (km/s): 2.160

Principal results: Site 760 (proposed Site EP10A′, latitude 16°55.32′S, longitude 115°32.48′E, water depth 1969.7 m) is located 5 km north (upslope and downdip) of Site 759 at the top of Wombat Plateau. This site was chosen to drill the post-Norian Mesozoic record in order to investigate the early rift, drift, and subsidence history of the region, as well as Mesozoic magnetobiostratigraphy and sea-level fluctuation history.

The 506-m-thick cored section consists of an upper 17.2-m-thick interval of Quaternary foraminifer nannofossil ooze (Subunit IA, 0–17.2 meters below sea floor, or mbsf), unconformably overlying 4.5 m of lower Upper Pliocene nannofossil ooze (Subunit IB, 17.2–21.7 mbsf), which in turn is underlain by 58.4 m of upper Eocene to Upper Miocene nannofossil ooze (Unit II, 21.7–80.1 mbsf). Below this eupelagic sequence is a major unconformity with a 40-cm-thick manganese crust, overlying 4.4 m of variegated, olive-yellow, massive to laminated silty claystone to sandstone with Mn nodules and fragments of Mn-oxide crust (Unit III, 80.1–84.9 mbsf); the latter deposit is apparently a lag formed during late Cretaceous(?) to Eocene time.

Below this unconformity we penetrated 422 m of Triassic (late Carnian to Norian) rocks. The uppermost Triassic Unit IV (84.9–210.9 mbsf) consists of 126.0 m of siliciclastic rocks (mainly dark-gray silty claystones) interbedded with clayey siltstone to silty sandstone with rootlets and minor occurrences of coal. These rocks were deposited in a marginal-marine (marsh to lagoonal) environment with local subaerial exposure that allowed soil profiles to develop. The underlying Unit V (210.9–284.9 mbsf) consists of 74.5 m of silty claystone, clayey siltstone, and silty sandstone with cross-lamination and bioturbation. Mollusks and coccoliths occur at the base of this unit, which was deposited in a shallow-marine (estuarine or distributary bay) setting with minor channels.

Below this is Unit VI (284.9–464.05 mbsf), which consists of 178.65 m of interbedded fossiliferous limestone, silty claystone, clayey siltstone, and silty sandstone, indicating a fluctuating shallow-marine, lagoonal/intertidal to carbonate bank/shelf environment. Near or above the Carnian/Norian boundary we recovered a conglomerate (rudstone) with reworked, rounded limestone and volcanic rock pebbles that might indicate a transgression and erosion of preexisting shallow-water carbonates and early-rift volcanics. The lowermost unit, Unit VII (464.05–506.0 mbsf), consists of 41.95 m of Carnian silty claystone, clayey siltstone, and silty sandstone with coccoliths and siderite layers, but without limestone interbeds. We attribute this facies to a protected shallow-water tidal flat or lagoonal setting, but cannot exclude a deeper-water prodelta environment.

Spores and pollen proved again most versatile in dating the marginal-marine sediments of Carnian to Norian age. Triassic nannofossils, some of them undescribed forms, were observed at two levels in the Triassic. A few late Norian foraminifers were found in the more calcareous middle part of the Triassic sequence, as were traces of radiolarians.

Because of severe bridging problems, downhole logging was restricted to the upper part of the hole between 80 and 150 mbsf.

BACKGROUND AND OBJECTIVES

Background

Site 760 is located approximately 5 km downdip (upslope) of Site 759, on the southeastern edge of the Wombat Plateau (Fig. 1). Therefore, the background for Site 759 (see "Background and Objectives," Site 759 chapter) also serves as background for Site 760. The drilling results at Site 759 showed that the sediments below the Neogene section on the

[1] Haq, B. U., von Rad, U., et al., 1990. *Proc. ODP, Init. Repts.*, 122: College Station, TX (Ocean Drilling Program).

[2] Shipboard Scientific Party is as given in the list of Participants preceding the contents.

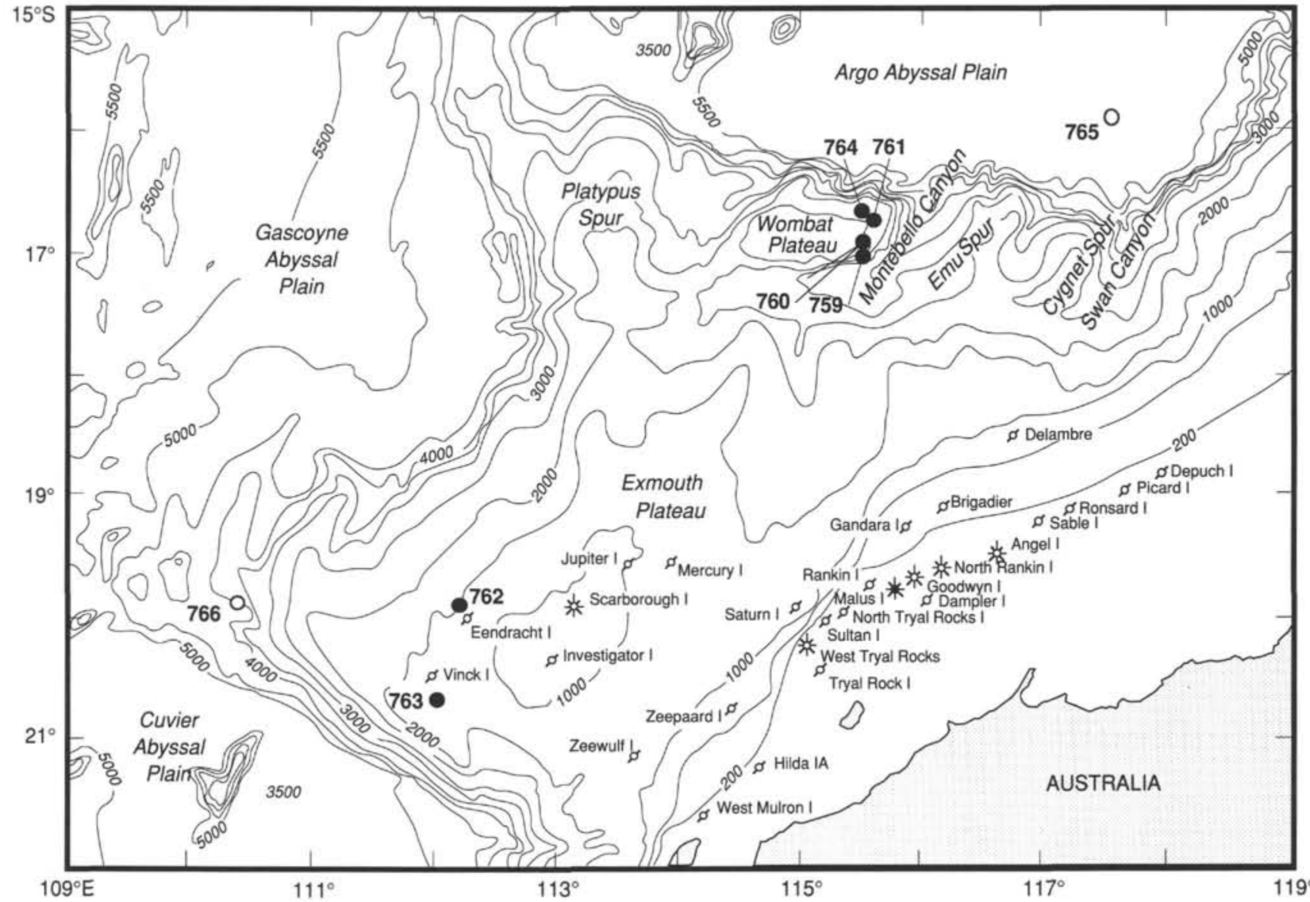

Figure 1. Bathymetric map of Exmouth Plateau region showing locations of ODP sites (closed circles = Leg 122 sites, open circles = Leg 123 sites) and commercial wells. Leg 122 sites 759 and 760 are at the position of proposed Site EP10A. Bathymetry in meters (Exon, unpubl. data).

flank of Wombat Plateau are entirely Triassic and that the younger Mesozoic record was missed at that site. The recovery of this younger section is crucial to the dating of the breakup unconformity and the understanding of the late rift history of the Exmouth Plateau.

To recover the younger section, Site 760 was located upslope from Site 759, northward of the point at which three unconformities on the seismic record merge. Site 760 was expected to recover a section intermediate in age between that recovered at Site 759 and the younger section anticipated at proposed Site EP9E (Site 761). As only trace amounts of hydrocarbon gases were recorded at Site 759, the drilling of Site 760 was judged to be safe and thus was approved by the Ocean Drilling Program (ODP) and the JOIDES Pollution Prevention and Safety Panel (PPSP).

Objectives

Site 760 was designed to recover a Mesozoic section younger than that encountered at Site 759 (Carnian) and overlain by sediments of Paleogene to Neogene age. Nevertheless, the main objectives for the two sites were the same (see "Background and Objectives," Site 759 chapter) and included (1) reconstructing the early breakup, uplift, and subsidence history, (2) documenting sea level changes, and (3) refining chronostratigraphy.

OPERATIONS

Hole 760A

JOIDES Resolution was underway to Site 760 at 2115 hr (local time, or LT), 11 July 1988. After a short seismic survey, beacon SN 404 was dropped at 2315 hr near 16°55.32′S, 115°32.48′E. The hole was to be cored using the advanced piston corer/extended core barrel system (APC/XCB) and a Security M84F IADC Code 6-1-7 bit was selected. The bottom hole assembly (BHA) consisted of the 11-7/16-in. bit, long bit sub, seal bore collar, landing saver sub, long top sub, latch sub, seven 8-1/4-in. drill collars, one cross over (XO), one 7-1/4-in. drill collar, and two stands of 5-1/2-in. drill pipe.

Core 122-760A-1H recovered 7.7 m of sediment (Table 1), which established seafloor to be at 1981.1 m from the dual elevator stool (DES). Nine piston cores were taken to a penetration of 83.7 meters below sea floor (mbsf) before a pullout of 70,000 pounds required the termination of piston coring; recovery was 103%.

Coring continued with the XCB system. From 93.2 mbsf through 182.7 mbsf recovery decreased, averaging 33% (Fig. 2). The laminated claystone/siltstone in this interval was packing into the throat of the core catcher, preventing additional core from entering the barrel. In an effort to improve recovery, the cored interval was reduced to 5 m at 187.0 mbsf. This procedure was successful, as the recovery increased to an average of 78%

Table 1. Coring summary, Site 760.

Core no.	Date (July 1988)	Time (local)	Depth (mbsf)	Cored (m)	Recovered (m)	Recovery (%)
122-760A-						
1H	12	1030	0.0–7.7	7.7	7.73	100.4
2H	12	1100	7.7–17.2	9.5	10.09	106.2
3H	12	1130	17.2–26.7	9.5	9.91	104.3
4H	12	1320	26.7–36.2	9.5	9.83	103.5
5H	12	1345	36.2–45.7	9.5	9.09	95.7
6H	12	1415	45.7–55.2	9.5	10.09	106.2
7H	12	1450	55.2–64.7	9.5	9.77	102.8
8H	12	1520	64.7–74.2	9.5	9.94	104.6
9H	12	1700	74.2–83.7	9.5	9.90	104.2
10X	12	1820	83.7–93.2	9.5	5.44	57.3
11X	12	2000	93.2–102.7	9.5	1.71	18.0
12X	12	2105	102.7–112.2	9.5	3.00	31.6
13X	12	2230	112.2–116.2	4.0	1.92	48.0
14X	13	0000	116.2–125.7	9.5	1.18	12.4
15X	13	0115	125.7–135.2	9.5	0.53	5.6
16X	13	0230	135.2–144.7	9.5	8.23	86.6
17X	13	0350	144.7–154.2	9.5	1.82	19.2
18X	13	0440	154.2–163.7	9.5	0.30	3.2
19X	13	0645	163.7–173.2	9.5	4.55	47.9
20X	13	0815	173.2–182.7	9.5	3.75	39.5
21X	13	0910	182.7–187.9	5.2	1.62	31.2
22X	13	1030	187.9–192.9	5.0	4.92	98.4
23X	13	1115	192.9–197.9	5.0	3.05	61.0
24X	13	1150	197.9–202.9	5.0	1.29	25.8
25X	13	1245	202.9–207.9	5.0	8.09	161.8
26X	13	1340	207.9–212.9	5.0	3.68	73.6
27X	13	1430	212.9–217.9	5.0	2.93	58.6
28X	13	1545	217.9–222.9	5.0	5.87	117.4
29X	13	1640	222.9–232.4	9.5	7.60	80.0
30X	13	1810	232.4–241.9	9.5	9.79	103.1
31X	13	2015	241.9–251.4	9.5	5.70	60.0
32C	13	2200	251.4–254.4	(Wash and drill—3.0 m)		
33X	13	2245	254.4–259.4	5.0	6.49	129.8
34X	13	2350	259.4–264.4	5.0	1.58	31.6
35X	14	0100	264.4–269.4	5.0	8.21	164.2
36X	14	0250	269.4–278.9	9.5	2.00	21.1
37X	14	0420	278.9–283.9	5.0	4.28	85.6
38X	14	0620	283.9–284.9	1.0	0.50	50.0
Coring totals				281.9	196.58	69.7
Wash and drill = 3.0 m						
122-760B-						
1C	14	2055	0.0–89.9	(Wash and drill—89.9 m)		
2R	14	2200	89.9–99.4	9.5	1.18	12.4
3R	14	2300	99.4–108.9	9.5	2.06	21.7
4R	15	0000	108.9–118.4	9.5	1.38	14.5
5C	15		118.4–283.0	(Wash and drill—164.6 m)		
6R	15	1325	283.0–292.5	9.5	2.77	29.2
7R	15	1540	292.5–302.0	9.5	3.82	40.2
8R	15	1820	302.0–311.5	9.5	4.59	48.3
9R	15	1955	311.5–321.0	9.5	4.90	51.61
0R	15	2050	321.0–330.5	9.5	3.36	35.4
11R	15	2230	330.5–340.0	9.5	5.19	54.6
12R	16	0023	340.0–349.5	9.5	4.25	44.7
13R	16	0150	349.5–359.0	9.5	3.54	37.3
14R	16	0250	359.0–368.5	9.5	6.63	69.8
15R	16	0435	368.5–378.0	9.5	2.51	26.4
16R	16	0700	378.0–387.5	9.5	6.20	65.3
17R	16	0900	387.5–397.0	9.5	4.94	52.0
18R	18	1000	397.0–406.5	9.5	3.16	33.3
19R	16	1140	406.5–416.0	9.5	6.37	67.1
20R	16	1450	416.0–425.5	9.5	7.49	78.8
21R	16	1745	425.5–435.0	9.5	6.22	65.5
22R	16	2025	435.0–444.5	9.5	6.00	63.2
23R	16	2215	444.5–454.0	9.5	6.63	69.8
24R	17	0100	454.0–463.5	9.5	0.14	1.5
25R	17	0230	463.5–468.0	4.5	3.46	36.4
26R	17	0525	468.0–477.5	9.5	4.54	47.8
27R	17	0730	477.5–487.0	9.5	9.81	103.3
28R	17	0950	487.0–496.5	9.5	6.32	66.5
29R	17	1200	496.5–506.0	9.5	6.16	64.8
Coring totals				251.5	123.02	48.9
Wash and drill = 254.5 m						

for the next 40 m. Three 9.5-m cores were taken with an average recovery of 81%. At 251.4 mbsf the XCB cutter shoe and 3 in. of the barrel broke off and were left in the hole. The Atride center mill was run in place of the XCB and 3 m of hole was made in 15 min. Coring continued to 284.9 mbsf, whereupon the bit torque increased and the drilling rate decreased to nearly zero (Fig. 3A). This was interpreted as evidence that the bit had failed either from wear and/or junk damage, and thus no further coring was possible. Although no significant amount of gas had been detected, the bit was raised to 105 mbsf and a 200-sack cement plug was emplaced. Operations at Hole 760A were concluded at 1300 hr (LT) 14 July.

Hole 760B

As deeper penetration was needed to achieve the scientific objectives of the site, the ship was moved 20 m north to drill Hole 760B. The plan was to drill the second hole using the rotary-core-barrel (RCB) system through the intervals well recovered in Hole 760A to 283.0 mbsf (the total depth of Hole 760A), whereupon coring would be resumed. Intervals poorly recovered in Hole 760A were to be recored with the RCB in Hole 760B. A 9-7/8-in. Security M84F IADC Code 6-1-7 bit was used; the BHA, which contained a mechanical bit release, was the same as used at Hole 759A.

The Atride center bit was installed in the core bit, and Core 121-760B-1C was drilled to 89.9 mbsf, at which depth RCB coring commenced. In Hole 760A, the interval from 103 to 116 mbsf had produced recovery of only 29%. For comparison, a portion of the same interval was re-cored with the RCB to determine if recovery would improve. However, recovery decreased to 16% (Fig. 4).

The center bit was reinstalled and the hole drilled to 283.0 mbsf. From this depth, RCB coring was resumed to 506.0 mbsf (Fig. 3B). At Site 760, as at Site 759, the recovered material was older than expected and the scientific party thought that their objectives could be better achieved at another site (see "Background and Objectives," Site 761 chapter, this volume). Overall recovery for Hole 760B was 49%.

While coring Hole 760B a 5-barrel mud sweep was pumped every third core; no abnormal torque or drag occurred until the last core was attempted (506.0 mbsf), at which point the drag increased to 50,000 lbs. A 20-barrel mud sweep and reaming reduced the drag to normal.

After logging (see "Downhole Measurements," this chapter, for a synopsis of logging operations), the thrusters and hydrophones were raised and secured and *JOIDES Resolution* departed for Site 761 (EP9E) at 0075 hr (LT), 19 July 1988.

LITHOSTRATIGRAPHY

Introduction

Site 760 consisted of two holes, 760A and 760B. Hole 760A was cored to 284.9 mbsf; twenty-nine cores were recovered from Hole 760B, including 3 spot cores from the sequence penetrated in Hole 760A, 2 center-bit runs, and 24 cores taken continuously between 283.0 and 506.0 mbsf (below the section penetrated in Hole 760A). Rocks and sediments at Site 760 were divided into seven lithologic units, summarized in Table 2 and Figure 5. The abundance of sedimentary components is recorded in Figure 6. Coring disturbance was minor; recovery increased with depth in the holes. Lithologic units are discussed in descending order.

Unit I (0–21.7 mbsf)

Interval 122-760A-1H-1 to -3H-4.

Unit I consists of Quaternary foraminifer nannofossil ooze (Subunit IA) and upper Pliocene nannofossil ooze with foraminifers (Subunit IB).

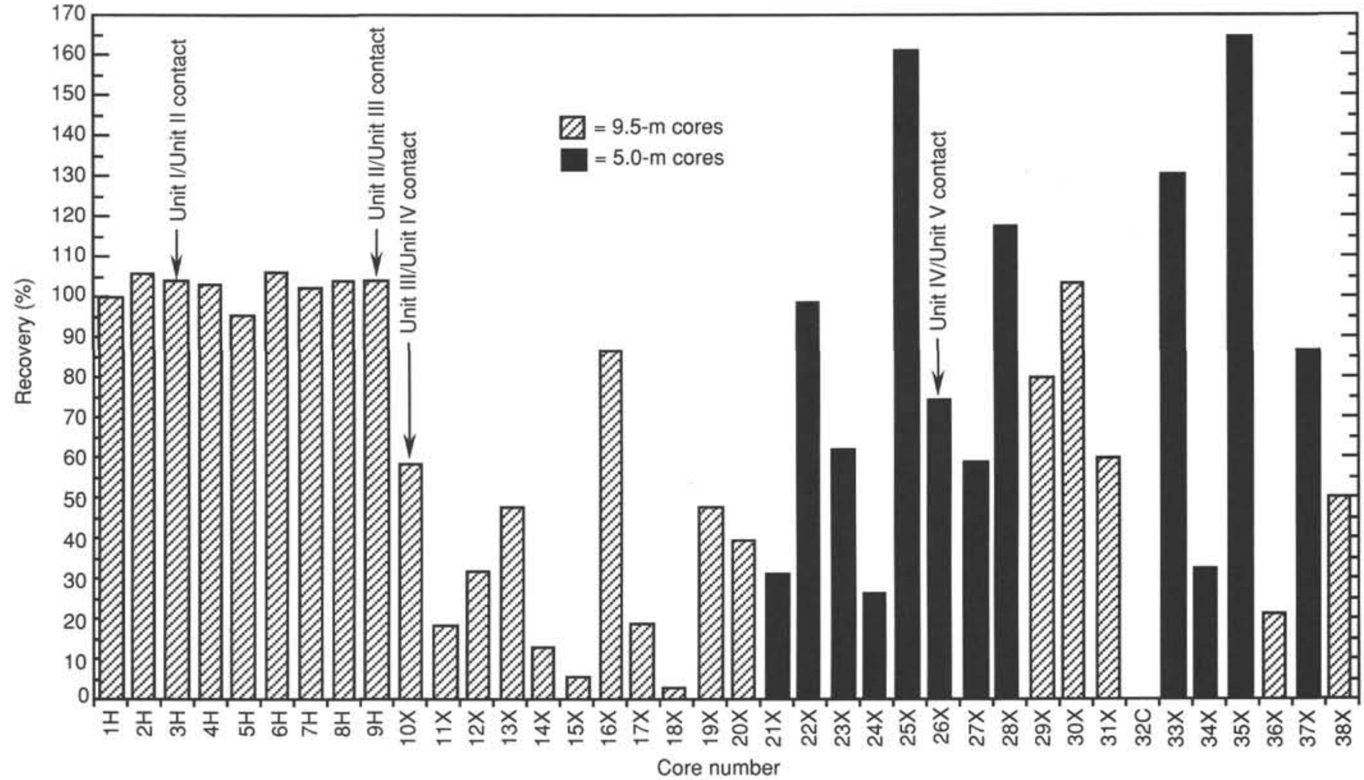

Figure 2. Core number versus recovery (%) for Hole 760A. A core-type of "C" denotes center-bit or wash cores, with no sediment recovered *in situ*.

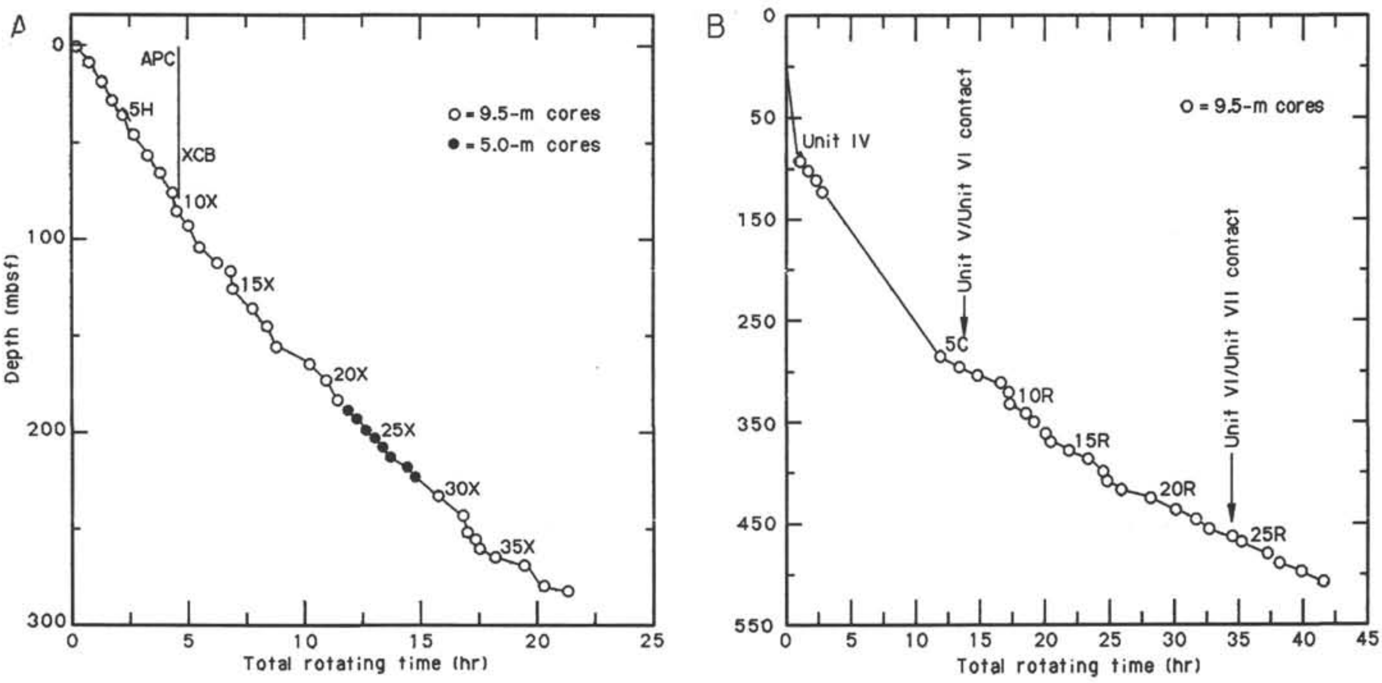

Figure 3. Total rotating time (hr) versus depth (mbsf). **A.** Hole 760A. **B.** Hole 760B.

Subunit IA (0–17.2 mbsf)

Interval 122-760A-1H-1 through -2H-CC.

Subunit IA consists of 17.2 m of Quaternary foraminifer nannofossil ooze. Cyclic sequences, represented by 5- to 50-cm-thick alternating color bands, occur through the upper 10.1 m of this subunit; these are thicker (30–160 cm) and less apparent in the lower 7.1 m of the section (i.e., Interval 122-760A-2H-1, 90–125 cm; see Fig. 7). Alternating pink (5Y 7/3 to 5Y 7/4), light gray (5YR 7/1), and light greenish-gray bands, 3–50 cm thick, characterize the upper 3 m. Light

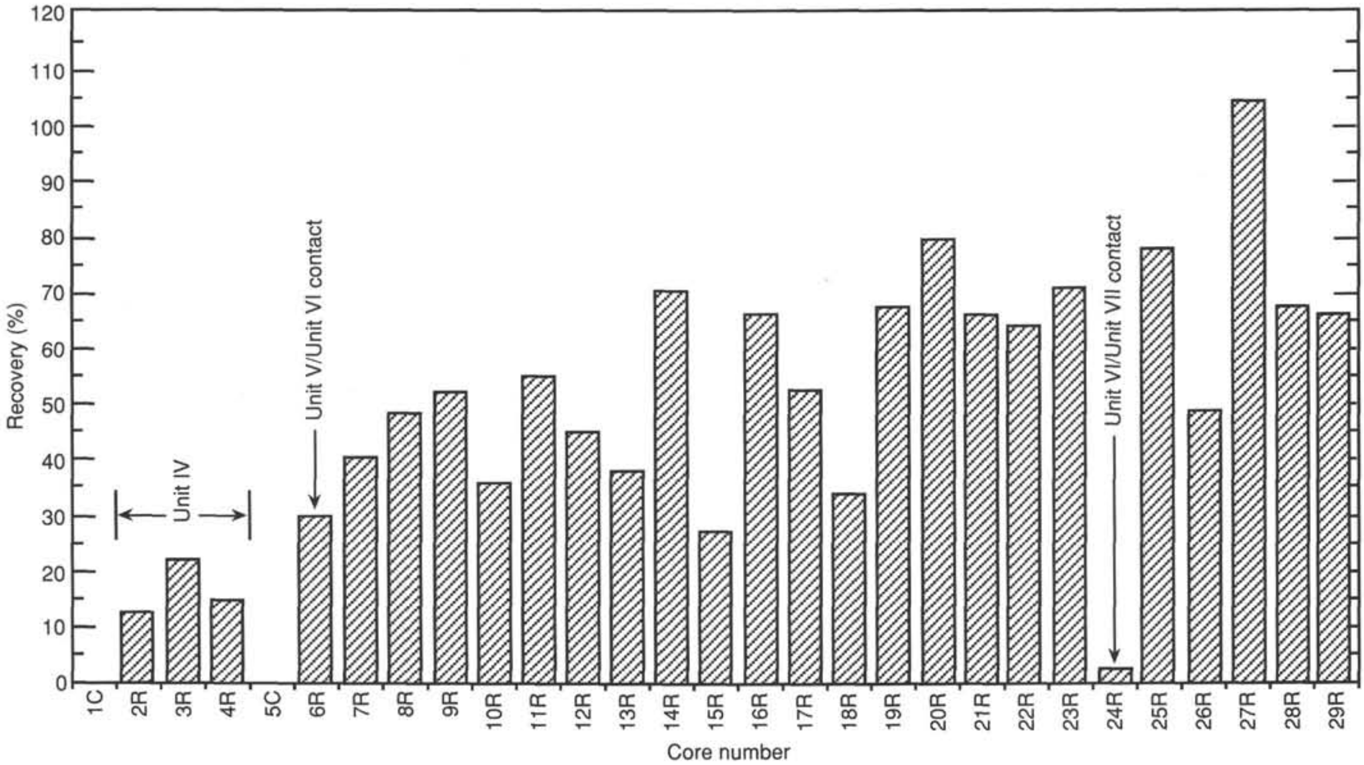

Figure 4. Core number versus recovery (%), Hole 760B. A core-type of "C" denotes center-bit or wash cores, with no sediment recovered *in situ*.

greenish-gray (10Y 7/1) and gray (2.5Y 6/0) to light gray (2.5Y 7/0) color bands are interlayered from 3 mbsf to the base of the subunit. Below 10.6 mbsf, 70- to 160-cm-thick gray layers alternate with 10–40-cm-thick greenish gray layers. Individual color bands are generally structureless, except for minor color-mottling attributed to bioturbation.

Subunit IB (17.2–21.7 mbsf)

Interval 122-760A-3H-1 to -3H-4.

Subunit IB consists of 4.5 m of white (10YR 8/1) to light gray (10YR 7/1) nannofossil ooze with foraminifers. Faint color bands, 15–30 cm thick, are present (e.g., 122-760A-3H-3, 25–75 cm; see Fig. 8). This subunit is generally structureless, with minor bioturbation. Discoasters are abundant.

Unit II (21.7–80.1 mbsf)

Interval 122-760A-3H-4 to -9H-4, 140 cm.

Unit II is composed of 58.4 m of generally structureless nannofossil ooze and nannofossil ooze with foraminifers and minor clay; sporadic bioturbation occurs throughout. Sediments range from upper Miocene to upper Eocene, with a disconformity between the lower Oligocene and upper Eocene at 71.02 mbsf (Core 122-760A-8H-4, 82 cm; see "Biostratigraphy," this chapter). White (10YR 8/1) to light gray (2.5Y 7/2) intervals, 6 and 14 m thick, alternate with white (10YR 8/1) to very pale brown (10YR 8/3) layers, 9.5 and 28.9 m thick. Foraminifers and clay minerals occur as minor components (in variable abundance) admixed with nannofossils. Foraminifer-rich layers occur in Sections 122-760A-4H-1 to -CC (generally 15%–25% foraminifers), 122-760A-6H-6 to -7H-7 (10%–25% foraminifers), and 122-760A-9H-2 to -4 (25%–60% foraminifers).

Unit III (80.1–84.9 mbsf)

Interval 122-760A-9H-4, 140 cm to -10X-1, 115 cm.

Note that Core 122-760A-9H recovered 9.9 m of sediment; however, the maximum core recovery in ODP calculations is 9.5 m. Therefore, the additional 0.4 m of sediment recovered in this core and described here exceed the 4.8 m "officially" recovered (see "Explanatory Notes," this volume, for a discussion of sediment recovery calculations).

Unit III is 4.8 m thick and consists of (from top to bottom): a 40-cm-thick manganese crust, a 360-cm-thick variegated and texturally diverse siliciclastic layer, a 41-cm-thick layer of sandy siltstone containing manganese nodules, and a 74-cm-thick layer of variegated and texturally diverse siliciclastic sediments. Unit III is undated, but separates lower Eocene pelagic ooze (above) from Norian siliciclastic sediments (below). A strong reflector marking a prominent angular unconformity on reflection seismic data probably correlates with the manganese crust at the top of Unit III (see "Seismic Stratigraphy," Site 761 chapter, this volume).

The manganese crust at the top of Unit III consists of black (10YR 2/1), soft, uncemented manganese oxide nodules in a 40-cm-thick layer (Fig. 9). These nodules have a yellowish core of carbonate or siliciclastic pebbles.

Underlying this manganese crust are 3.6 m of variegated claystones and silty to fine-grained sandstones, with hues ranging from light grayish-brown (2.5Y 6/2) and light olive brown (2.5Y 5/4), to pale olive (5Y 6/4) and pale yellow (5Y 7/3). The upper 1.6 m are well-bedded, with 10–20-cm-thick claystone beds containing thin (1–2 mm) siltstone laminae, alternating with 7–15-cm-thick beds of fine-grained sandstone containing thin (1–10 mm) claystone laminae. Scattered iron

Table 2. Lithostratigraphy of Site 760.

Unit	Lithology	Cores	Depth (mbsf)	Thickness (m)	Environment	Age
IA	Foraminifer-nannofossil ooze, light gray to greenish-gray.	122-760A-1H-1, 0 cm to -2H-CC	0.0–17.2	17.2	Pelagic; cyclic color bands, 40–50 cm thick.	Quaternary
IB	Nannofossil ooze with foraminifers, white to light gray.	122-760A-3H-1, 0 cm to -3H-4	17.2–21.7	4.5	Pelagic; structureless, minor bioturbation, vague color bands.	Late Pliocene
II	Nannofossil ooze, white to pale brown, contains clay and foraminifers in part.	122-760A-3H-4 to -9H-4, 140 cm	21.7–80.1	58.4	Pelagic; structureless except for minor mottling due to bioturbation.	Late Miocene to Late Middle Eocene
III	Manganese oxide layer, 40 cm thick, overlying variegated olive yellow to brownish-yellow, massive to laminated silty claystone and silty sandstones with MnO_2 nodules.	122-760A-9H-4, 140 cm to -10X-1, 115 cm	80.1–84.9	4.8	MnO_2 layer sits on major unconformity represented by variegated sands and silts.	Unconformity; early Eocene and Cretaceous
IV	Siliciclastic interval, black to dark gray claystone interbedded with dark greenish-gray clayey siltstone to silty sandstone with root-mottling and minor occurrences of coal.	122-760A-10X-1, 115 cm to -26X-2, 150 cm and 122-760-2R to -4R	84.9–210.9	126.0	Marginal marine (estuarine or distributary bay) to subaerial (soil profile).	Late Triassic (Norian)
V	Siliciclastic interval black to dark gray, parallel-laminated to massive or bioturbated silty claystones interbedded with greenish-gray, parallel- to cross-laminated siltstones to sandstones with upward-fining sequences and occasional mollusk fragments; glauconite decreases in abundance uphole.	122-760A-26X-CC, 0 cm to -38X and 122-760B-6R-1, 0 cm to -6R-2, 40 cm	210.9–284.9 283.0–285.4	74.5	Shallow to marginal marine (estuarine to distributary bay or tidal flat with channels).	Late Triassic (Norian)
VI	Interbedded fossiliferous limestones and siliciclastics, dark gray to black silty claystones interbedded with gray grainstones, packstones, wackestones, and mudstones, and minor silty quartz sandstones, with minor algal mats, rootlets, coal, pyrite, and vertical burrows.	122-760B-6R-2, 40 cm to -25R-1, 55 cm	284.9–464.05	178.65	Shallow marine, tidal flat with carbonate banks?	Late Triassic (Norian to Carnian)
VII	Siliciclastic interval black to dark gray silty claystone with minor dark greenish-gray silty sandstone; parallel laminations, sideritic nodules and concretionary layers, molluscan shells, and upward-fining sequences.	122-760B-25R-1, 55 cm to -29R-CC	464.05–506.0	41.95	Shallow marine, tidal flat and channels, or prodelta.	Late Triassic (Carnian)

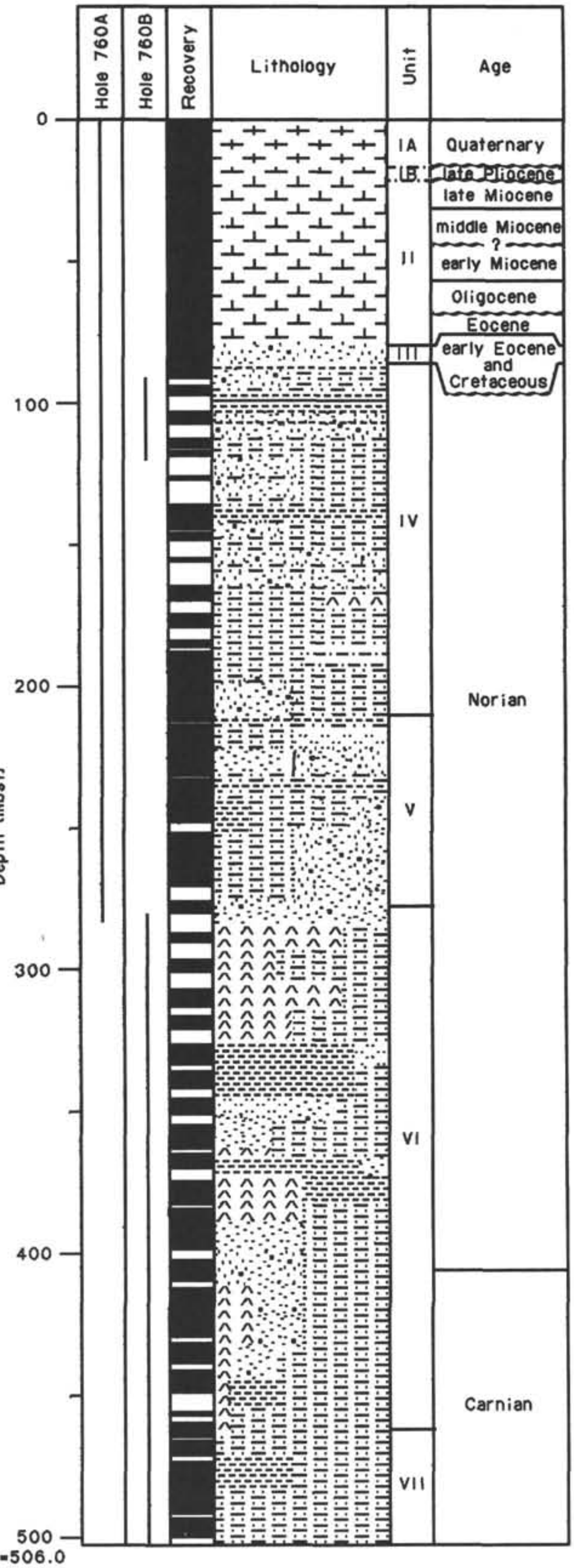

Figure 5. Lithologic column for Holes 760A and 760B, showing core number and type, recovery, generalized lithology, lithologic unit, and age. Black in recovery column indicates recovered intervals. Key to lithological symbols is in the "Explanatory Notes" chapter, this volume.

oxide and manganese oxide nodules occur locally within this well-bedded interval. The lower 2.0 m consist of pale olive (5Y 6/4) to pale yellow (5Y 7/3), structureless, uncemented, fine-grained silty sand.

A second layer of manganese oxide occurs 3.6 m below the base of the upper manganese crust (122-760A-10X-1, 0-40 cm). These are fragments 1 mm to 5 cm in size that are dispersed in a disturbed, 41-cm-thick sandy siltstone layer. This second manganese layer overlies a 74-cm-thick variegated zone of brownish-yellow (10YR 6/8) to olive yellow (2.5Y 6/6) sandy siltstone with minor sand and clay. Two thin manganese oxide layers (<1 mm thick) occur in the lower 10 cm of this variegated zone, with the lower boundary of Unit III placed at the lowest layer of manganese oxide nodules.

Approximately 110 m.y. are represented by Unit III and its bounding surfaces (see "Biostratigraphy," this chapter), suggesting that this unit contains one or more unconformity surfaces representing periods of nondeposition and subaerial or submarine erosion/exposure. The occurrence of two oxidized, variegated siliciclastic intervals, each overlain by layers enriched in manganese oxide nodules, suggests that two cycles of erosion and hardground formation were probably involved in the deposition of Unit III.

Unit IV (84.9–210.9 mbsf)

Interval 122-760A-10X-1, 115 cm to -26X-2, 150 cm, and Interval 122-760B-2R to -4R.

Unit IV is the first of the major siliciclastic intervals encountered at Site 760. It consists of black (N/2) to dark gray (5Y 4/1) silty claystones, and dark gray (5Y 4/1) to dark greenish gray (10Y 5/2) clayey siltstones, sandy siltstones, and fine-grained sandstones. The unit is 126.0 m thick, and contains late Triassic (Norian) microfossils.

The cores consist of silty claystones interbedded with clayey siltstones and minor sandy siltstones and sandstones. "Rootlets" and/or algal stringers (e.g., Interval 122-760A-10X-1, 108–138 cm; see Fig. 10) are characteristic biogenic structures observed in Unit IV (Fig. 6). Some of the "rootlets" may have been filled with pyrobitumen or dead oil (see "Organic Geochemistry," this chapter). Well-developed soil profiles are also present, associated with some minor occurrences of coal (Intervals 122-760A-26X-2, 104–105 cm, and -26X-2, 110–115 cm). There are also minor occurrences of pyrite nodules (first encountered in Section 122-760A-21X-1) and siderite (first encountered in Core 122-760A-20X-1, 95 cm, and -20X-1, 115 cm). Parallel and cross-laminated beds are present in the lower portion of the unit, in the transitional zone to the underlying Unit V (i.e., 192.9–210.9 mbsf; see Fig. 11). Bioturbation is rare to absent within the cores, and no marine fossils were observed.

Microscope examination showed that the silty claystones and clayey siltstones contain clay minerals, quartz, carbonaceous opaque material, minor feldspar, rock fragments, and accessory minerals.

The presence of soil profiles, root or algal stringer structures and coal, and the absence of marine fossils suggest a marginal-marine environment (marsh to lagoon?) with intermittent periods of subaerial exposure. The predominance of terrestrial palynomorphs and freshwater algae in Unit V (see "Biostratigraphy," this chapter) provides corroborative evidence for a marginal to nonmarine environment of deposition. The occurrence of a marine palynomorph assemblage (e.g., acritarchs and a diverse dinoflagellate assemblage in Sample 122-760A-25X-2, 74–76 cm; see "Biostratigraphy," this chapter), about 4 m above an inferred soil profile, suggests that marine incursions alternated with periods of subaerial exposure.

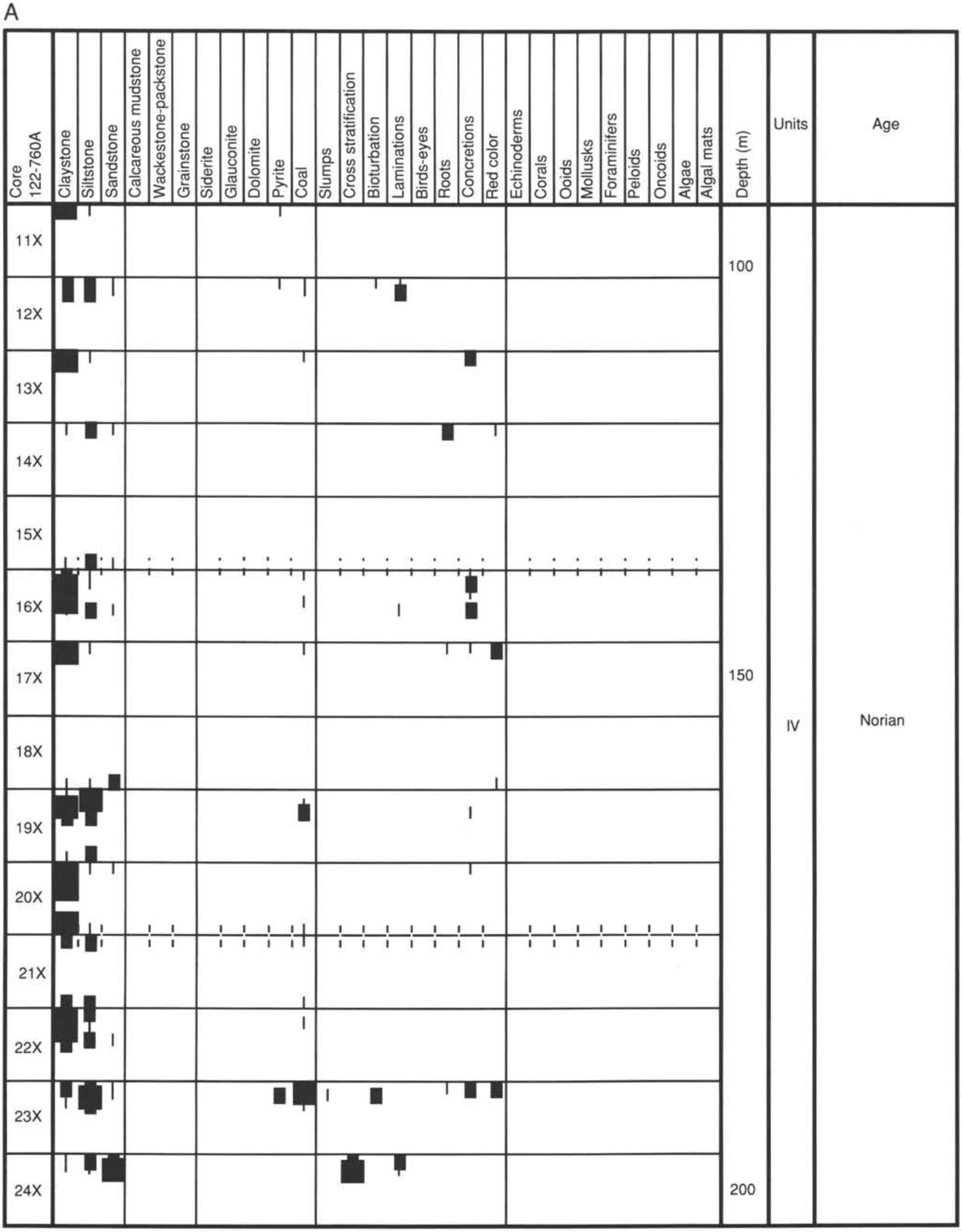

Figure 6. Sequential changes of sedimentological components of Site 760. Width of bar indicates relative abundance: thin bar = trace; thicker bar = common; thickest bar = abundant. **A.** Hole 760A. **B.** Hole 760B.

A (cont.)

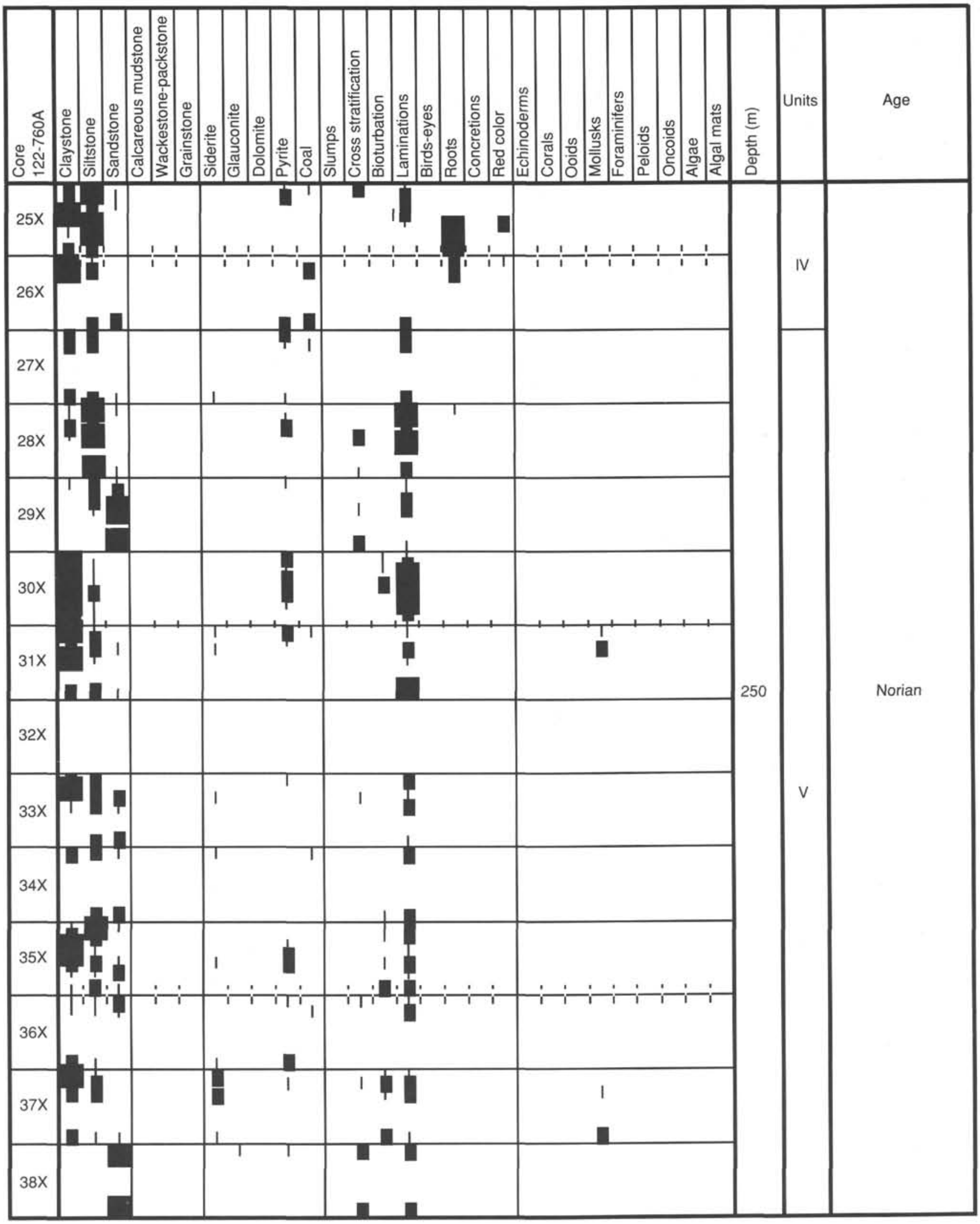

Figure 6. (continued).

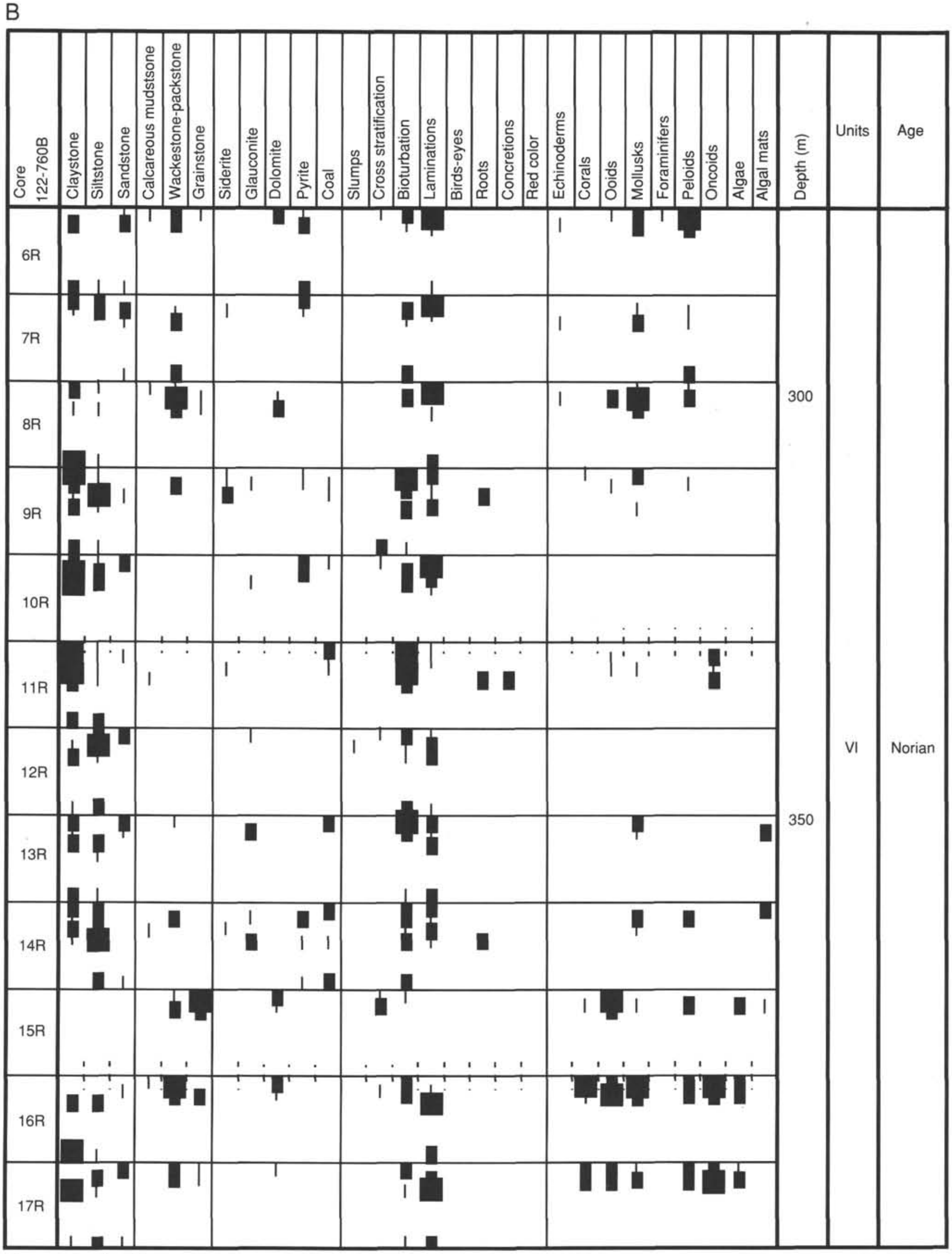

Figure 6 (continued).

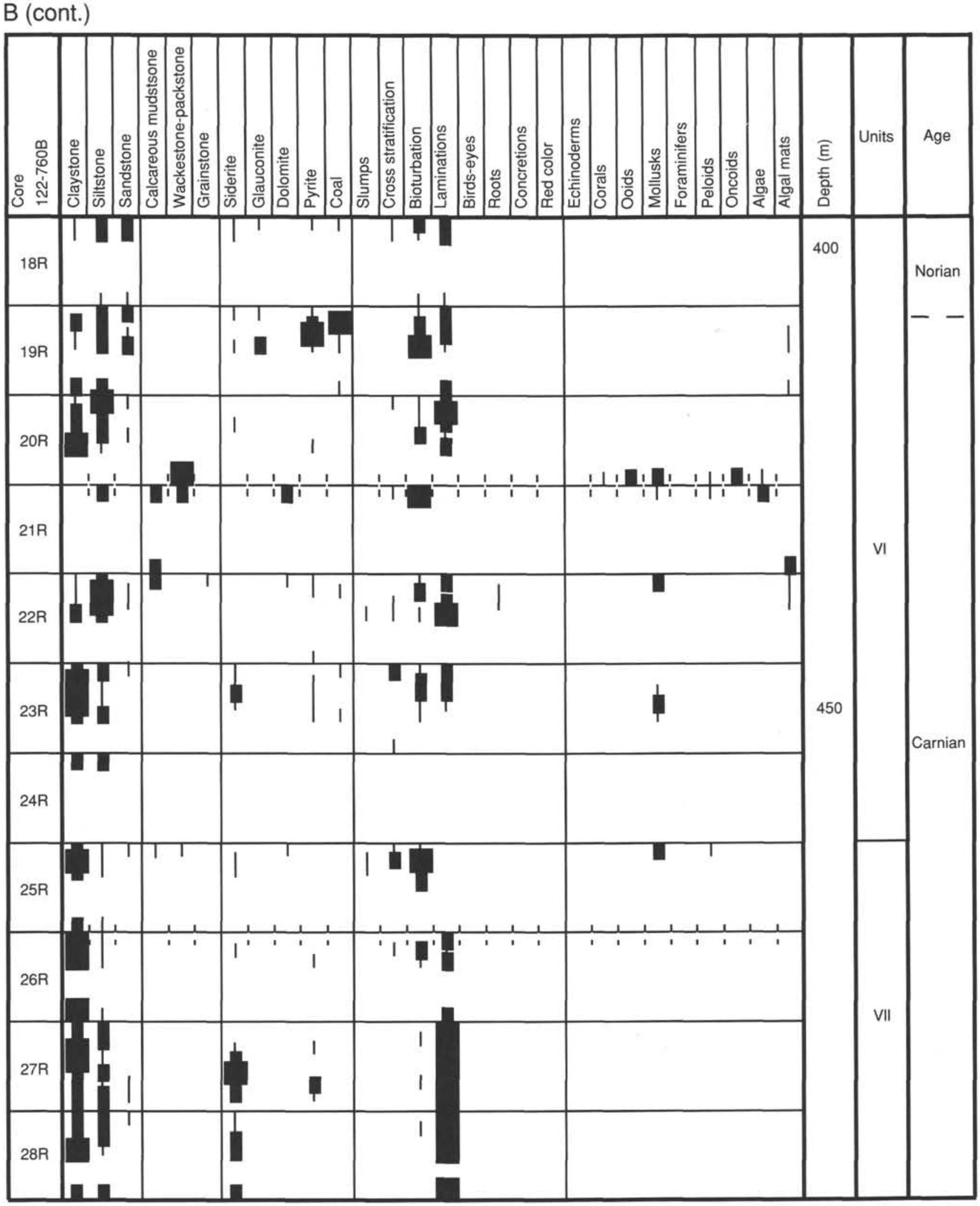

Figure 6 (continued).

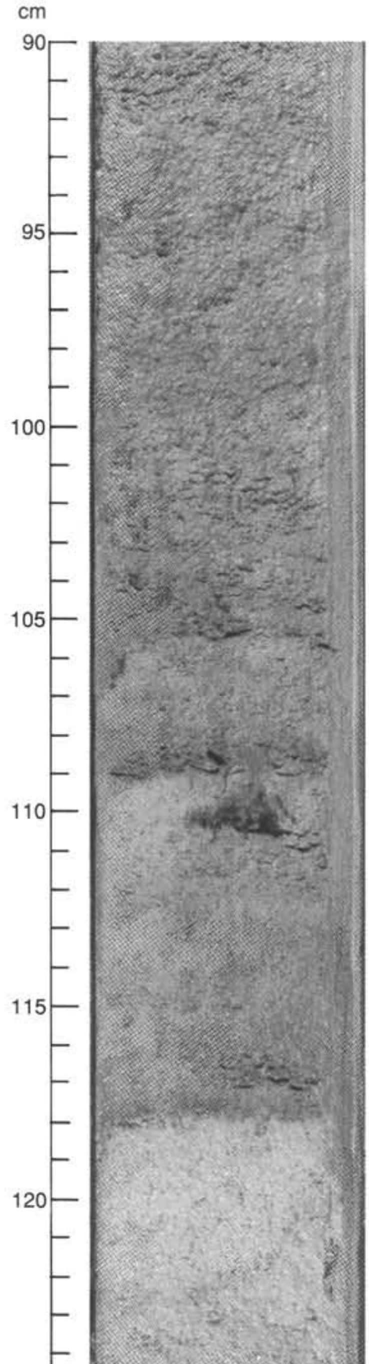

Figure 7. Interval 122-760A-2H-1, 90–125 cm. Foraminifer nannofossil ooze of Subunit IA, characterized by cyclic color changes.

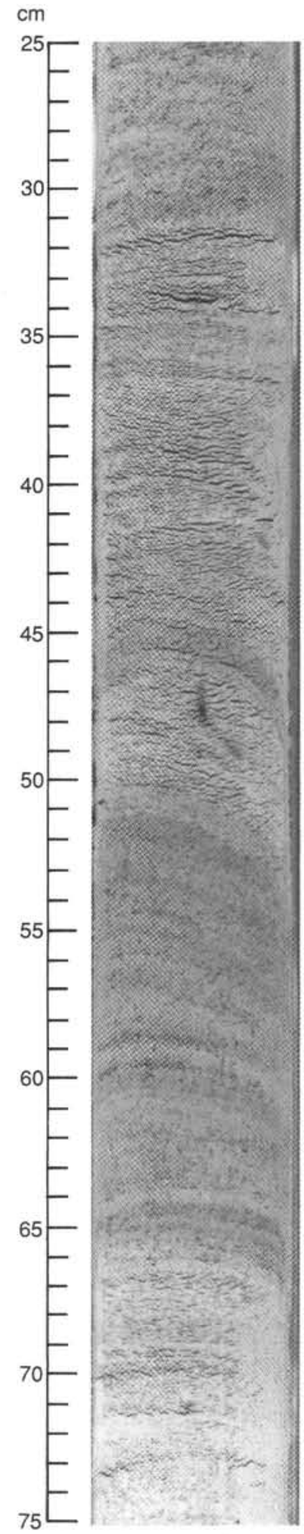

Figure 8. Interval 122-760A-3H-3, 25–75 cm. Nannofossil ooze of Subunit IB, characterized by cyclic interlayers of white and light gray bands.

Unit V (210.9–284.9 mbsf)

Cores 122-760A-26X-CC through -38X and 122-760B-6R-1 to -6R-2, 40 cm.

Unit V is a 74.5-m-thick siliciclastic interval dated as Norian (late Triassic). The siliciclastic sediments and rocks are dark greenish gray (10Y 5/2) clayey siltstones, sandy siltstones, and sandstones, and dark gray (5Y 4/1) to black (N2) silty claystones.

Three 20- to 27-m-thick upward-fining sequences make up Unit V: (1) a poorly recovered sequence, 284.9–259.4 mbsf (25.5 m thick, Core 122-760A-38X to Core -34X); (2) 259.4–232.4 mbsf (27.0 m thick, Core 122-760A-33X to Core -30X); and (3) from 232.4 to the top of Unit V at 210.9 mbsf (Core

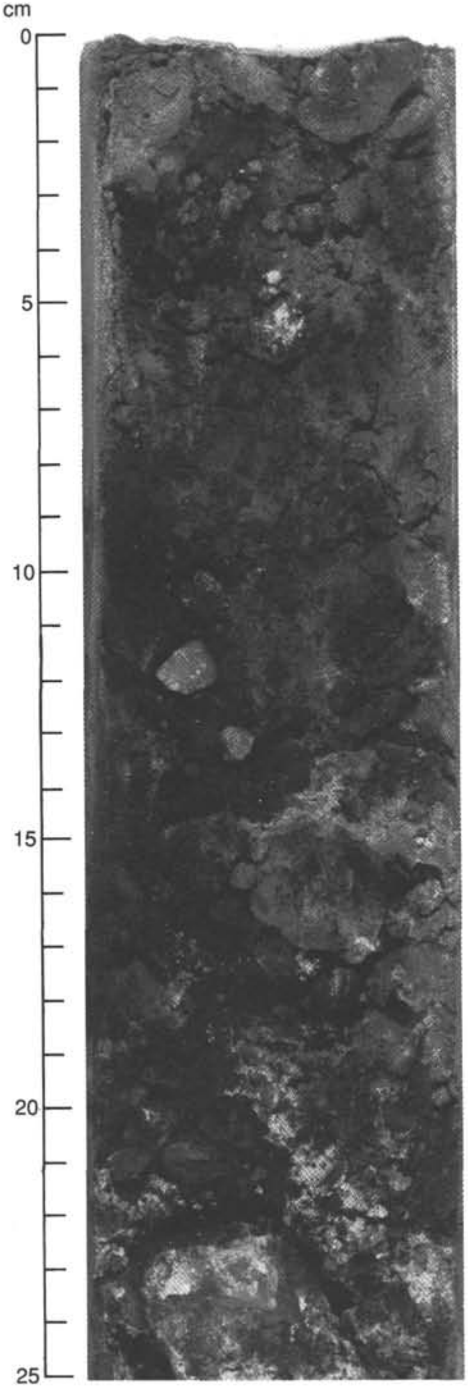

Figure 9. Interval 122-760A-9H-5, 0–25 cm. Manganese oxide crust of Unit III, consisting of black manganese oxide nodules with yellowish carbonate or siliciclastic pebbles at the center.

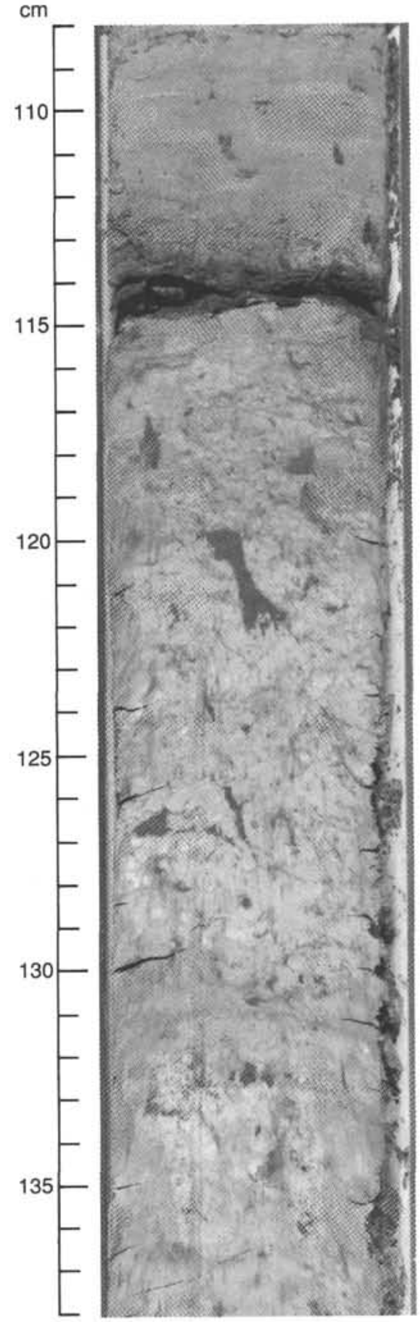

Figure 10. Interval 122-760A-10X-1, 108–138 cm. Mottled silty claystone of Unit IV. Many former rootlet soil profiles are present.

122-760A-29X to Core -26X-CC), and continuing up into Unit IV (to Core 122-760A-25X-5). The basal portion of these upward-fining sequences consists of parallel- and cross-laminated, silty to coarse-grained sandstones, with quartz as the dominant mineral. Parallel-laminated (and to a lesser extent cross-laminated) siltstones to silty claystones compose the remainder of the upward-fining sequences. Nodules and disseminated grains of pyrite (Fig. 12), carbonaceous matter, and bioturbation structures are common in the finer-grained intervals.

Mollusk shells and fragments, thin coquina layers, and calcite-cemented sandstone are present at the bottom of the lowermost upward-fining sequence (Cores 122-760A-37X and -38X). These lithologies overlap in depth with carbonate wackestone and packstone recovered in Hole 760B (Sections 122-760B-6R-1 and -6R-2). On the basis of similar lithologies and depths, we correlate Core 122-760A-38X with the upper part of Core 122-760B-6R, and place the boundary between Units V and VI at 284.9 mbsf (i.e., at the base of Core 122-760A-38X, and in Core 122-760B-6R-2, 40 cm; 284.9 mbsf).

The above sequences and characteristics suggest a marginal-marine environment with probable channelized se-

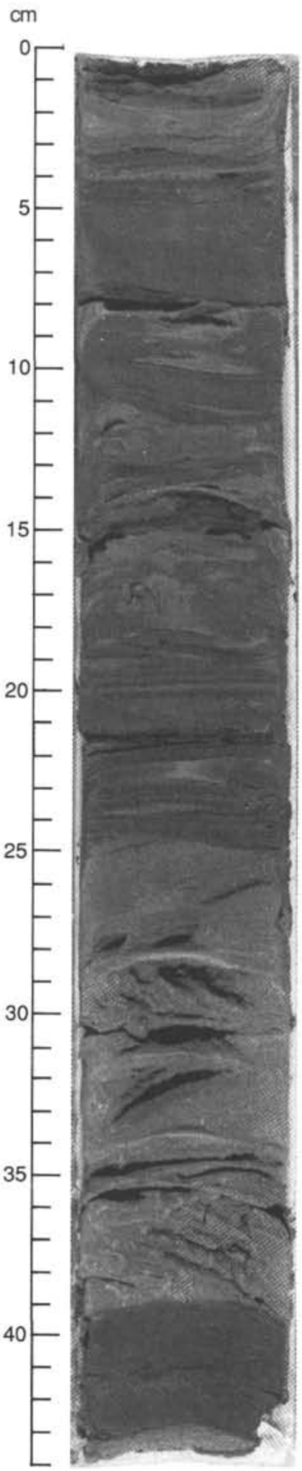

Figure 11. Interval 122-760A-24X-CC, 0–44 cm. Parallel laminated silty claystone interbedded with cross-laminated silty sandstone of Unit IV.

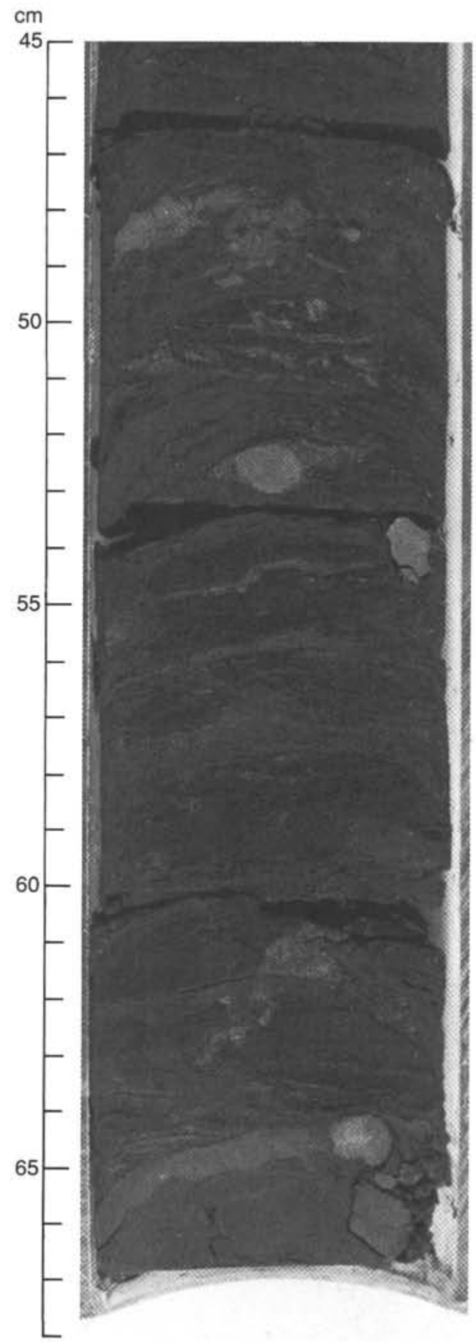

Figure 12. Interval 122-760A-26X-CC, 45–68 cm. Interbedded clayey siltstone and silty claystone of Unit V. They are generally carbonaceous and are parallel-laminated. Many pyrite nodules occur locally.

quences. Palynomorph assemblages from Unit V are dominated by nonmarine forms and others not typically found in a marine setting (here termed "atypically marine") except for Sample 122-760A-37X-CC, which contains a diverse marine assemblage (see "Biostratigraphy," this chapter). Together these data suggest a shallow-marine influence at the base of Unit V, evolving into a brackish or freshwater channelized distributary system (deltaic, distributary bay, estuarine, or marsh environment).

Unit VI (284.9–464.05 mbsf)

Interval 122-760B-6R-2, 40 cm to -25R-1, 55 cm.

Unit VI consists of interbedded carbonates and siliciclastic sedimentary rocks, is 178.65 m thick, and is Norian-Carnian (late Triassic) in age. The Norian/Carnian boundary was placed in the lower part the unit, between Cores 122-760B-18R and -19R (see "Biostratigraphy," this chapter).

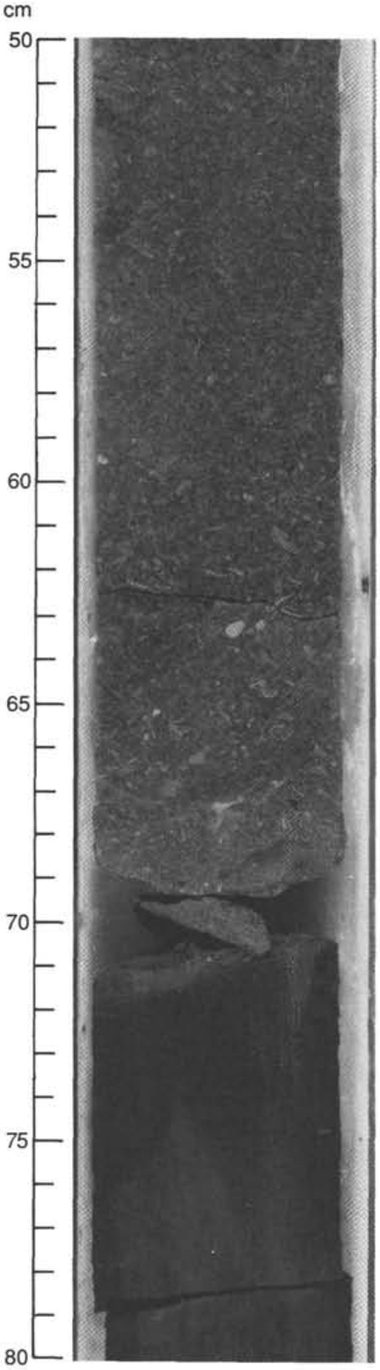

Figure 13. Interval 122-760B-17R-2, 50–80 cm. Silty claystone and interbedded carbonate grainstone of Unit VI. The silty claystone is structureless and moderately bioturbated. The carbonate grainstone interbed is normally graded with a slightly erosional base and mainly consists of peloids, molluscan shells, algae, and intraclasts.

The lithologies in Unit VI include dark gray (5Y 4/1) clayey siltstones, black (N2) silty claystones, and gray (2.5Y 7/2) grainstones, wackestones, carbonate mudstones, and quartz-rich silty sandstones. The clayey siltstones and silty claystones are volumetrically the dominant fraction, and are interbedded with the fossiliferous limestones and quartz-rich silty sandstone layers (e.g., Interval 122-760B-17R-2, 50–80 cm; Fig. 13).

Mineralogically, the clayey siltstones and silty claystones have been described in Unit IV and at Site 759. The suite of fossiliferous limestones (grainstones, packstones, wackestones, and mudstones) is very similar to that described at Site 759. At Site 760, carbonate rocks are abundant in three discrete intervals: Cores 122-760B-6R to -9R, Cores 122-760B-14R to -17R, and Cores 122-760B-20R to -24R (see Fig. 5). Limestone fragments found at the top of Core 122-760B-19R are considered to be contamination from overlying limestones that fell into the hole.

Major components easily recognized in the carbonate grainstones, wackestones, and packstones are peloids (including oolites and oncolites), bioclasts (e.g., mollusk and echinoderm fragments, scleractinian corals, and algae such as dasycladaceans; Interval 122-760B-21R-1, 100–150 cm; see Fig. 14), and intraclasts.

Microscope study suggests that some of the intraclasts are volcanic in origin and are andesitic or rhyolitic in composition. Micritic envelopes surround many bioclasts and intraclasts, evidence of the work of boring algae and bacteria. Glauconite and minor amounts of pyrite also occur in some of the fossiliferous limestones. Micrite is the dominant constituent between grains in the wackestones and packstones, and micritic ghosts in some grainstones suggest that neomorphic sparite is present.

Many of the carbonate rocks contain a high percentage of secondary dolomite. Overly close packing and sheltering effects were also observed within the packstones and grainstones. Many of the bioclastic limestones show graded bedding and cross-laminations, suggesting that they were current deposited. As an illustration of the microfacies diversity, Sample 122-760B-8R-2, 18–21 cm, (303.7 mbsf) is a foraminifer algal pelmicrite. Sample 122-760B-17R-2, 15–17 cm (389.2 mbsf) is a quartz-bearing algal oolitic-oncolitic pelsparite (grainstone) with reworked altered volcanic rock fragments, calc-alkaline in composition. Lastly, Sample 122-760B-20R-CC (425 mbsf), is a bioclastic algal mollusk grainstone to mudstone. It is apparent from this cursory discussion that the carbonate rocks at Sites 760 and 759 were deposited under diversified marine conditions and a detailed microfacies analysis is needed.

Throughout most of Unit VI many small ripples, cross-beds, and parallel laminations were observed in all of the lithologies, indicating current action. In addition, many areas are intensely bioturbated, containing well-preserved vertical burrows. Dewatering structures (Fig. 15) and other structures derived from soft-sediment deformation (e.g., flame structures, convolute laminations, and load casts) are present.

Minor occurrences of coal were found in Core 122-760B-14R, Sections 122-760B-19R-3 and 19R-4, and Core 122-760B-22R (Fig. 16). Some "rootlets" and/or algal filaments occur above and below these thin coal layers and seams. The silty sandstones associated with the coal appear matted and are poorly sorted. Pyrite was observed from Cores 122-760B-7R through -22R (Figs. 12 and 16) mainly in the form of pyritized burrows and nodules. Where present, palynomorph assemblages from Unit VI sediments reflect largely nonmarine to restricted-marine influences (see "Biostratigraphy," this chapter).

The above features and lithologies suggest deposition in a marginal-marine environment, in the vicinity of interfingering siliciclastic and shallow-water carbonate deposystems. The siliciclastic sediments were largely current deposited, and were subjected to bioturbation; the carbonates contain peloidal (oolitic-oncolitic) and bioclastic (algal-molluscan-foraminifer) components derived from a shallow- to marginal-marine environment. A more detailed environmental interpretation will follow from further shore-based studies.

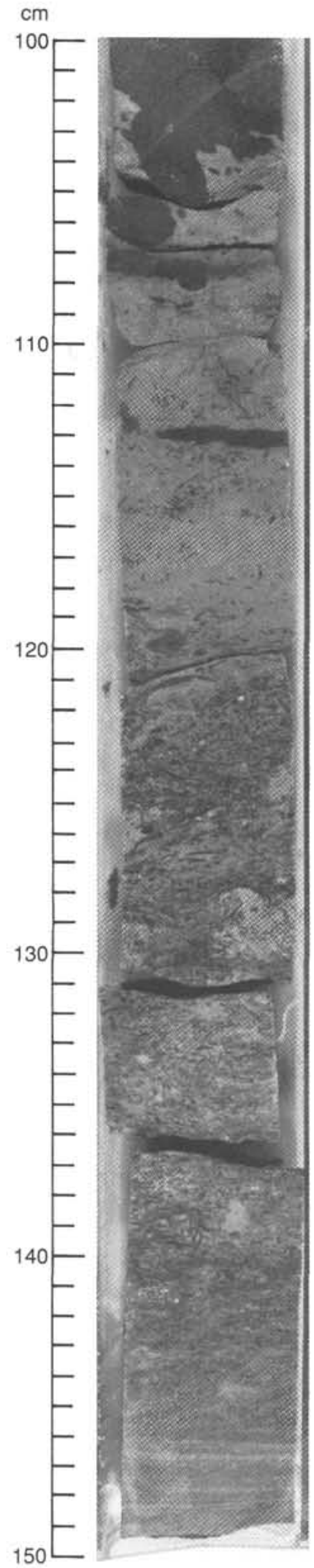

Figure 14. Interval 122-760B-21R-1, 100–150 cm. Carbonate packstone of Unit VI. Dasycladacean algae are typically observed, together with many peloids and molluscan shell fragments. This packstone is generally massive but includes minor cross- and parallel laminations at the base.

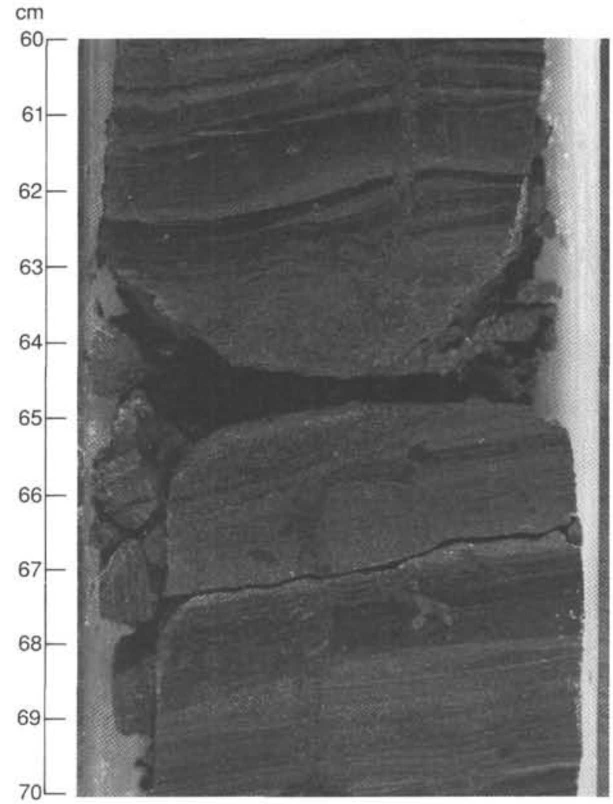

Figure 15. Interval 122-760B-22R-3, 60–70 cm. Dewatering structures in parallel laminated silty claystones of Unit VI.

Unit VII (464.05–506.0 mbsf)

Interval 122-760B-25R-1, 55 cm, through -29R-CC.

Unit VII is a siliciclastic sequence of rocks that has a stratigraphic thickness of 41.95 m, and has been defined as Carnian (late Triassic). Black (N2/4) silty claystone, dark gray (5Y4/1) clayey siltstone, and dark greenish gray (10Y5/2) silty sandstone are the dominant lithologies. The silty claystone, clayey siltstone, and silty sandstone are interlaminated and interbedded. Coarser-grained rocks are more abundant towards the bottom of the unit, suggesting a general upward-fining trend.

Mineralogically, these rocks are similar to the overlying silty claystone, clayey siltstone, and silty sandstone of Units IV–VI. The clayey siltstone contains parallel laminations, many of which are "sideritic." The frequency of these sideritic layers (and also of sideritic nodules) increases with depth in the unit. Within the small channel deposits (e.g., Core 122-760B-29R) are many graded intervals. Structures produced by soft-sediment deformation are also common in the lower portion of the unit (Core 122-760B-28R) and include small slumps and synsedimentary faults. The only fossil fragments observed in hand specimen are mollusk shells found in Core 122-760B-29R. Pyrite is common toward the bottom of the unit; small pyrite nodules were observed in Cores 122-760B-27R through -29R. Biogenic sedimentary structures are moderately to poorly preserved (Fig. 6).

The sediments of Unit VII could have been deposited either in a distal prodelta setting, or in a protected shallow water setting (i.e., tidal flat, estuarine or back bay). Energy conditions were generally lower for this unit than for the overlying Unit VI. Chemically reducing conditions were present at least locally in the sediment column, giving rise to siderite intervals.

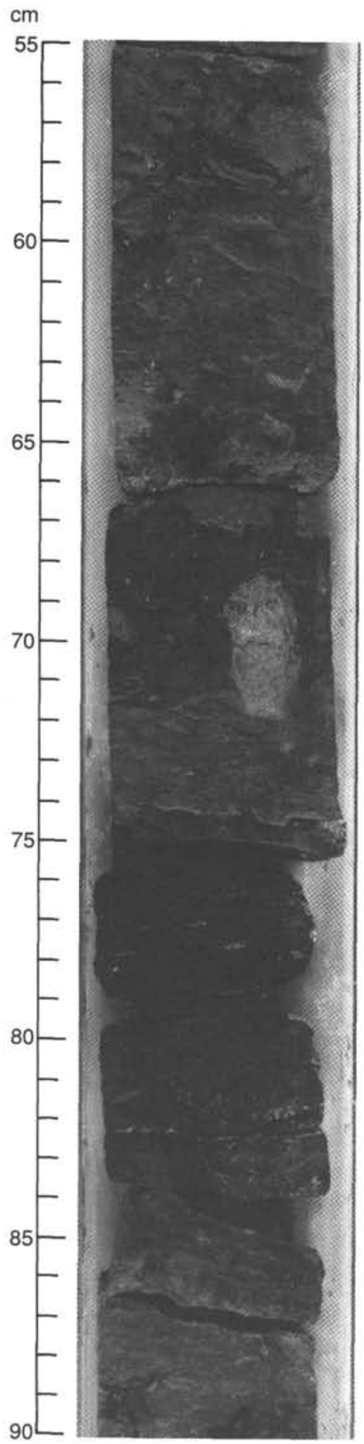

Figure 16. Interval 122-760B-22R-2, 55–90 cm. A coal layer (75–80 cm) and coal fragments (80–90 cm) are intercalated in moderately bioturbated sandy siltstone of Unit VI. The sandy siltstones also contain some algal stringers and rootlet profiles. Some burrows are filled with pyrite.

Triassic Lithostratigraphy and Sedimentologic History of Sites 759 and 760

The alternative hypotheses discussed in the following paragraphs regarding the Triassic lithostratigraphy and sedimentologic history of Sites 759 and 760 were derived from preliminary data and reflect the differing viewpoints of the shipboard sedimentologists.

We agree as to the general suite of environments in which the Triassic sediments accumulated (see Table 2, this chapter; and Table 2, Site 759 chapter, this volume). The sediments of most open-marine nature (prodelta) are at the bottom of Site 759 (Unit V). The remainder of the Triassic sediments at Site 759 (Units IV and III) represent alternating paralic claystones and neritic limestones (delta plain). Triassic paralic claystones and neritic limestones are present throughout Site 760 (Units VII–V), except for parts of Unit IV where subaerial exposure and soil-profile development occurred (as determined by facies analysis). These soil horizons underlie the major angular unconformity (late Eocene to late Triassic) observed on seismic records.

However, we differ in opinion as to whether the two sites overlap in part, or whether there is a gap between repeating sedimentary cycles (with all the Triassic sediments of Site 760 thereby younger than those of Site 759).

The evidence for overlap of the two sites is as follows:

1. Preliminary biostratigraphy suggests that the ages at the bottom of Hole 760B overlap with the ages at Site 759, and that Core 122-759B-14R-CC correlates with Core 122-760B-17R-CC.
2. Both sites contain similar sedimentary cycles of siliciclastic sediments and limestones.
3. There is a preliminary match between some of the limestone units at the two sites.
4. The seismic profiles suggest at first examination that there is no overlap. However, there are structural complexities in that Site 760 is on a small upthrown fault block (horst), and that the reflectors vanish in diffractions in the southern fault-scarp of the southern Wombat Plateau, which could hide a major fault between the two holes. It is therefore possible that these faults complicate the obvious seismic correlation. Thus, the possibility of overlap between the two sites is dependent in part on subjective seismic-reflector interpretation.

The evidence for a gap between the two sites is as follows:

1. Preliminary petrographic examination of limestones and siliciclastic sediments indicates the existence of very complex microfacies relations that change vertically on the scale of centimeters. Such vertical facies changes must represent equivalent lateral variations (Walther's Law). Thus there is no reason to suggest that the sediments should correlate in detail.
2. Closer examination of the sequences in which different lithologies are observed indicates that they are acyclic in stratigraphic position. A good example of this is the sediments above and below the observed coal seams and coal layers. The order of appearance is not predictable, suggesting a complex, migrating, and fluctuating environment, or the resedimentation of the carbonate beds into a siliciclastic system.
3. The most obvious seismic interpretation is that the base of Hole 760B is about 50 m above the top of the Triassic section in Hole 759A. The fault offset at the horst is not enough to cause overlap in the holes.
4. The paleontological ages are very preliminary and the presence of unconformities still has to be confirmed.

Whether or not the two sites overlap does not significantly influence the sedimentological interpretation. Large sedimentary cycles are evident within the Triassic on the Wombat Plateau. These clearly are complex and represent fluctuating nearshore marine and deltaic environments.

Opinions also differ as to the environments and geological settings responsible for producing these sedimentary sequences. Preliminary shipboard analysis suggested two alternative hypotheses (Figs. 17–19); both scenarios draw on regional background information indicating that during the Late Triassic, deposition was largely fluviatile on what is the present-day northwest Australian shelf, fluviodeltaic to the north, and restricted distal deltaic to the south of Sites 759 and 760. Areas of shallow-water carbonate banks provided a source for carbonate detritus interbedded with siliciclastic sediments (Cook, Smyth, and Vos, 1985).

Scenario 1: Marine Transgression-Regression Model[3]

Triassic rocks encountered at Site 760 can be divided into two major depositional sequences separated by an inferred regional unconformity (Fig. 17). Each sequence represents a deltaic environment; the younger depositional sequence (DS-2) begins at the unconformity with a shallow marine carbonate unit, representing the marine transgression that occurred after the erosion of the upper part of the older depositional sequence (DS-1).

Depositional Sequence 1 (DS-1)

This sequence consists of siltstones and claystones with some sandstone and carbonate interbeds. Fine laminations, micro-cross-laminations, grading, and bioturbation are the most common sedimentary structures in these sediments (Figs. 6 and 17). Shell fragments and pyrite are present. A coal seam occurs in Core 122-760B-22R. The carbonates are generally carbonate mudstones and wackestones; where interbedded with the fine-grained clastic sediments (which in turn are laminated and micro-cross-laminated) there are sharp contacts.

Sequence DS-1 probably represents the proximal part of a prodelta environment. The overlying part of the sequence (including the distributary-mouth-bar sequence and the bay fill deposits) were possibly eroded; this is suggested by the unconformity, marked by a questionable basal conglomerate (pebbles in the top of Core 122-760B-19R probably represent downhole contamination) and a tentative age gap (Fig. 17). Evidence for a prodelta environment includes parallel color bands in claystone, thin graded silt and silty clay, parallel laminations, bioturbation, and the remnants of a shallow marine fauna. The silts and clays were apparently deposited from suspension in the prodelta environment whereas the sandstones probably formed in the distal parts of the distributary-mouth-bar of the delta. The carbonate material may have been derived from an adjacent carbonate platform and transported to the site.

Depositional Sequence 2 (DS-2)

Sequence DS-2 commences with a carbonate-cemented conglomeratic sandstone, finer-grained clastics, and a coal seam (Fig. 17). The basal clastics are succeeded by shallow-marine carbonates (Cores 122-760B-14R to -18R) ranging in texture from carbonate wackestone to grainstone. They include fragments of marine organisms such as mollusks, echinoderms, and corals, as well as oolites, peloids, and intraclasts. Pyrite is a common diagenetic mineral in the carbonates. These carbonates probably mark a transgression after a major erosional event that followed the deposition of sequence DS-1.

Soon after the marine transgression, deltaic conditions prevailed and prodeltaic sediments were deposited on top of the shallow-water carbonates, followed by distributary-mouth-bar and bay-fill deposits of sequence DS-2. Alternations of siltstone, silty claystone, sandstone, and limestone in Cores 122-760B-13R through -29X represent the prodelta environment of DS-2. Parallel laminations, micro-cross-laminations, grading, and bioturbation are common features, and the presence of glauconite and marine shell fragments support the prodelta interpretation.

Progressing upward from the prodelta sequence to the distributary-mouth-bar deposits, the amount and thickness of the sandstones increase, marine fossils are more scarce, and plant debris first occurs (i.e., Cores 122-760A-29X to -19X. Sedimentary structures (e.g., small-scale laminae, ripples, and graded sand units) are much more common in this relatively shallow-water depositional environment.

The uppermost part of sequence DS-2 (Core 122-760A-18X to the unconformity capping the Triassic rocks) represents the bay-fill deposits of the delta, and is characterized by alternating silts and silty clays, and thin layers of sandstone with plant debris and siderite nodules.

Comparison of Sites 759 and 760 shows that the carbonate rocks encountered at Hole 759B (Cores 122-759B-7R to -16R) appear to be very similar in lithology and stratigraphy to those found at Site 760 (Cores 122-760B-14R to -17R), suggesting that the Triassic rocks of the two sites may correlate in part. Sequence DS-2 (Site 760) may have developed at Site 759 above the shallow-water carbonates, but was largely removed by pre-early Miocene erosion and thus only the lowermost part of its prodelta sediments were preserved. Preliminary paleontological data indicates that sequence DS-1 (Site 760) is younger than the rock package underlying the shallow marine carbonates at Site 759; it thus may represent the upper part of the package, although they appear to be very similar in succession.

Scenario 2: Migrating Delta-Lobe Model (Static Sea Level)[4]

The environments associated with deltas are complex. For simplicity, we divide the deltaic complex into three zones: (1) the *prodelta environment* (that part of the delta below the effective depth of wave erosion, lying beyond the delta front); (2) the *delta front* (the zone that includes the shoreline and seaward-dipping profile extending offshore); and (3) the *delta plain* (the area behind the delta front, characterized by active and abandoned distributary channels separated by shallow-water environments and emergent or near-emergent surfaces).

The lowermost sediments at Hole 759B are a prodelta facies, consisting of well-bedded silty claystones with marine coccoliths, some radiolarians, and evidence of small-scale sediment gravity flows. The remainder of the Triassic sediments at Site 759 (and those found at Site 760) are closely analogous with modern-day delta-plain environments. These environments include distributary channels, back bays, tidal flats, swamps, marshes, and subaerially exposed soils. All of the environments are recognized from the sediments described at Sites 759 and 760. However, there is disagreement over the existence of an unconformity between Cores 122-759A-16R and -17R, and its correlation to a conglomerate

[3] Shore-based studies indicate that Scenario 2 is more likely than Scenario 1.

[4] As previously noted, shore based studies indicate that Scenario 2 is more likely than Scenario 1.

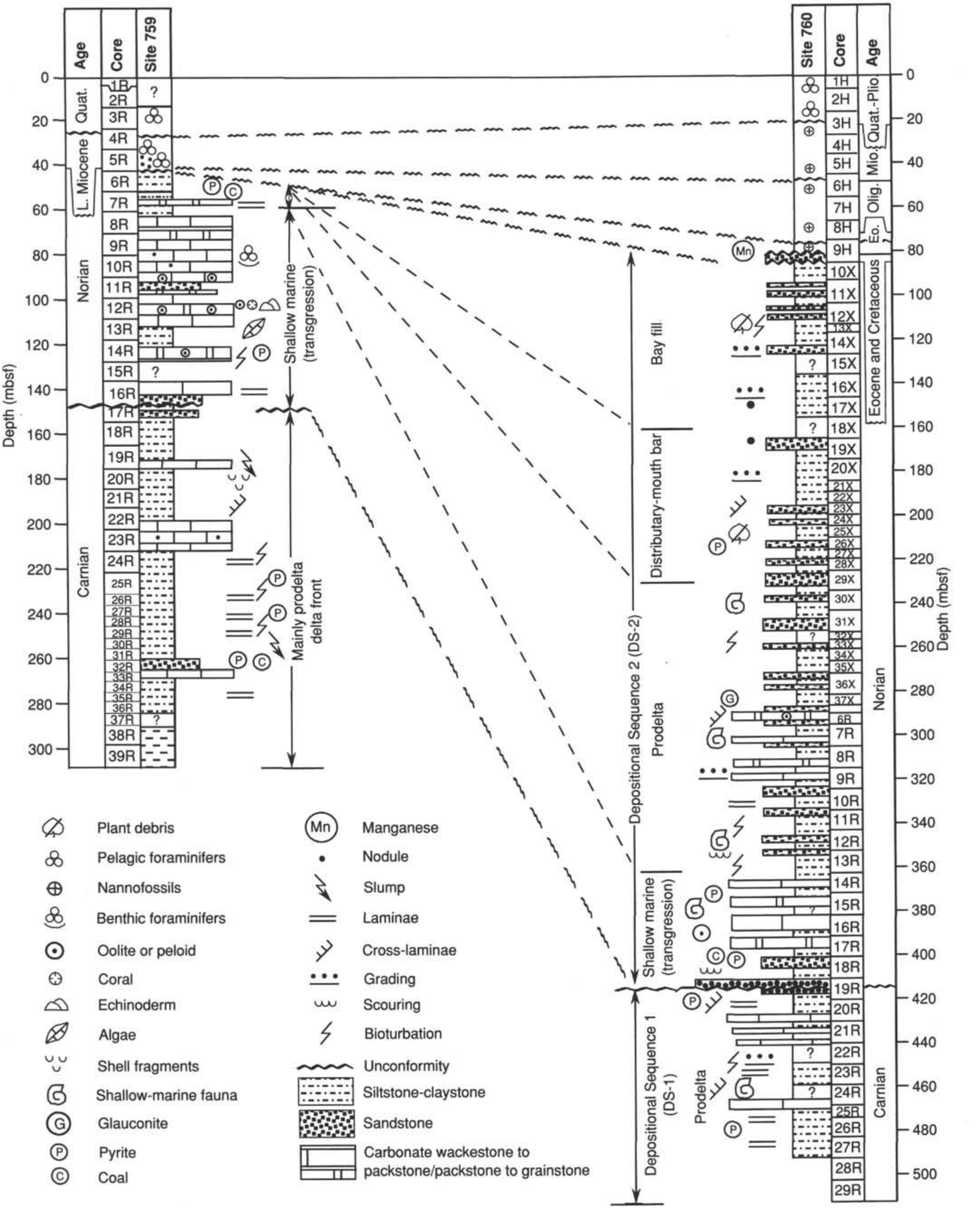

Figure 17. Depositional environments and correlation of Site 759 and 760. This is a tentative shipboard correlation that will be modified by more detailed shore-based studies.

(possibly downhole contamination) that overlies the equivalent unconformity at Hole 760B.

An alternative model for the formation of the complex facies relationships observed at Sites 759 and 760 is that they are analogous to the formation and areal distribution of the delta complexes and lobes in the pre-modern and modern Mississippi delta (Fig. 18A). Four major pre-modern delta complexes comprising 15 lobes have been recognized (Frazier, 1967). Channel switching causes the pre-existing delta lobe to be abandoned and a new delta lobe to be initiated elsewhere. Sediment supply to the formerly active delta diminishes and it ceases to prograde. Basinal processes (e.g., wave and current action) are enhanced in the absence of sediment supply, and local reworking, compaction, and subsidence continue. Post-abandonment modifications are analogous to many of the environments observed at Sites 759 and 760 (Fig. 18B). Clayey silts, sands, coquinas, oyster beds, swamps, tidal flats, and carbonaceous sediments can be attributed to lateral migration of a delta-lobe complex rather than to sea-level fluctuation.

The observed interbedded limestone deposits can easily fit into the migrating delta-lobe model. Normal marine conditions (under which carbonate sediments could accumulate) prevail in the areas away from the active delta plain or lobe. With time, the active lobe is abandoned and a new lobe forms, burying the carbonates. Subsidence of the abandoned lobe could produce an environment suitable for carbonate formation. The depocenter of delta-plain sediments alternating with carbonates could migrate back and forth with time. Carbonates preserved on one lobe would correlate laterally to delta-plain sediments that formed at the same time on an adjacent lobe, and vice versa; thus sediments of similar composition need not laterally correlate in detail (Fig. 19).

BIOSTRATIGRAPHY

Introduction

Holes 760A and 760B were drilled approximately 5 km northeast of Site 759 in order to obtain a more complete stratigraphic section. Calcareous nannofossils and planktonic foraminifers provided accurate age dating for the upper pelagic carbonate part of the section, down to Core 122-760A-9H (see Fig. 20 and Table 3 for summaries of nannofossil and foraminifer biostratigraphic results, respectively). We used palynomorphs to date the upper Triassic section in both holes as Norian and Carnian. Both the Norian and the Carnian intervals yielded calcareous nannofossil assemblages. The Carnian microflora is the oldest yet reported. Very few radiolarians were recovered at Site 760.

Calcareous Nannofossils

Occurrence and Preservation

The upper eight cores from Hole 760A contain abundant, well-preserved Cenozoic calcareous nannofossils. The upper part of Core 122-760A-9H also contains well-preserved nannofossils, but in the lower part of this core the preservation is much poorer. Cores 122-760A-10H to -34X are barren of nannofossils. Cores 122-760A-35X to -37X and 122-760B-25R to -29R contain variably abundant but predominantly poorly preserved Triassic nannofossils. Core 122-760A-38X is barren; Cores 122-760B-2R to -24R are also barren.

Cenozoic Biostratigraphy

The high diversity of nannofossil species in the upper part of Hole 760A allows the high-resolution zonation of Martini (1971) to be applied. In several cores, however, the primary zonal markers are absent and we have relied on secondary markers (see Martini, 1971; Perch-Nielsen, 1985) for correlation to the Martini zonal scheme.

The interval from Sample 122-760A-1H-1, 100–101 cm, to -1H-4, 100–102 cm, is Quaternary in age. The co-occurrence of *Gephyrocapsa oceanica* and *Emiliania huxleyi* and the absence of *Pseudoemiliania lacunosa* indicate a mixed NN20–NN21 assemblage. The interval from Sample 122-760A-1H-5, 100–101 cm, through -2H-6, 88–90 cm, was assigned to NN19, given that *Pseudoemiliania lacunosa* occurs but indigenous discoasters do not.

Sample 122-760A-2H-7, 29–31 cm, belongs in Zone NN16, as indicated by the co-occurrence of *Pseudoemiliania lacunosa* and *Discoaster surculus*. Sample 122-760A-2H-CC is, however, in Zone NN11, as indicated by *Discoaster quinqueramus*.

Samples 122-760A-3H-1, 30–32 cm, to -3H-3, 30–32 cm, are also in Zone NN16, given that *P. lacunosa* and *D. surculus* both occur, suggesting that sediment slumped from higher up in the hole was redrilled. Samples 122-760A-3H-4, 30–31 cm, and -3H-5, 30–32 cm, also belong in NN11 because *Reticulofenestra umbilica* and *Discoaster neohamatus* both occur. The sequence passes into Zone NN10 in Core 122-760A-3H-6, 63–65 cm, as indicated by the presence of *Catinaster calyculus* and *Discoaster bellus*, and the absence of *D. hamatus* and *D. quinqueramus*. *Discoaster hamatus* appears in Sample 122-760A-3H-7, 71–73 cm, and -3H-CC, indicating Zone NN9.

The interval from Sample 122-760A-4H-2, 90–92 cm, to -4H-3, 90–92 cm, is in Zone NN8, given that *Catinaster coalitus* occurs but *Discoaster hamatus* does not. Sample 122-760A-4H-4, 90–92 cm, contains rare *D.* cf. *D. kugleri* and lacks *Catinaster coalitus* and *Cyclicargolithus floridanus*; therefore, we tentatively place it in Zone NN7. Samples 122-760A-4H-6, 90–92 cm, to -5H-1, 30–31 cm, are assigned to Zone NN6, given the co-occurrence of *Cyclicargolithus floridanus* and *Discoaster braarudii*, and the absence of *Sphenolithus heteromorphus*.

We first noted *Sphenolithus heteromorphus* in Sample 122-760A-5H-2, 30–32 cm; it occurs with *Discoaster druggii*, thus indicating Zone NN5. Species indicative of Zone NN5 also occur from Samples 122-760A-5H-4, 30–32 cm, to -5H-6, 30–32 cm. We did not find *Helicosphaera ampliaperta* (always a rare species) in this interval, and thus could not identify Zone NN4 with certainty. The co-occurrence of *Sphenolithus heteromorphus* and *S. belemnos* in Sample 122-760A-5H-CC indicates Zone NN3. Sample 122-760A-6H-1, 13–15 cm, also lies within Zone NN3. *Triquetrorhabdulus carinatus* and *Discoaster druggii* occur together from Sample 122-760A-6H-2, 30–32 cm, to -6H-CC, indicating Zone NN2.

Sample 122-760A-7H-1, 30–32 cm, belongs in Zone NN1, as *T. carinatus* is abundant and *D. druggii* and *Sphenolithus ciperoensis* do not occur. We assign Samples 122-760A-7H-2, 30–32 cm, to -7H-5, 30–32 cm, to Zone NP25 on the basis of *Sphenolithus ciperoensis* being present and *S. distentus* and *S. predistentus* being absent. Samples 122-760A-7H-6, 30–32 cm, to -7H-CC belong in Zone NP24, as indicated by the co-occurrence of *S. ciperoensis*, *S. distentus*, and *S. predistentus*.

Sample 122-760A-8H-1, 30–32 cm, consists of redrilled sediment slumped downward from Zone NP25. Sample 122-760A-8H-2, 30–32 cm, is in NP23, as indicated by the absence of the zonal boundary species, *Reticulofenestra umbilica* and *Sphenolithus ciperoensis*, and the presence of *S. pseudoradians*. Samples 122-760A-8H-3, 30–32 cm, and -8H-4, 4–6 cm, also belong in Zone NP23, because *Reticulofenestra umbilica*, *Cyclococcolithus formosus*, *Discoaster saipanen-*

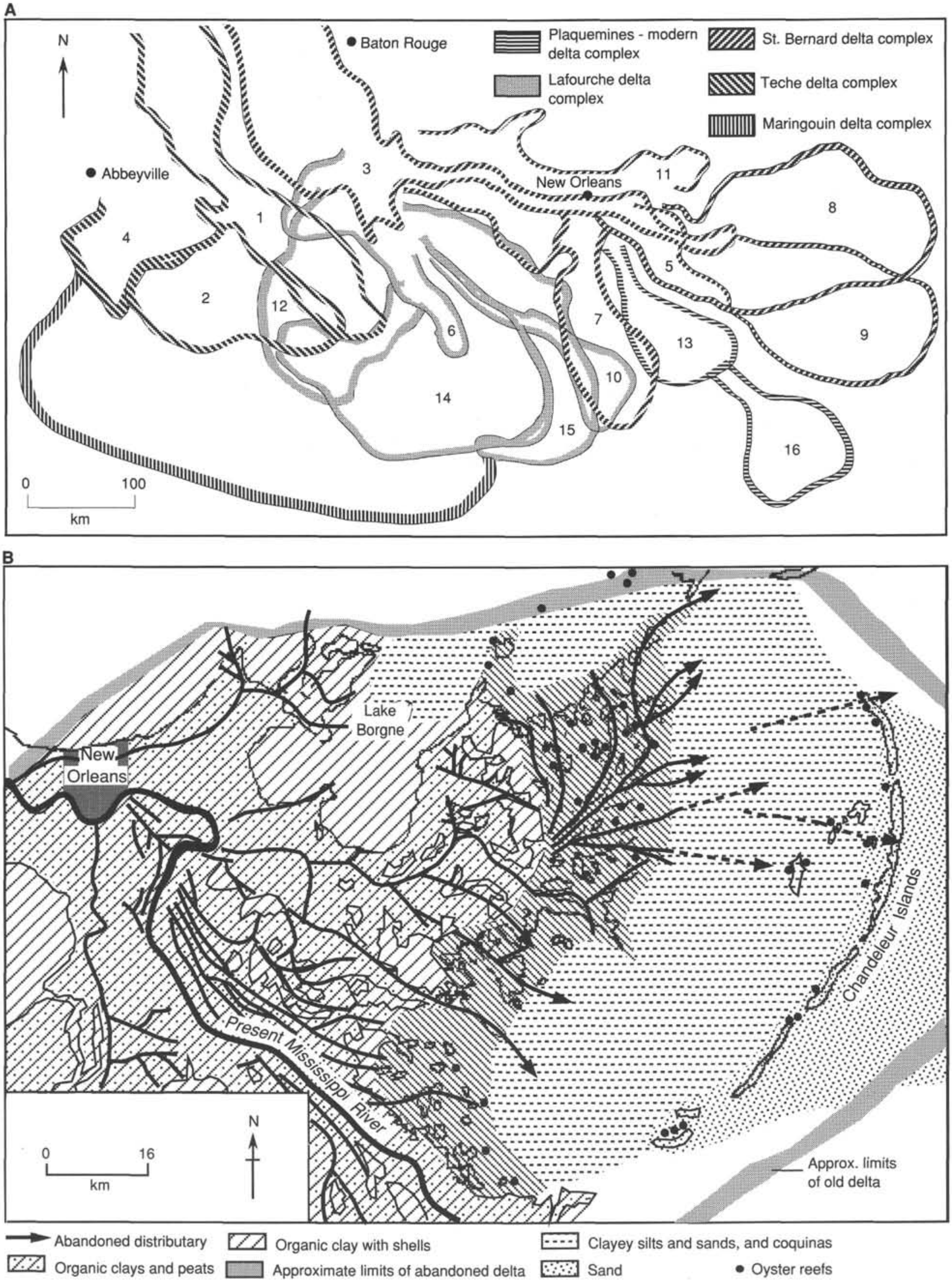

Figure 18. **A.** Areal distribution of pre-modern and modern delta complexes and lobes, Mississippi delta. Numbers in delta-lobe complexes show progression from youngest (1) to oldest (16) (after Frazier, 1967, and Fisher et al., 1969). **B.** Abandoned St. Bernard Lobe of pre-modern Mississippi delta, and post-abandonment modifications (after Coleman and Gagliano, 1964).

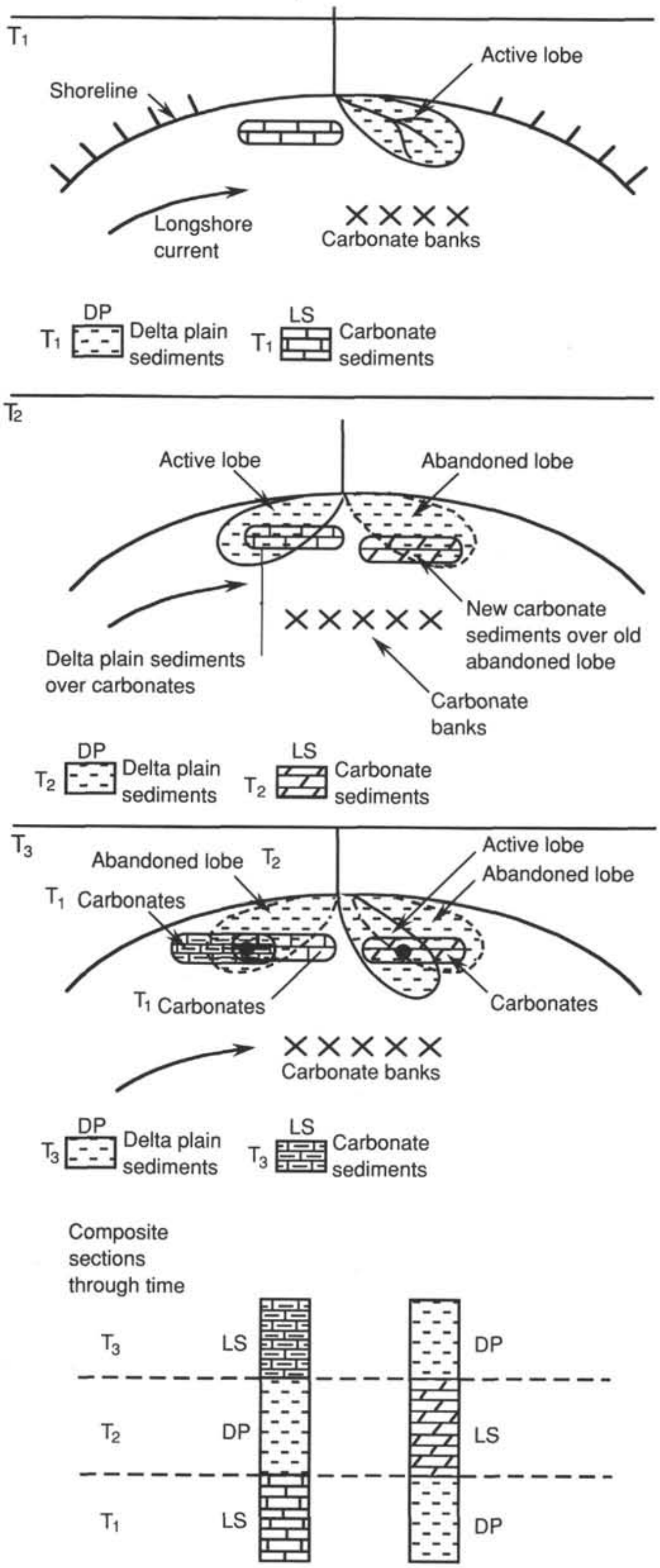

Figure 19. Formation of alternating sediment sequences by a laterally migrating delta-lobe complex. T_1 = time 1, T_2 = time 2, T_3 = time 3, DP = delta plain sediments, LS = carbonate sediments.

Core-section (122-760A-)	Nannofossil Zone	Series
1H -1 to 1H-4	NN20-21	Holocene and upper Pleistocene
1H-5 to 2H-6	NN19	lower Pleistocene
2H-7	NN16	upper Pliocene
2H-CC	NN11	upper Miocene
3H-1 to 3H-3	NN16	upper Pliocene
3H-4 to 3H-5	NN11	upper Miocene
3H-6	NN10	
3H-7 to 3H-CC	NN9	
4H-1 to 4H-3	NN8	
4H-4 to 4H-5	NN7	middle Miocene
4H-6 to 5H-1	NN6	
5H-2 to 5H-6	NN5	
		? ? ?
5H-CC to 6H-1	NN3	lower Miocene
6H-2 to 6H-CC	NN2	
7H-1	NN1	
7H-2 to 7H-5	NP25	upper Oligocene
7H-6 to 8H-1	NP24	
8H-2 to 8H-4	NP23	lower Oligocene
8H-4 to 9H-1	NP20	upper Eocene
9H-2 to 9H-4	???	lower-Middle Eocene
9H-5 to 9H-6	NP10-11 and NC?	lower Eocene and Cretaceous

Figure 20. Cenozoic calcareous nannofossil biostratigraphy, Hole 760A. Wavy lines indicate hiatuses. Dot-and-dash lines indicate possibly redrilled slumped material.

sis, and *D. barbadiensis* occur and *Sphenolithus pseudoradians* does not. Sample 122-760A-8H-4, 136–138 cm, belongs in Zone NP20 given that *Discoaster saipanensis* occurs and that *Ericsonia formosa* and *Reticulofenestra umbilica* are common. Zone NP20 continues downward to Sample 122-760A-8H-CC, and into Sample 122-760A-9H-1, 14–16 cm.

The interval from Sample 122-760A-9H-2, 28–30 cm, to -9H-4, 30–32 cm, contains poorly preserved lower to middle Eocene nannofossils, and Section 122-760A-9H-5 contains

Table 3. Planktonic foraminifer zonal boundaries identified at Site 760.

Core, section, interval (cm)	Zone	Age
122-760A-		
1H-CC to 2H-6, 88–90	N22	Pleistocene
2H-7, 20–22 to 3H-3, 29–31	N21–N19	Pliocene
3H-4, 80–82 to 3H-CC	N17A	Late Miocene
4H-CC	N13	late Middle Miocene
5H-1, 30–32 to 5H-4, 30–32	N12–N9	Middle Miocene
5H-5, 30–32 to 5H-CC	N8	late Early Miocene
6H-1, 13–15 to 6H-2, 30–32	N8?–N6?	Early Miocene
6H-3, 30–32 to 6H-4, 30–32	N4B	Early Miocene
6H-5, 30–32 to 7H-1, 30–32	N4A	Late Oligocene
7H-2, 30–32 to 7H-CC	P22–P21	Late Oligocene
8H-1, 30–32 to 8H-3, 30–32	P20–P19	Early Oligocene
8H-4, 4–6	P18	Early Oligocene
8H-4, 136–138 to 9H-5, 34–36	P17–P16	Late Eocene
8H-5, 30–32 to 9H-5, 34–36	Not zoned	Eocene to Santonian
9H-6, 34–36 to	Barren	Indeterminate
122-760B-		
6R-CC		
7R-CC to 14R-3, 20–22	Not zoned	Carnian

mixed lower Eocene and upper Cretaceous nannofossils. *Fasciculithus typmpaniformis* and *Discoaster multiradiatus* occurring together in Section 122-760A-9H-5, 34–36 cm, suggest Zones NP10 to NP11.

Hiatuses occur in the upper Pliocene (between Zones NN16 and NN19) and in the lower Oligocene (between Zones NP20 and NP23; see Fig. 20). A hiatus is tentatively indicated between Zones NN3 and NN5, but as mentioned in the preceding discussion, the marker species for NN4 is always rare and study of additional samples may show that this zone is present.

Mesozoic Biostratigraphy—Triassic

Triassic nannofossils were found in Sections 122-760A-35X-CC to -37X-CC, and in Samples 122-760B-25R-CC to -28R-CC. Assemblages observed at the base of Hole 760A were composed largely of a small form classified as *Tetralithus* sp. A more diverse assemblage was observed at the base of Hole 760B consisting of *Hayococcus floralis, Tetralithus* sp., and several other undescribed forms. Nannofossils from Hole 760A appear to be composed predominantly of calcite; however, most specimens observed from Hole 760B appear to have been replaced by siderite. None of the observed forms have been described in Jurassic or younger rocks, and the fossils therefore appear to be Triassic in age. Comparison of the assemblages recovered from the bases of Holes 759B, 760A, and 760B may yield some relative age information that can be compared with ages given by other microfossil groups. The assemblages from Holes 759B and 760A are completely different, whereas those at Hole 760B are a mixture of the two end-members. This may indicate that the sediments recovered at the base of Hole 760B are intermediate in age to those recovered at the base of the other two holes. Alternatively, the higher-diversity assemblage in Hole 760B may be a result of favorable preservation.

Foraminifers

Occurrence and Preservation

The upper nine cores in Hole 760A yielded abundant, well-preserved, low-latitude planktonic foraminiferal faunas. In the lower part of Core 122-760A-9H, abundance and preservation deteriorate and the bottom section (Section 122-760A-9H-6) is barren of foraminifers. All samples from the underlying sediments of Hole 760A proved to be barren of foraminifers. Results are summarized in Table 3.

A few samples from Hole 760B yielded sparse but well-preserved foraminiferal faunas, all of late Triassic age.

Cenozoic Biostratigraphy

The Cenozoic (down to and including Samples 122-760A-9H-5, 34–36 cm) yielded rich and diverse planktonic foraminiferal faunas of fully tropical character. Although virtually all Cenozoic ages younger than Paleocene are represented, there are several hiatuses that reduce the total thickness and average sedimentation rates. Nevertheless, the sediments do not bear much evidence of condensation resulting from dissolution or low primary productivity.

Neogene

The consistent presence of *Globorotalia truncatulinoides* down to and including Sample 122-760A-2H-6, 88–90 cm, indicates a Pleistocene age (Zone N22).

Pliocene ages were obtained from the assemblages from Sample 122-760A-2H-7, 20–22 cm (Zone N21, with *Globorotalia tosaensis*), down to Sample 122-760A-3H-3, 29–31 cm (Zone N19, with *Globorotalia tumida* and *Sphaeroidinella dehiscens*). There may be a stratigraphic break at the top of the Pliocene interval that is marked by the abrupt appearance of typical *G. tosaensis* assemblage without gradational forms to *G. truncatulinoides*.

Another stratigraphic break in the microfaunas was observed between Zone N19 and the highest Miocene (in Sample 122-760A-3H-4, 80–82 cm), which belongs to Zone N17A with its typical assemblage of *Globorotalia plesiotumida*, but without *G. tumida* and *Pulleniatina primalis*. It would thus appear that Zones N18 and N17B are missing. Zone N17A was recognized down to and including Sample 122-760A-3H-CC.

Core 122-760A-4H was not studied in detail. Sample 122-760A-4H-CC was dated as late Middle Miocene (Zone N13) on the presence of *Globorotalia fohsi robusta*. From the calcareous nannofossil data, it would appear that the Upper and uppermost Middle Miocene (Tortonian and upper Serravallian) are both complete, within the accuracy limits of biostratigraphic resolution.

The upper part of Core 122-760A-5H shows a rapid succession of Middle Miocene zones (from N11 or N12 down to N9) as indicated by the successive representatives of the *Globorotalia fohsi* group. Sample 122-760A-5H-4, 30–32 cm, is the lowest one to contain *Orbulina suturalis* and marks the base of Zone N9. The lower part of Core 122-760H-5H belongs to Zone N8 given that successive members of the *Globigerinoides sicanus-Praeorbulina* lineage of the latest Early Miocene are present.

Core 122-760A-6H is entirely early Miocene in age. The upper part of this core is difficult to date due to an apparent absence of zonal markers, but on the basis of calcareous nannofossil evidence it should correspond to Zones N5 to N6.

The simultaneous appearance of *Globorotalia kugleri* and *Globoquadrina binaiensis* in Sample 122-760A-6H-3, 30–32 cm, marks the top of Zone N4. The presence of *Globoquadrina dehiscens* and *Globigerinoides primordius* down to and including Sample 122-760A-6H-4, 30–32 cm, identifies the lower Miocene part of Zone N4 (i.e., Zone N4B).

Paleogene

The Oligocene is remarkably complete in Hole 760A. The Miocene/Oligocene boundary was placed within Zone N4, at the lowest occurrence of *Globoquadrina dehiscens* (in Sample

122-760A-6H-4, 30–32 cm). Below that, Core 122-760A-6H and Sample 122-760A-7H-1, 30–32 cm, contain both *Globoquadrina praedehiscens* and *Globigerinoides primordius*, indicating youngest Oligocene Zone N4A.

Further down, the zonation depends largely on the distinction between *Neogloboquadrina opima opima* and *Neogloboquadrina opima nana* for discrimination between Zones P22 and P21; this zonal boundary is present but could not be drawn accurately.

Sample 122-760A-7H-CC is the deepest to contain *Globigerina angulisuturalis* and marks the base of Zone P21.

From Sample 122-760A-8H-1, 30–32 cm, down to and including Sample 122-760H-8H-3, 30–32 cm, are combined Zones P20 and P19; this represents the first downhole evidence of early Oligocene (Rupelian); the top of the Rupelian may actually be slightly higher than the top of P19/20 according to Haq et al. (1987). The highest occurrence of *Pseudohastigerina* in Sample 122-760A-8H-4, 4–6 cm, marks the top of Zone P18 (earliest Oligocene).

The highest evidence of Eocene, with *Turborotalia cerroazulensis* (the typical, angular form *T. cerroazulensis cocoaensis*), and *Globigerapsis* spp. is found in Sample 122-760A-8H-4, 136–138 cm. In this sample, a variety of middle and late Eocene forms including *Morozovella spinulosa* and *Truncorotaloides topilensis* are also present. Down to the lowest sample with Eocene planktonics (i.e., Sample 122-760A-9H-5, 34–36 cm), mixed Late, Middle, and Early Eocene faunas occur, probably due to repeated mixing and winnowing in a deep-marine environment, although downhole contamination cannot be ruled out. Some Cretaceous forms were also found in this sample.

More detailed sampling of the Eocene interval is necessary in order to obtain a more complete record of *in-situ* and reworked elements.

Mesozoic Biostratigraphy

Cretaceous

As mentioned above, Sample 122-760A-9H-5, 34–36 cm, contains some Upper Cretaceous foraminifers. These include *Globotruncana linneiana*, indicating a Santonian to Maestrichtian age. It is possible, however, that this occurrence is due to reworking at the base of the Eocene section.

Triassic

No foraminifers were found in the Triassic part of the section in Hole 760A.

In Hole 760B, only a few washed samples yielded foraminifers. An age not older than late Norian can be assigned to a small assemblage in Sample 122-760B-8R-CC, including *Involutina liassica* or *Involutina turgida* (Zaninetti, 1976); the same form was also found in Sample 122-760B-14R-3, 20–22 cm, together with *Lingulina tenera* and *Eoguttulina* spp. These occurrences constrain the age of a monotypic assemblage of *Agathammina austroalpina* observed in a thin section of a limestone from higher in the section (Sample 122-760B-7R-CC), as well as the entire interval in between, to Norian or Rhaetian.

Lower in Hole 760B, thin sections of limestone samples were studied from limestones down to and including Sampie 122-760B-15R-1, 59–60 cm. Of these, Sample 122-760B-9R-2, 35–38 cm, contained the most age-diagnostic fauna, with *Glomospirella friedli* and *Trocholina permodiscoides*? occurring together, most probably indicating a Norian age.

Shore-based thin-section study of the Triassic limestones may provide the first foraminiferal biostratigraphy for the Norian and Carnian of this region.

Radiolarians

The sediments drilled from Hole 760A contain few radiolarians because of the unsuitable facies. Consequently, all samples had to be studied as wet-sieved residues instead of as strewn slides. Sample 122-760A-1H-CC, contains rare but fairly well-preserved Quaternary radiolarians assignable to either the *Amphirhopalum ypsilon* or *Anthrocyrtidium angulare* Zones of Sanfilippo et al. (1985). Characteristic taxa include *Axoprunum angelinum*, *Collosphaera huxleyi*, *Lamprocyrtis nigriniae*, *Phormostichoartus marylandicus*, spyrids (gen. et sp. indet.), *Stylacontarium acquilonium*, and *Stylatractus* sp. Faunal composition remains nearly unchanged down to Sample 122-760A-2H-5, 88–90 cm. Radiolarians are extremely rare and only fragmentary from Sample 122-760A-2H-CC to -6H-CC. Fragments of *Dorcadospyris* sp. were recovered in Sample 122-760A-7H-CC, indicating an age range of middle Miocene to early Oligocene. Rare specimens of *Podocyrtis trachoides* occur in Sample 122-760A-8H-7, 29–31 cm, and *Spongatractus pachystylus* occurs in 122-760A-8H-CC; both taxa indicate a middle to late Eocene age. Unfortunately, no radiolarians were recovered from Samples 122-760A-9H-CC to -37X-CC.

The sediments in Hole 760B are also largely devoid of radiolarians. Sample 122-760B-2R-CC is barren, but Sample 122-760B-3R-CC contains several twisted radiolarian spines as well as poorly preserved, three- and four-rayed radiolarians with outlines similar to the Jurassic genera *Pseudocrucella* and *Homeoparonaella*, respectively. Three- and four-rayed forms have been reported in Late Triassic (Norian) rocks in western North America (Blome, 1984), but are only abundant in latest Triassic (late Norian) and younger Jurassic strata, which suggests that the sediments in Sample 122-760B-3R-CC may be as young as Jurassic in age. No radiolarians were recovered from Samples 122-760B-4R-CC to -29R-CC. Rare, shallow-water ostracodes, mollusks, and coral fragments were recovered in Sample 122-760B-8R-CC. Ostracodes were also observed in Sample 122-760B-16R-CC. Carbonized wood fragments, plant cuticle, and megaspores were recovered from Samples 122-760B-2R-CC, -12R-CC, -13R-CC, -14R-CC, -17R-CC, -19R-CC, and -23R-CC.

Palynology

The upper ten cores in Hole 760A are barren of palynomorphs. The intervals from Core 122-760A-11H through -37X and from Core 122-760B-6R through -18R contain palynomorph assemblages of variable abundance and preservation. Both intervals are Norian in age and belong to the *Minutosaccus crenulatus* Zone (Dolby and Balme, 1976; Helby et al., 1987).

Most samples of the interval from Core 122-760B-19R through -29R contain a rich palynomorph assemblage with moderate to good preservation. The interval is Carnian in age (*Samaropollenites speciosus* Zone, Subunit B, according to Dolby and Balme, 1976) and is comparable with the interval below Sample 122-759B-20R, 60–64 cm, in Hole 759B.

Hole 760A

Sample 122-760A-11X-1, 82–85 cm, contains a diverse but moderately preserved palynoflora. The presence of *Minutosaccus crenulatus*, *Falcisporites australis*, *Samaropollenites speciosus*, and *Enzonalasporites vigens* indicates the *Minutosaccus crenulatus* Zone (Norian). Acritarchs and an undescribed species of the dinoflagellate genus *Dapcodinium* are abundant. The presence of only one dinoflagellate species in the assemblage points to a restricted-marine environment. The palynoflora of Sample 122-760A-11X-CC is dominated by terrestrial palynomorphs. The presence of the freshwater algae *Plaesiodictyon* and *Bartenia communis* and the absence of dinoflagellates indicate a nonmarine environment. All core-catcher samples from Cores 122-760A-12X through -19X are barren of palynomorphs.

Samples 122-760A-20X-CC, -21X-CC, and -22X-CC contain a nonmarine palynomorph assemblage, as recorded in Sample 122-760A-11X-CC. All core-catcher samples from Core 122-760A-23X through -25X are barren of palynomorphs. In contrast, Sample 122-760A-25X-2, 74–76 cm, contains acritarchs and a diverse dinoflagellate assemblage with *Suessia listeri*, *Suessia swabiana*, and *Shublikodinium* spp. The presence of dinoflagellates (specially of *Suessia* spp.) indicates marine conditions.

Samples 122-760A-26X-CC and -27X-CC contain a nonmarine palynomorph assemblage. Samples 122-760A-28X-CC and -29X-CC are barren. Sample 122-760A-30X-CC contains an assemblage indicative of unusual marine conditions similar to Sample 122-760A-11X-1, 82–85 cm. All core-catcher samples from Core 122-760A-31X through -36X contain a nonmarine palynomorph assemblage (except for the barren Sample 122-760A-34X-CC).

In Sample 122-760A-37X-CC, a diverse acritarch and dinoflagellate assemblage (with several species of *Shublikodinium* and an undescribed species of *Rhaetogonyaulax*) indicates marine conditions.

Hole 760B

The interval from Core 122-760B-6R through -18R contains a predominantly marginal marine palynomorph assemblage characterized by the presence of few dinoflagellate specimens of the *Shublikodinium/Heibergella* group, the "atypically marine" alga *Botryococcus* and the freshwater alga *Plaesiodictyon*. The assemblage of Samples 122-760B-6R-CC and -8R-1, 42–44 cm, points to a more restricted marine environment, indicated by the absence of dinoflagellates and the presence of few acritarchs and *Botryococcus*. Nonmarine conditions are reflected in Samples 122-760B-9R-1, 74–76 cm, -12R-CC, -14R-CC, and -17R-2, 74–77 cm. Samples 122-760B-11R-CC and -18R-CC are barren.

The interval from Sample 122-760B-19R-2, 76–78 cm, through -22R-4, 74–76 cm, is characterized by the dominance of cuticles and the abundant occurrence of *Plaesiodictyon*. Only few acritarchs and a small number of *Tasmanites* in Sample -21R-CC indicate a slight marine influence at the base of this interval.

From Sample 122-760B-25R-CC to -29R-CC there is a moderately to well-preserved palynomorph assemblage that is dominated by pollen. Cuticules are common, whereas acritarchs, *Botryococcus*, and *Plaesiodictyon* are rare. Both the palynomorph assemblage and the presence of calcareous nannofossils in this interval point to an environment similar to the interval from Core 122-759B-25R through -39R at Site 759 (i.e., delta front to prodelta).

PALEOMAGNETICS

We used the pass-through cryogenic magnetometer to measure the archive sections from Cores 122-760A-1H through -38X and from Cores 122-760B-2R to -29R (excluding badly disturbed intervals). After the natural remanent magnetization (NRM) was measured, the sections were routinely demagnetized to 9 mT and remeasured.

Cenozoic Sediments in Hole 760A

The data provided by the archive halves presented clearly positive and negative inclinations, especially after 9-mT alternating-field (AF) demagnetization (Figs. 21A and 21B). This treatment seemed sufficient to remove an unstable secondary component. In order to detect variations in magnetic properties with depth, at least one discrete sample per section from Cenozoic sediments was subjected to stepwise AF demagnetization. All of the discrete samples were measured using the spinner magnetometer. In general, 8–15 mT was sufficient to remove the soft overprints (Fig. 22). For most of the APC cores, the whole-core measurements were fairly good and agreed well with both the discrete-sample data and the expected magnetic inclination for the site (−32°). Therefore, the data provided by measurement of the archive halves with the cryogenic magnetometer after 9-mT demagnetization were interpreted as magnetic-polarity reversals. The magnetic-polarity stratigraphy observed in the Cenozoic at Hole 760A was divided into four intervals:

1. Sections 122-760A-1H-1 through -2H-6 (corresponding to Subunit IA, Pleistocene foraminifer-nannofossil ooze): the results were interpreted in terms of polarity except for the first section, which displayed extensive coring disturbance. Such coring-induced disruption is common in the tops of cores. The results are of acceptable quality and document the polarity sequence through Chron C1. The intensity values after 9-mT demagnetization average about 3.5 mA/m and fluctuate between 1.0 and 10 mA/m. Several reversals were detected within this Pleistocene unit: Brunhes/Matuyama at 9 mbsf, the upper Jaramillo (Ju) at 12 mbsf, and the lower Jaramillo (Jl) at 14 mbsf (Fig. 21A).
2. Sections 122-760A-2H-7 through -3H-3 (corresponding to Subunit IB, late Pliocene nannofossil ooze with foraminifers): the intensity values after 9-mT demagnetization average 7 mA/m, and exhibit an anomalous high (about 35 mA/m) in the top 40 cm of Section 122-760A-3H-1. One reversal was detected at 17.5 mbsf within this late Pliocene unit (Fig. 21A). According to biostratigraphic data (see "Biostratigraphy," this chapter), this reversal could be correlated to one of the subchrons within Gauss Chron (Haq et al., 1987).
3. Sections 122-760A-3H-4 through -9H-4 (corresponding to Unit II, late Miocene to late Eocene nannofossil ooze): the results show a complicated pattern with many reversals, especially within the Miocene. A long reversed interval was detected in the upper Oligocene.
4. Sections 122-760A-9H-5 through -9H-6 (corresponding to Unit III, late Eocene to Cretaceous sandstone and siltstone): the intensity values after 9-mT demagnetization are very low (averaging 0.5 mA/m), with small fluctuations. No reversal was detected within this unit.

Triassic Sediments at Holes 760A and 760B

Hole 760A

All of the archive sections from Hole 760A are strongly magnetized. The NRM of 50% of the sections could not be measured with the cryogenic magnetometer because the magnetization was too high (given the total volume of the half-core). All of the measured sections lost 50%–60% of their remanent intensity with 9-mT AF demagnetization, but there was no major change in the magnetization directions that clearly indicated negative and positive inclinations. However, even after 9-mT demagnetization some very strongly magnetized sections could not be measured.

A pilot set of 10 discrete samples from Cores 122-760A-12X through -33X was measured with the spinner magnetometer and demagnetized with the Schonstedt AF-demagnetizer. An initial soft component of the NRM was removed at 5 mT and the intensity decreased dramatically. Above this field a stable component (either of normal or reversed polarity) was isolated. These results suggest that the data provided by the

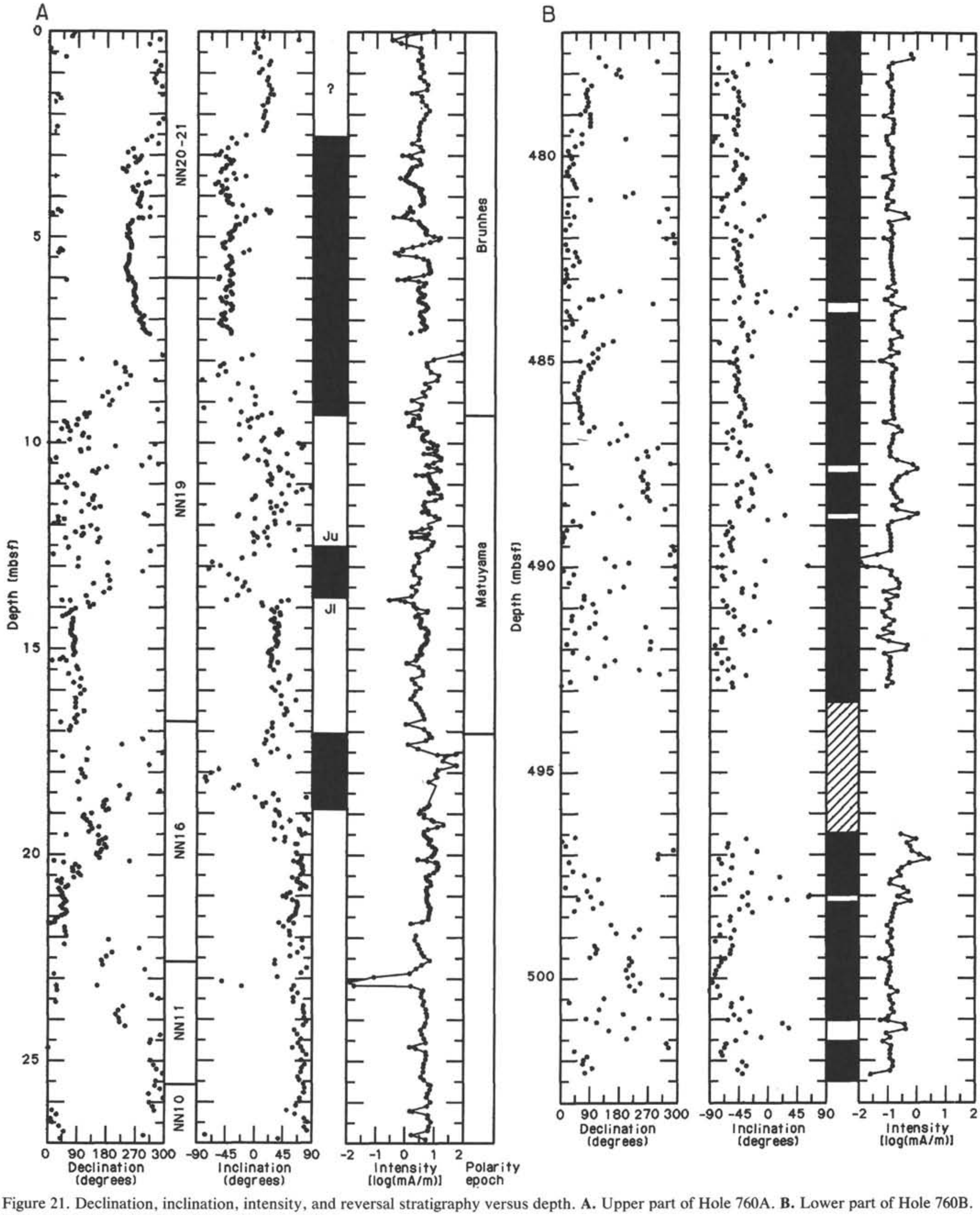

Figure 21. Declination, inclination, intensity, and reversal stratigraphy versus depth. **A.** Upper part of Hole 760A. **B.** Lower part of Hole 760B. Note unrecovered interval indicated by hatching.

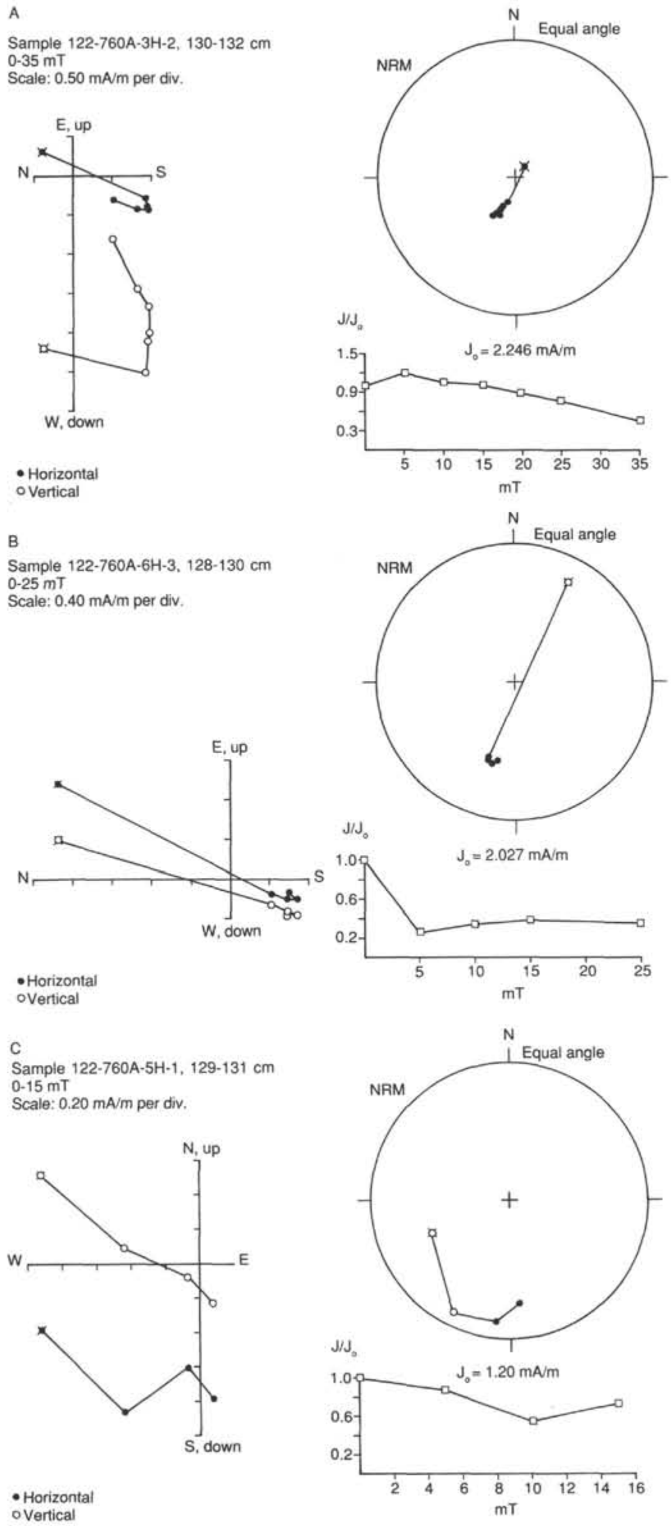

Figure 22. Vector endpoint diagrams, equal-angle stereographic projections, and intensity decay curves, Site 760. **A, B.** Single component of magnetization. **C.** Unstable component.

archive-half measurements after 9-mT demagnetization can be interpreted as magnetic polarity reversals.

Hole 760B

The archive halves from Hole 760B are weakly magnetized, except for Cores 122-760B-2R and -3R, which were too high to be measured with the cryogenic magnetometer. The 9-mT AF treatment was similar to that for Hole 760A. The magnetic polarity seemed normal within most of the sediments of this hole, but some reversed-polarity zones were observed from Cores 122-760B-7R through -12R. The three deepest cores of Hole 760B (Cores 122-760B-27R through -29R) showed a few spikes in sections with positive inclination and strong intensity, even after 9-mT demagnetization (Fig. 21B). These spikes were previously observed in Hole 759B (see "Paleomagnetics," Site 759 chapter), but disappeared at 9-mT AF treatment. We do not know the origin of these anomalies or whether they may be interpreted as reversed magnetic polarity zones. More shore-based investigations on discrete samples, using thermal demagnetization and magnetic mineralogy analysis, are necessary.

SEDIMENTATION RATES

Sedimentation rates for Hole 760A were plotted using the biostratigraphic data presented in the "Biostratigraphy" section of this chapter (Fig. 23). Methodology used to calculate sedimentation rates is outlined in the "Explanatory Notes" (this volume).

Only data points for Hole 760A are plotted in Figure 23. Triassic sedimentation rates could not realistically be calculated, given only one discrete age boundary in the entire section (i.e., the Norian/Carnian boundary). The minimum sediment accumulation rates are about 4 cm/k.y. for the Norian and about 1.3 cm/k.y. for the Carnian.

The Cenozoic sedimentation rates are very low for highly calcareous pelagic sediments. The average rate is about 0.2 cm/k.y. for most of the late Eocene to Recent; this is about one-fifth of usual rate for this type of sediment. There are a few exceptions: the Quaternary has rather high sedimentation rates (probably enhanced by a lack of compaction), and the lowermost Miocene is represented by a fair thickness of sediments as well, although the sedimentation rate of about 0.4 cm/k.y. is still quite low.

We note that the two small hiatuses in the early Pliocene and the early Miocene (Fig. 23) were preceded by episodes of relatively high sedimentation rates.

Overall, the sedimentation rates for Hole 760A are typical of condensed sequences. However, we note that all of the recovered Cenozoic sediments are normal pelagic carbonates with little or no evidence of being enriched in terrigenous or other noncalcareous matter, and our preliminary conclusion is that the section probably conceals a number of biostratigraphically undetectable hiatuses.

ORGANIC GEOCHEMISTRY

Shipboard organic geochemical analyses at Site 760 consist of 108 determinations of inorganic carbon, 151 Rock-Eval and total organic carbon (TOC) analyses, and 77 measurements of low-molecular-weight hydrocarbons. The procedures used for these determinations are outlined in the "Explanatory Notes" (this volume) and are described in detail by Emeis and Kvenvolden (1986).

Inorganic Carbon Results

Samples taken for physical-property measurements (67 from Hole 760A and 41 from Hole 760B) were analyzed for inorganic carbon content (Table 4). The calcium carbonate

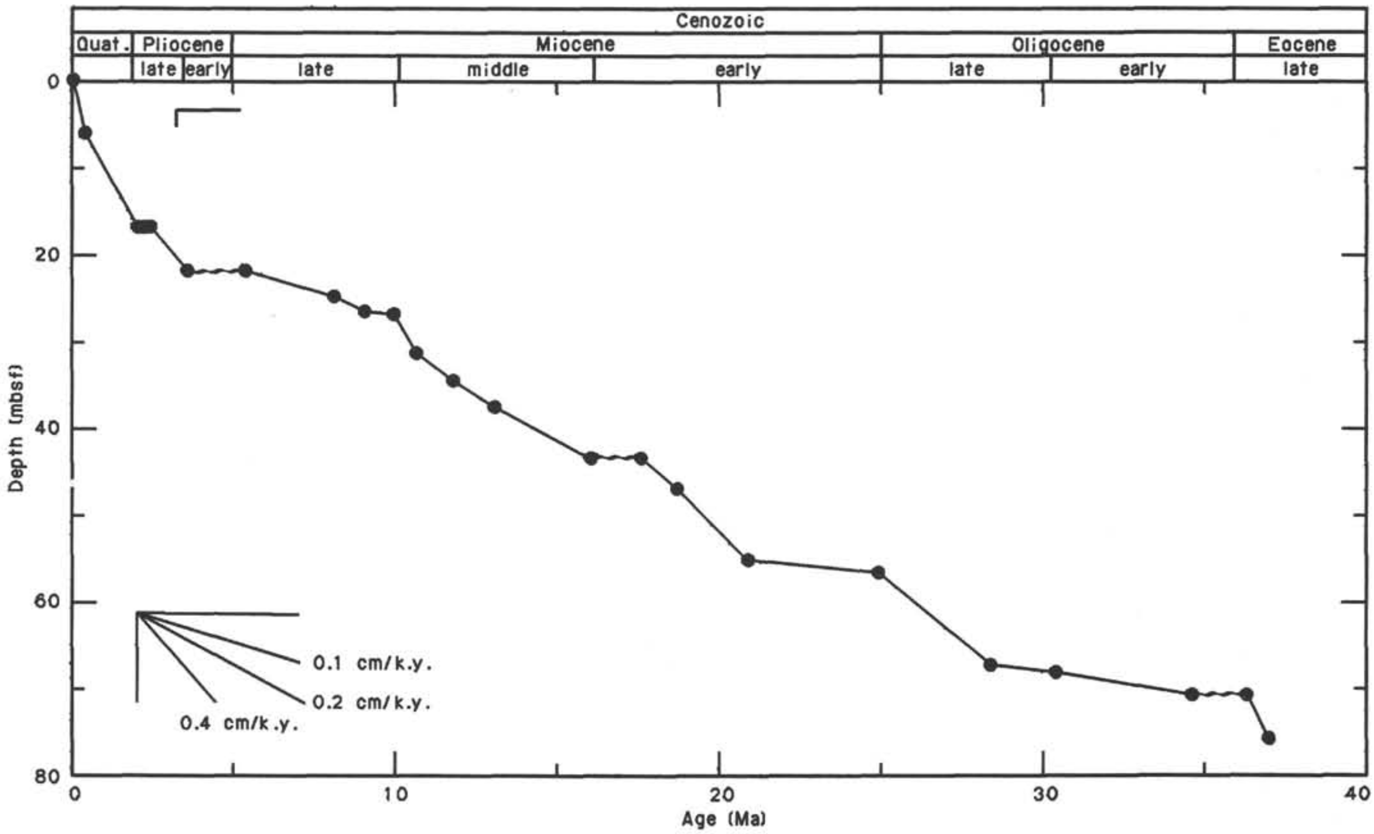

Figure 23. Sedimentation rates of Hole 760A. Hiatuses shown in wavy lines. Standard error bars for depth and age are at top left. See "Explanatory Notes," this volume, for a discussion of sedimentation-rate calculation methods.

content (estimated by multiplying the determined value for inorganic carbon by a factor of 8.33) ranged from less than 0.1% to over 97% of sediment dry weight. The upper 80 m of Hole 760A was dominated by nannofossil-foraminifer oozes. Deeper samples from Hole 760A and those from Hole 760B were interbedded clastics and limestones. Few samples had an intermediate carbonate content.

Rock-Eval and TOC Results

Rock-Eval and TOC results from samples from Holes 760A and 760B are given in Table 5. Many of the data are scattered. While some results are suspected of being erroneous (see "Organic Geochemistry," Site 759 chapter), much of the scatter may be attributed to the presence of mixed organic-matter types and variable levels of oxidation, recycling, and reworking.

The TOC content is generally less than 3%, except for a few samples of coal or coaly material in Cores 122-760B-13R and -14R (350–365 mbsf). For these samples, up to 18% TOC is observed. Many samples (notably the carbonates and some greenish silty clastics) have very low organic carbon contents (<0.2% TOC).

The organic matter is interpreted to be dominated by type III (higher land plant) debris on the basis of the low hydrogen index (HI) values (Fig. 24). A few samples (including the low-TOC greenish, silty material noted above from Cores 122-760A-12X to -16X) have very high HI values (>1000 in many cases). These results were first suspected of arising from contamination by the plastic core barrel liner. However, this was proved unlikely because the headspace gas samples (which also produced high Rock-Eval HI values) were taken from the centers of cores as soon as they arrived on deck and before any cutting or other manipulation had taken place. Furthermore, analyses of the plastic gave relatively high oxygen index (OI) values, which are not observed for most of the samples in question. The low to moderate OI values also argued against the possibility of analytical error of the TOC content because the same value is used in the denominator of both the HI and OI parameters. The high hydrogen index values may indicate the presence of a very reactive bitumen phase that may be natural (pyrobitumen or "dead oil") or an unknown contaminant (pipe dope?). Liquid petroleum and volatile lubricants or other contaminants have been ruled out because of the low S_1 yields (<0.25 mg hydrocarbons/g rock). The samples in which this phenomenon is observed contained black stringers that could be interpreted as rootlets, organic-matter-filled veins, or fragments of algal debris in the form of rip-up clasts. Additional work, including solvent extraction/fractionation and gas chromatography, and possibly organic petrology, is needed to resolve the significance of these observations.

Low-Molecular-Weight Hydrocarbon Results

Results of the routine measurements of low-molecular-weight hydrocarbons are listed in Table 6. In the uppermost 475 m of the two holes, methane concentrations in the headspace vials were generally 4 ± 2 ppm with rare excursions to 10 to 20 ppm; ethane concentrations were less than about 1 ppm. Where traces of ethane were noted but were below the concentration threshold of the integrator, the ratio of methane/ethane (C_1/C_2) was estimated visually to be similar to those samples for which integrator areas were available (i.e., about 10 to 20). In the bottom 25 m of Hole 760B, however, the concentrations of both C_1 and C_2 rose dramati-

Table 4. Concentrations of inorganic carbon and calcium carbonate in samples from Holes 760A and 760B. Inorganic carbon concentrations were measured coulometrically. Calcium carbonate percentages were calculated assuming the carbonate contents to be pure calcite. All percentages are on a whole, dry-weight basis. The lithology of each sample is indicated.

Core, section, interval (cm)	Depth (mbsf)	Inorganic carbon (%)	$CaCO_3$ (%)	Lithology
122-760A-				
1H-2, 22–24	1.72	10.33	86.08	Light-colored ooze
1H-4, 56–58	5.06	9.06	75.49	Light-colored ooze
2H-2, 72–74	9.92	9.70	80.80	Light-colored ooze
2H-4, 56–58	12.76	9.94	82.83	Light-colored ooze
2H-6, 96–98	16.16	9.75	81.24	Light-colored ooze
3H-2, 66–69	19.36	9.35	77.91	Light-colored ooze
3H-3, 60–62	20.80	9.53	79.41	Light-colored ooze
3H-6, 68–70	25.38	10.87	90.58	Light-colored ooze
4H-2, 80–82	29.00	10.91	90.91	Light-colored ooze
4H-4, 80–82	32.00	10.09	84.08	Light-colored ooze
5H-2, 86–88	38.56	10.51	87.58	Light-colored ooze
5H-4, 86–88	41.56	10.23	85.24	Light-colored ooze
5H-6, 86–88	44.56	10.47	87.24	Light-colored ooze
6H-2, 86–88	48.06	9.19	76.58	Light-colored ooze
6H-4, 86–88	51.06	7.79	64.91	Brown nannofossil ooze
6H-6, 91–93	54.11	9.12	75.99	Brown nannofossil ooze
6H-2, 86–88	57.56	9.30	77.40	Brown nannofossil ooze
7H-4, 86–88	60.56	10.83	90.24	Brown nannofossil ooze
7H-6, 74–77	63.44	10.74	89.49	Brown nannofossil ooze
8H-2, 86–88	67.06	10.32	85.99	Orange ooze
8H-4, 86–88	70.06	10.95	91.24	Light grey ooze
8H-6, 86–88	73.06	11.15	92.91	Light grey ooze
9H-2, 86–88	76.56	11.17	93.08	Light brown sandy ooze
9H-4, 86–88	79.56	10.25	85.41	Light brown sandy ooze
9H-6, 27–29	81.97	0.07	0.58	Claystone
10X-2, 86–88	86.06	0.03	0.24	Olive claystone
10X-4, 18–20	88.38	0.03	0.24	Olive claystone
11X-1, 70–72	93.90	0.04	0.33	Black mudstone
12X-1, 88–90	103.58	0.03	0.24	Grey sandstone
12X-2, 58–60	104.78	0.04	0.33	Black mudstone
13X-1, 87–89	113.07	0.02	0.16	Dark grey mudstone
14X-1, 19–20	116.39	0.02	0.16	?
16X-2, 120–122	137.90	0.02	0.16	Black claystone
16X-4, 89–91	140.59	0.02	0.16	Black claystone
17X-1, 65–68	145.35	0.01	0.08	Black claystone
19X-1, 55–57	164.25	0.61	5.08	?
19X-2, 59–61	165.79	0.04	0.33	?
20X-2, 11–13	174.81	0.16	1.33	Dark grey claystone
20X-2, 133–135	176.03	0.17	1.41	Sand
21X-1, 27–30	182.97	0.01	0.08	Dark grey claystone
21X-1, 74–76	183.44	0.01	0.08	?
22X-2, 57–60	189.97	0.02	0.16	Sandstone
22X-2, 134–136	190.74	0.01	0.08	?
22X-3, 32–35	191.22	0.07	0.58	?
23X-1, 18–20	193.08	0.50	4.10	?
24X-1, 76–78	198.66	0.05	0.41	Sand
25X-3, 31–33	206.21	0.02	0.16	Dark grey claystone
26X-1, 107–109	208.97	0.03	0.24	Dark grey claystone
26X-CC, 21–23	211.79	0.01	0.08	Dark grey claystone
27X-1, 145–147	214.35	0.21	1.74	Siltstone
27X-CC, 21–24	216.04	7.25	60.41	Indurated carbonate sandstone
28X-2, 120–122	220.60	0.02	0.16	Black siltstone
28X-3, 103–105	221.93	0.02	0.16	Black siltstone
29X-4, 54–56	227.94	0.01	0.08	Sandstone
30X-1, 32–35	232.72	0.08	0.66	Claystone (mudstone)
30X-7, 10–13	241.50	0.07	0.58	Black claystone (mudstone)
31X-1, 54–55	242.44	0.03	0.24	Black sandy claystone
31X-3, 54–55	245.44	5.36	44.66	Carbonate sandstone
33X-1, 36–38	254.76	0.10	0.80	Black claystone
33X-4, 80–82	259.70	0.04	0.33	Black claystone
34X-1, 91–93	260.31	0.16	1.33	Green siltstone
35X-2, 76–78	266.66	0.01	0.08	Black siltstone
35X-4, 87–89	269.77	0.22	1.83	Black siltstone
36X-2, 2–4	270.92	0.11	0.91	Claystone
37X-2, 14–16	280.54	1.45	12.08	?
37X-CC, 12–14	283.30	0.12	0.99	?
38X-1, 16–18	284.06	10.33	86.08	Sandstone
122-760B-				
6R-1, 16–18	283.16	10.92	90.00	?
6R-2, 99–102	285.49	0.16	1.33	Claystone
7R-1, 147–149	293.97	0.12	1.00	Claystone
7R-3, 27–29	295.77	10.45	87.05	Limestone
8R-1, 63–67	302.63	0.09	0.75	Claystone
8R-3, 63–67	305.63	11.60	96.63	Limestone
9R-2, 15–17	313.15	0.77	6.41	?
10R-1, 103–105	322.03	0.28	2.33	Black claystone
11R-1, 27–29	330.77	0.67	5.58	Green grey claystone
11R-2, 88–90	332.88	0.94	7.83	Green sandy claystone
12R-1, 119–121	341.19	0.02	0.17	Sandstone
12R-3, 81–84	343.81	0.06	0.50	Dark grey claystone
13R-1, 122–125	350.72	0.08	0.67	Black claystone
13R-2, 41–44	351.41	0.01	0.08	Grey claystone
14R-2, 30–32	360.80	11.18	93.13	Limestone
14R-CC, 17–19	365.80	0.02	0.17	Black claystone
14R-CC, 17–19	365.80	0.01	0.08	Black claystone
15R-1, 54–56	369.04	11.70	97.46	Limestone
16R-1, 134–136	379.34	11.70	97.46	Limestone
16R-4, 69–71	383.19	0.15	1.25	?
17R-1, 9–11	387.59	6.94	57.81	Carbonate sandstone
17R-2, 58–60	389.58	1.33	11.08	Limestone
17R-3, 84–86	391.34	0.08	0.67	Black claystone
19R-1, 72–74	407.22	0.33	2.75	Sandstone
19R-3, 98–101	410.48	0.23	1.92	?
20R-1, 126–131	417.26	0.05	0.42	Claystone
20R-3, 142–144	420.42	0.30	2.50	?
21R-3, 50–53	429.00	0.04	0.33	Siltstone
21R-4, 58–62	430.58	3.74	31.15	Claystone
22R-1, 24–26	435.24	10.22	85.13	Limestone
22R-4, 127–129	440.77	0.11	0.92	Sandstone
23R-1, 145–148	445.95	0.12	1.00	Black claystone
23R-3, 50–52	448.00	0.75	6.25	?
25R-1, 17–19	463.67	11.11	92.55	Grey limestone
25R-2, 23–25	465.23	0.08	0.67	Black claystone
26R-3, 18–20	471.18	0.23	1.92	Dark grey mudstone
27R-3, 74–76	481.24	0.56	4.66	?
28R-2, 76–78	489.26	0.31	2.58	?
28R-4, 64–66	492.14	0.32	2.67	?
29R-1, 8–10	496.58	0.29	2.42	?
29R-3, 116–118	500.66	0.30	2.50	Sandstone

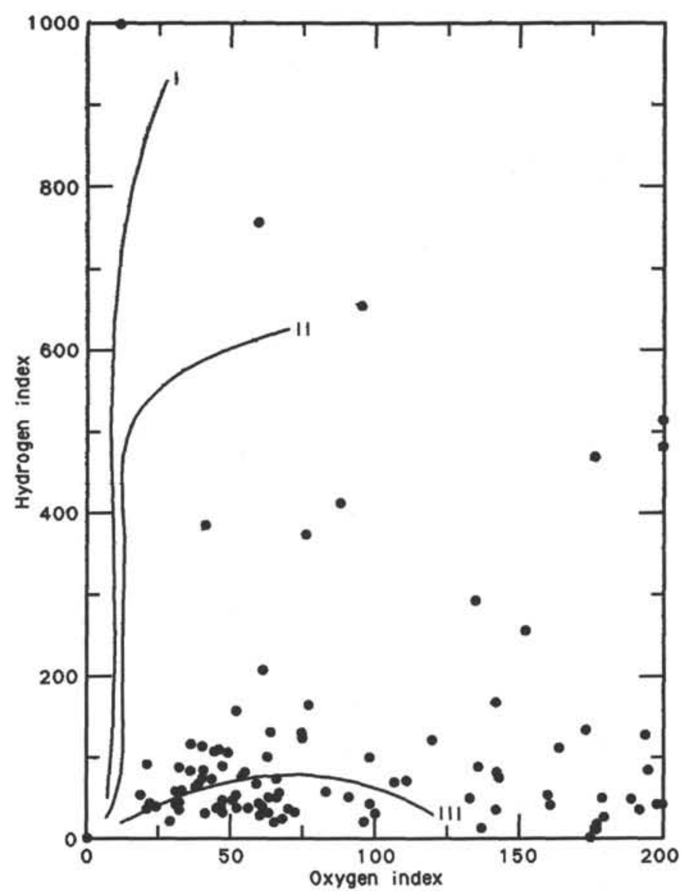

Figure 24. Van Krevelen-type plot of Rock-Eval hydrogen and oxygen index values for samples from Holes 760A and 760B. Units for HI are mg total hydrocarbons/g total organic carbon; for OI, mg CO_2/g total organic carbon.

Table 5 Results of Rock-Eval analyses of samples from Holes 760A and 760B. Total organic carbon (TOC) percentages are on a whole, dry-weight basis.

Core, section, interval (cm)	Depth (mbsf)	Sample weight (mg)	T_{max} (°C)	S_1	S_2	S_3	PI	S_2/S_3	PC	TOC (%)	HI	OI	Lithology
122-760A-													
1H-2, 22–24	1.72	107.4	365	0.00.	0.04	1.93	0.00	0.02	0.00	0.01	4001	9300	Light-colored ooze
2H-6, 96–98	16.16	102.1	377	0.16	0.73	1.89	0.18	0.38	0.02	0.10	730	1890	Light-colored ooze
2H-2, 72–74	9.92	100.9	459	0.10	0.40	2.22	0.20	0.18	0.04	0.05	800	4440	Light-colored ooze
2H-5, 145–150	15.15	103.3	274	0.01	0.01	1.46	0.50	0.00	0.00	0.01	100	14600	Light-colored ooze
3H-3, 60–62	20.80	105.3	308	0.07	0.00	1.95	1.00	0.00	0.00	0.00	0	0	Light-colored ooze
4H-2, 80–82	29.00	110.9	308	0.01	0.00	1.39		0.00	0.00	0.02	0	6950	Light-colored ooze
5H-2, 86–88	38.56	102.1	308	0.02	0.00	1.53	1.00	0.00	0.00	0.00	0	0	Light-colored ooze
6H-4, 86–88	51.06	111.7	553	0.08	0.74	1.61	0.10	0.45	0.06	0.07	1057	2300	Brown nannofossil ooze
8H-6, 86–88	73.06	110.2	528	0.00	0.08	0.64	0.00	0.12	0.00	0.01	800	6400	Brown nannofossil ooze
9H-5, 145–150	81.65	101.9	569	0.02	5.60	0.33	0.00	16.96	0.46	0.47	1191	70	Brown nannofossil ooze
9H-4, 86–88	79.56	102.9	230	0.00	0.00	1.15		0.00	0.00	0.00	0	0	?
9H-5, 27–29	80.47	99.2	454	0.09	1.60	0.27	0.05	5.92	0.14	0.13	1230	207	Light brown sandy ooze
9H-6, 27–29	81.97	101.3	471	0.00	1.48	0.26	0.00	5.69	0.12	0.12	1233	216	Claystone
10X-4, 18–20	88.38	99.9	537	0.03	0.97	0.31	0.03	3.12	0.08	0.08	1212	387	Olive claystone
10X-4, 18–20	88.38	101.9	512	0.00	0.88	0.32	0.00	2.75	0.07	0.07	1257	457	Olive claystone
10X-2, 86–88	86.06	99.9	584	0.10	0.65	0.43	0.14	1.51	0.06	0.06	1083	716	Olive claystone
10X-5, 145–150	91.15	102.2	464	0.58	5.78	0.08	0.09	72.25	0.53	0.53	1090	15	?
11X-1, 0–1	93.20	99.4	453	1.25	6.09	0.07	0.17	87.00	0.61	0.61	99	811	?
11X-1, 70–72	93.90	100.2	428	0.05	1.76	0.78	0.03	2.25	0.15	2.13	82	36	Black claystone
12X-2, 589–60	110.09	103.8	436	0.00	1.48	0.46	0.00	3.21	0.12	1.27	116	36	Black claystone
12X-2, 0–1	104.20	103.7	456	0.00	3.78	0.05	0.00	75.60	0.31	0.37	1021	13	?
12X-1, 88–90	103.58	100.3	460	0.00	1.18	0.14	0.00	8.42	0.09	0.10	1180	140	Grey sandstone
13X-1, 0–1	112.20	100.2	459	0.00	3.93	0.31	0.00	12.67	0.32	0.52	755	59	?
13X-1, 87–89	113.07	101.0	468	0.00	0.88	0.88	0.00	1.00	0.07	1.87	47	47	Dark grey claystone
14X-1, 19–20	116.39	99.4	511	0.02	0.76	0.32	0.03	2.37	0.06	0.07	1085	457	?
14X-1, 0–5	116.20	101.0	464	0.24	5.64	0.14	0.04	40.28	0.49	0.54	1044	25	?
14X-1, 0–5	116.20	100.0	492	0.00	1.30	0.58	0.00	2.24	0.10	0.16	812	362	?
14X-1, 0–5	116.20	101.3	466	0.00	1.85	0.48	0.00	3.85	0.15	0.19	973	252	?
16X-2, 120–122	137.90	101.7	434	0.00	0.72	0.28	0.00	2.57	0.06	0.14	514	200	Black claystone
16X-4, 89–91	140.59	101.4	442	0.01	0.71	0.43	0.01	1.65	0.06	0.57	124	75	Black claystone
16X-4, 124–125	140.94	99.6	440	0.00	2.54	0.52	0.00	4.88	0.21	0.68	373	76	Black claystone
16X-4, 140–150	141.10	103.6	447	0.01	1.44	0.21	0.01	6.85	0.12	0.22	654	95	?
17X-1, 0–3	144.70	101.6	451	0.00	1.18	0.70	0.00	1.68	0.09	0.46	256	152	?
17X-1, 65–68	145.35	100.8	426	0.00	0.53	0.22	0.00	2.40	0.04	0.11	481	200	Black claystone
19X-1, 55–57	164.25	102.8	514	0.00	0.44	0.85	0.00	0.51	0.03	0.04	1100	2125	?
19X-2, 59–61	165.79	100.9	453	0.00	0.82	0.38	0.00	2.15	0.06	0.28	292	135	?
19X-1, 55–57	164.25	101.7	509	0.00	0.49	0.93	0.00	0.52	0.04	0.05	980	1860	?
19X-2, 140–150	166.60	102.8	449	0.02	2.97	0.32	0.01	9.28	0.24	0.77	385	41	?
20X-2, 11–13	174.81	99.8	434	0.01	1.33	2.03	0.01	0.65	0.11	1.82	73	111	Dark grey claystone
20X-2, 133–135	176.03	102.8	441	0.01	1.43	2.68	0.01	0.53	0.12	1.87	76	143	Sand
20X-1, 148–150	174.68	104.3	432	0.01	1.13	1.62	0.01	0.69	0.09	1.95	57	83	Dark grey claystone
21X-1, 27–30	182.97	100.2	434	0.02	1.31	0.82	0.02	1.59	0.11	3.40	38	24	Dark grey claystone
21X-1, 0–2	182.70	105.7	452	0.00	0.92	0.90	0.00	1.02	0.07	0.75	122	120	?
21X-1, 74–76	183.44	102.4	472	0.00	0.81	0.61	0.00	1.32	0.06	1.94	41	31	?
22X-3, 32–35	191.22	101.6	476	0.00	0.77	1.12	0.00	0.68	0.06	0.68	113	164	?
22X-2, 57–60	189.97	101.7	471	0.02	0.61	0.38	0.03	1.60	0.05	0.60	101	63	Sandstone
22X-2, 134–136	190.74	101.0	497	0.00	1.08	0.32	0.00	3.37	0.09	0.52	207	61	?
22X-2, 148–150	190.88	101.0	451	0.00	0.53	0.52	0.00	1.01	0.04	0.53	100	98	?
23X-1, 18–20	193.08	99.8	516	0.00	0.36	0.58	0.00	0.62	0.03	0.11	327	527	?
23X-1, 148–150	194.38	99.8	437	0.00	0.57	0.33	0.00	1.72	0.04	0.44	129	75	?
24X-1, 0–2	197.90	104.3	434	0.00	0.57	0.86	0.00	0.66	0.04	0.80	71	107	?
24X-1, 76–78	198.66	100.6	455	0.00	0.82	0.74	0.00	1.10	0.06	1.24	66	59	Sand
25X-3, 31–33	206.21	100.9	451	0.00	0.74	0.34	0.00	2.17	0.06	0.69	107	49	Dark grey claystone
25X-5, 0–1	208.90	107.1	449	0.00	0.61	0.78	0.00	0.78	0.05	0.45	135	173	?
26X-CC, 21–23	ERR	101.4	430	0.02	0.87	0.47	0.02	1.85	0.07	1.49	58	31	Dark grey claystone
26X-1, 107–109	208.97	102.1	447	0.00	0.59	0.24	0.00	2.45	0.04	0.08	737	300	Dark grey claystone
27X-1, 145–147	214.35	101.0	471	0.00	1.20	3.40	0.00	0.35	0.10	2.12	56	160	Siltstone
27X-CC, 21–24	ERR	102.0	437	0.00	0.15	3.56	0.00	0.04	0.01	0.67	22	531	Carbonate sandstone
27X-2, 0–1	214.40	99.8	461	0.00	0.74	3.76	0.00	0.19	0.06	1.63	45	230	?
28X-2, 120–122	220.60	102.9	439	0.01	1.28	0.71	0.01	1.80	0.13	0.29	38	21	Black siltstone
28X-4, 0–1	222.40	110.5	463	0.00	0.80	0.23	0.00	3.47	0.06	0.10	800	230	?
28X-3, 103–105	221.93	99.7	472	0.00	0.70	0.41	0.00	1.70	0.05	1.05	66	39	Black siltstone
29X-4, 54–56	227.94	102.6	505	0.00	0.67	0.30	0.00	2.23	0.05	0.05	1340	600	Sandstone
29X-4, 0–1	227.40	101.3	491	0.00	0.52	0.12	0.00	4.33	0.04	0.04	1300	300	?
30X-7, 10–13	241.50	104.5	437	0.01	0.78	1.09	0.01	0.71	0.06	1.79	43	60	Black claystone
30X-1, 32–35	232.72	106.2	438	0.00	1.36	1.68	0.00	0.80	0.11	2.66	51	63	Claystone
30X-5, 140–150	239.80	102.2	438	0.07	2.35	0.88	0.03	2.67	0.22	0.69	87	32	?
30X-6, 0–1	239.90	102.1	440	0.00	0.95	0.88	0.00	1.07	0.07	2.70	35	32	?
31X-1, 54–55	242.44	104.2	437	0.01	0.95	0.58	0.01	1.63	0.08	1.56	33	8	Black sandy claystone
31X-3, 0–1	244.90	100.3	469	0.02	1.15	2.06	0.02	0.55	0.09	2.26	50	91	?
31X-3, 54–55	245.44	105.4	401	0.00	0.00	0.42	0.00	0.00	0.03	0.00	0	400	Carbonate sandstone
33X-1, 36–38	254.76	103.6	502	0.01	0.48	1.09	0.02	0.44	0.04	1.50	32	72	Black claystone
33X-4, 80–82	259.70	100.4	505	0.00	0.84	1.00	0.00	0.84	0.07	2.15	39	46	Black claystone

Table 5 (continued).

Core, section, interval (cm)	Depth (mbsf)	Sample weight (mg)	T_{max} (°C)	S_1	S_2	S_3	PI	S_2/S_3	PC	TOC (%)	HI	OI	Lithology
34X-1, 91–93	260.31	105.1	573	0.00	0.16	0.57	0.00	0.28	0.01	0.03	533	1900	Green siltstone
35X-2, 76–78	266.66	102.8	462	0.00	0.55	0.29	0.00	1.89	0.04	0.61	90	47	Black siltstone
35X-4, 87–89	269.77	98.6	440	0.02	1.52	3.83	0.01	0.39	0.12	0.12	1266	3191	Black siltstone
35X-4, 87–89	269.77	104.3	439	0.12	1.35	3.56	0.08	0.37	0.12	2.67	50	133	Black siltstone
35X-2, 76–78	266.66	103.7	465	0.00	0.50	0.27	0.00	1.85	0.04	0.67	74	40	Black siltstone
35X-3, 140–150	268.80	102.0	448	0.01	2.72	4.68	0.00	0.58	0.22	3.28	82	142	?
36X-2, 2–4	270.92	104.8	478	0.00	0.70	1.60	0.00	0.43	0.05	0.82	85	195	Claystone
37X-2, 14–16	280.54	101.1	421	0.00	0.15	1.40	0.00	0.10	0.01	0.79	18	177	?
37X-CC, 12–14	ERR	100.2	464	0.00	0.70	1.34	0.00	0.52	0.05	1.91	36	70	?
38X-1, 16–18	284.06	99.9	271	0.00	0.00	1.00	0.00	0.00	0.57	0.00	0	0	
122-760B-													
2R-1, 0–1	89.90	101.5	578	0.04	0.47	0.62	0.08	0.75	0.04	0.04	1175	1550	?
2R-1, 58–60	90.48	99.9	451	0.00	1.12	0.53	0.00	2.11	0.09	0.68	164	77	Black claystone
3R-1, 114–116	100.54	100.6	436	0.01	1.49	1.33	0.01	1.12	0.12	1.99	74	66	Black claystone
3R-1, 149–150	100.89	102.5	445	0.00	1.02	1.59	0.00	0.64	0.08	2.57	39	61	?
4R-1, 0–2	108.90	101.9	455	0.00	0.80	0.27	0.00	2.96	0.06	0.51	156	52	?
4R-1, 68–70	109.58	100.5	449	0.00	0.61	0.23	0.00	2.65	0.05	0.13	469	176	Black claystone
5C-2, 102–103		102	435	0.00	0.10	0.99	0.00	0.10	0.00	0.72	13	137	?
6R-1, 16–18	283.16	101.2	428	0.00	0.01	0.66		0.01	0.00	0.26	3	253	Limestone
6R-2, 99–102	285.49	101.3	457	0.02	0.75	1.06	0.03	0.70	0.06	2.21	33	47	Claystone
7R-1, 147–149	293.97	101.1	437	0.00	0.90	1.20	0.00	0.75	0.07	2.89	31	41	Claystone
7R-2, 0–1	294.00	100.6	435	0.00	0.95	1.13	0.00	0.84	0.07	2.48	38	45	?
7R-3, 27–29	295.77	101.1	413	0.00	0.04	0.91	0.00	0.04	0.00	0.18	22	505	Limestone
8R-1, 0–1	302.00	100.5	483	0.00	1.33	2.02	0.00	0.65	0.11	1.48	89	136	?
8R-1, 63–67	302.63	101.9	487	0.01	0.89	1.19	0.01	0.74	0.07	1.78	50	66	Claystone
8R-3, 63–67	305.63	102	338	0.00	0.00	0.67		0.00	0.00	0.04	0	1675	Claystone
8R-CC, 27–28	ERR	101.6	436	0.00	0.61	1.24	0.00	0.49	0.05	2.05	29	60	?
9R-1, 0–1	311.50	102.3	433	0.00	0.40	1.20	0.00	0.33	0.03	1.84	21	65	?
9R-2, 15–17	313.15	101.6	274	0.00	0.00	0.02	0.00	0.00	0.00	0.00	0	0	?
9R-2, 15–17	313.15	100.7	431	0.01	0.68	1.82	0.01	0.37	0.05	2.66	25	68	?
9R-CC, 11–12	ERR	103.5	448	0.00	0.66	0.28	0.00	2.35	0.05	0.60	110	46	?
10R-1, 0–1	321.00	102.6	464	0.00	0.37	0.08	0.00	4.62	0.03	0.09	411	88	?
10R-1, 103–105	322.03	101.1	438	0.02	0.89	3.58	0.02	0.24	0.07	2.52	35	142	Black claystone
10R-1, 140–150	322.40	99.5	440	0.01	1.23	2.77	0.01	0.44	0.10	2.80	43	98	?
10R-3, 22–24	324.22	101.2	483	0.00	0.63	0.76	0.00	0.82	0.05	1.12	56	67	?
11R-1, 0–1	330.50	100.5	384	0.00	0.08	1.17	0.00	0.06	0.00	0.66	12	177	?
11R-1, 27–29	330.77	100.6	594	0.00	0.07	1.25	0.00	0.05	0.00	0.06	116	2083	Green grey claystone
11R-2, 88–90	332.88	100.2	502	0.07	0.06	1.13	0.58	0.05	0.01	0.03	200	3766	Green sandy claystone
11R-CC, 25–26	ERR	101.9	512	0.00	0.38	0.37	0.00	1.02	0.03	0.05	760	740	?
12R-1, 0–2	340.00	101.6	548	0.00	0.25	0.43	0.00	0.58	0.02	0.05	500	860	?
12R-1, 119–121	341.19	100.9	485	0.00	0.60	0.20	0.00	3.00	0.05	0.05	1200	400	Sandstone
12R-3, 81–84	343.81	100.6	441	0.00	1.26	0.72	0.00	1.75	0.10	2.12	59	33	Dark grey claystone
12R-3, 93–95	343.93	100.6	450	0.00	1.34	0.55	0.00	2.43	0.11	1.24	108	44	?
13R-1, 122–125	350.72	101.8	423	0.06	2.25	1.20	0.03	1.87	0.19	5.36	41	22	Black claystone
13R-1, 148–150	350.98	101.3	434	0.00	0.45	0.87	0.00	0.51	0.03	1.38	32	63	?
13R-2, 41–44	351.41	99.5	482	0.00	0.42	0.20	0.00	2.10	0.03	0.50	84	40	Grey claystone
13R-3, 28–29	352.78	101.5	519	0.00	1.76	0.87	0.00	2.02	0.14	1.35	130	64	?
14R-1, 0–2	359.00	101.5	444	0.00	1.51	1.06	0.00	1.42	0.12	1.90	79	55	?
14R-2, 30–32	360.80	99.6	306	0.00	0.00	0.70		0.00	0.00	0.04	0	1750	Limestone
14R-4, 120–122	364.70	59.2	426	0.20	16.72	3.81	0.01	4.38	1.41	18.10	92	21	?
14R-CC, 17–19	ERR	100.8	435	0.07	3.11	1.16	0.02	2.68	0.26	5.85	53	19	Black claystone
15R-1, 0–2	368.50	103.7	437	0.00	0.92	1.24	0.00	0.74	0.07	4.26	21	29	?
15R-1, 54–56	369.04	102.7	438	0.00	0.00	0.43		0.00	0.00	0.03	0	1433	Limestone
16R-1, 134–136	379.34	100.8	370	0.00	0.00	0.73		0.00	0.00	0.05	0	1460	Limestone
16R-3, 123–125	382.23	98.8	508	0.00	0.86	1.23	0.00	0.69	0.07	1.48	58	83	?
16R-4, 69–71	383.19	101	508	0.01	0.57	2.17	0.02	0.26	0.04	1.34	42	161	?
17R-1, 9–11	387.59	100.6	367	0.00	0.03	1.33	0.00	0.02	0.00	0.28	10	475	Carbonate sandstone
17R-2, 58–60	389.58	100.5	309	0.00	0.01	0.84		0.01	0.00	0.06	16	1400	Limestone
17R-2, 148–150	390.48	101.7	440	0.00	1.25	1.24	0.00	1.00	0.10	2.35	53	52	?
17R-3, 84–86	391.34	99.1	434	0.00	0.70	0.99	0.00	0.70	0.05	1.89	37	52	Black claystone
18R-2, 136–138	399.86	101.5	587	0.00	0.15	0.86	0.00	0.17	0.01	0.14	107	614	?
19R-1, 72–74	407.22	100.7	590	0.02	0.30	1.29	0.06	0.23	0.02	0.20	150	645	Sandstone
19R-3, 98–101	410.48	100.7	594	0.00	0.28	0.97	0.00	0.28	0.02	0.54	51	179	?
20R-1, 126–131	417.26	99.4	485	0.00	0.73	0.54	0.00	1.35	0.06	1.65	44	32	Claystone
20R-3, 142–144	420.42	100.8	427	0.00	0.36	1.60	0.00	0.22	0.03	1.66	21	96	?
21R-3, 50–53	429.00	100.2	540	0.00	0.61	0.66	0.00	0.92	0.05	1.29	47	51	Siltstone
21R-4, 58–62	430.58	101.1	333	0.00	0.01	0.64		0.01	0.00	0.08	12	800	Claystone
22R-1, 24–26	435.24	100.7	311	0.00	0.00	0.64		0.00	0.00	0.13	0	492	Limestone
22R-4, 127–129	440.77	101.8	547	0.00	0.76	1.15	0.00	0.66	0.06	0.59	128	194	Sandstone
23R-1, 145–148	445.95	100.6	520	0.00	0.42	1.31	0.00	0.32	0.03	1.30	32	100	Black claystone
23R-3, 50–52	448.00	100.6	434	0.00	0.30	2.03	0.00	0.14	0.02	1.13	26	179	?
25R-1, 17–19	463.67	100.7	422	0.00	0.03	0.86	0.00	0.03	0.00	0.11	27	781	Grey limestone
25R-2, 23–25	465.23	99.7	470	0.00	0.77	1.16	0.00	0.66	0.06	2.07	37	56	Black claystone
26R-3, 18–20	471.18	100.4	481	0.00	0.90	3.34	0.00	0.26	0.07	1.82	49	183	Dark grey claystone
27R-3, 74–76	481.24	100.1	481	0.00	0.59	6.15	0.00	0.09	0.04	1.66	35	370	?

Table 5 (continued).

Core, section, interval (cm)	Depth (mbsf)	Sample weight (mg)	T_{max} (°C)	S_1	S_2	S_3	PI	S_2/S_3	PC	TOC (%)	HI	OI	Lithology
28R-2, 76–78	489.26	100.2	460	0.00	0.64	3.35	0.00	0.19	0.05	1.74	36	192	?
28R-4, 64–66	492.14	101.5	439	0.00	0.80	3.68	0.00	0.21	0.06	1.85	43	198	?
29R-1, 8–10	496.58	100.8	439	0.00	0.76	3.51	0.00	0.21	0.06	1.75	43	200	?
29R-3, 116–118	500.66	99.4	514	0.00	0.61	2.35	0.00	0.25	0.05	1.24	49	189	Sandstone

Note: PI = production index; PC = pyrolyzed hydrocarbon; TOC = total organic carbon (determined on a whole, dry-weight basis); HI = hydrogen index; OI = oxygen index; ERR = error.

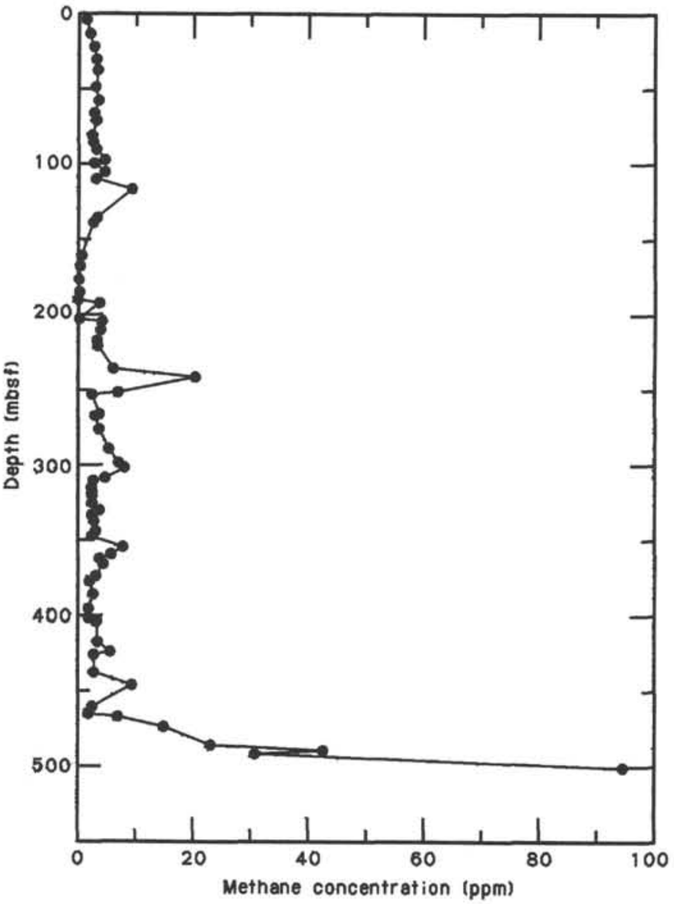

Figure 25. Downhole changes in concentration of methane (C_1) in samples from Holes 760A and 760B. Concentration is reported as in parts per million of the analyzed volume of gas obtained from headspace analyses of core samples.

cally to 97 and 4 ppm, respectively (Fig. 25). The C_1/C_2 ratio also increased somewhat, but stabilized at about 25.

These results indicate that the gas observed in samples from below the Tertiary oozes is thermogenic in origin (Claypool and Kvenvolden, 1983). This interpretation is consistent with the probable Triassic age of the rocks sampled, with the structural setting, and with the type III organic matter. The concentrations of gas throughout the upper portion of this site (and also those from nearby Hole 759B) may be indicative of an essentially open system wherein thermogenic gas has been generated downdip and is migrating updip and out of the rock at the seafloor.

Rapidly increasing concentrations of gas would be expected in a case where the effective permeability of a rock (e.g., shale) was reduced relative to the overlying units. This decreased permeability would result in more efficient retention of gases and could arguably be interpreted as a "cap" rock or reservoir seal. Diffusion migration of low-molecular-weight hydrocarbons in fine-grained rocks (especially near the contacts with more porous and permeable units) has been demonstrated (Leythaeuser et al., 1982; 1983). These workers have also observed that some migrational fractionation should be expected, favoring the lower-molecular-weight components. Gas lost during the coring and recovery operations would similarly be enriched in methane and hence reduce the measured C_1/C_2 ratio. The source of the thermogenic gases may have, therefore, a C_1/C_2 ratio similar to that observed in the headspace samples.

INORGANIC GEOCHEMISTRY

Introduction

The sampling program implemented at Site 760 differed from that carried out at Site 759 in order to obtain more detailed depth profiles of concentration gradients in the upper 100 m of Hole 760A. This was intended to better define some of the larger changes in concentrations observed at Site 759. Five-centimeter-long whole-round samples were obtained from each core in the first 100 m and squeezed (see "Explanatory Notes," this volume). Below 100 mbsf, every third core was sampled when sufficient sediment was recovered. A total of 22 samples were collected, although the last (Sample 122-760B-29R-4, 140–150 cm) did not yield any pore water. Bulk X-ray diffraction analysis of interstitial water squeeze cakes and other selected samples were performed later during the cruise, when regulated power was temporarily restored (see Table 7 of the Site 759 chapter, this volume).

Interstitial Waters

The methods employed for shipboard interstitial water analyses are described in the Explanatory Notes (this volume). Twenty-one water samples were analyzed (Fig. 26, Table 8). When ≤ 10 cm^3 of fluids were obtained, alkalinity and pH measurements were not carried out. Samples 122-760A-10X-2, 140–145 cm, -19X, 140–150 cm, through -35X, 140–150 cm, and -25R, 140–150 cm, fell in this category.

Magnesium (Mg^{2+}) and Calcium (Ca^{2+})

As at Site 759 (see "Inorganic Geochemistry," Site 759 chapter, this volume), the major constituents exhibit significant concentration changes as a function of depth below seafloor. In Figure 26 we present the depth profile for Mg^{2+}, the element that displays the largest downhole concentration gradient of the constituents determined. Its concentration (51.6 mM) at 5.9 mbsf is approximately 3% depleted relative to seawater (54.0 mM) and decreases sharply (to 39.3 mM) by 81.6 mbsf; it then rises (to 43.4 mM) at 86.6 mbsf, just below the boundary between Unit III (characterized by Mn oxides,

Table 6 . Concentrations of low-molecular-weight hydrocarbons of samples from Holes 760A and 760B. Analyses were done with the Carle gas chromatograph. Except where noted, data are from headspace samples. Concentrations are reported in parts per million (ppm) of headspace or vacutainer volume.

Core, section, interval (cm)	Depth (mbsf)	C_1	C_2	C_1/C_2
122-760A-				
1H-4, 145–150	6.0	1	nd	—
2H-5, 145–150	15.2	2	nd	—
3H-4, 120–125	22.9	3	nd	—
4H-6, 0–1	34.2	3	nd	—
5H-6, 0–1	43.7	3	nd	—
6H-6, 0–1	53.2	3	nd	—
7H-6, 0–1	62.7	4	nd	—
8H-4, 144–145	70.6	3	nd	—
8H-5, 121[a]	71.9	4	nd	—
9H-3, 0–5	77.2	3	nd	—
9H-6, 62[a]	82.3	3	nd	—
10X-3, 0–1	86.7	3	nd	—
11X-1, 0–1	93.2	3	nd	—
12X-1, 0–1	102.7	3	nd	—
13X-1, 0–1	112.2	3	nd	—
14X-1, 0–5	125.7	3	nd	—
16X-4, 124–125	140.9	3	nd	—
17X-1, 0–2	144.7	3	nd	—
19X-2, 123–125	166.4	3	nd	—
20X-1, 148–150	174.7	4	nd	—
21X-1, 0–2	182.7	3	nd	—
22X-2, 145–150	190.9	3	nd	—
23X-1, 148–150	194.4	5	tr	—
24X-1, 0–2	197.9	4	tr	—
25X-5, 0–1	208.9			
26X-2, 0–1	209.4	4	nd	—
27X-2, 0–1	214.4	4	nd	—
28X-4, 0–1	222.4	3	nd	—
29X-4, 0–1	227.4	3	nd	—
30X-6, 0–1	239.9	6	tr	—
31X-3, 0–1	244.9	21	1	19
33X-2, 0–1	255.9	7	tr	—
34X-1, 0–2	259.4	3	nd	—
35X-3, 123–125	268.6	4	nd	—
36X-1, 0–2	269.4	3	nd	—
37X-2, 148–150	281.9	4	nd	—
122-760B-				
2R-1, 0–1	89.9	3	nd	—
3R-1, 149–150	100.9	5	nd	—
4R-1, 0–2	108.9	4	nd	—
5C-2, 102–103		10	1	12
7R-2, 0–1	294.0	5	nd	—
8R-1, 0–1	302.2	33	nd	—
8R-CC, 27–28	306.6	8	1	8
9R-1, 0–1	311.5	5	nd	—
9R-CC, 11–12	316.4	3	nd	—
10R-1, 0–1	321.0	2	nd	—
10R-3, 22–24	324.2	3	nd	—
11R-1, 0–1	330.5	3	nd	—
11R-CC, 25–25	335.7	3	nd	—
12R-1, 0–2	340.0	3	nd	—
12R-3, 93–95	343.9	3	nd	—
13R-1, 148–150	351.0	3	nd	—
13R-3, 28–29	352.8	3	nd	—
14R-1, 0–2	359.0	8	nd	—
14R-4, 120–122	364.7	6	nd	—
15R-1, 0–2	368.5	4	nd	—
15R-2, 100–101	371.0	4	nd	—
16R-1, 0–2	378.0	3	nd	—
16R-3, 123–125	382.2	2	nd	—
17R-2, 148–150	390.5	3	nd	—
18R-2, 136–138	399.9	2	nd	—
19R-1, 0–2	406.5	2	nd	—
19R-2, 123–125	409.5	3	nd	—
20R-5, 0–1	422.0	4	nd	—
20R-CC, 35–36	423.5	4	nd	—
21R-4, 0–1	430.0	6	nd	—
21R-CC, 26–27	431.7	3	nd	—

Table 6 (continued).

Core, section, interval (cm)	Depth (mbsf)	C_1	C_2	C_1/C_2
22R-4, 148–150	441.0	3	nd	—
23R-CC, 30–32	451.1	10	1	7
25R-1, 0–5	463.5	3	nd	—
25R-2, 123–125	466.2	3	nd	—
26R-1, 0–2	468.0	2	nd	—
26R-3, 125–127	472.3	7	nd	—
27R-1, 0–5	477.5	15	1[b]	15
28R-1, 0–2	487.0	24	1[b]	21
28R-2, 123–125	489.7	43	2[b]	27
29R-1, 0–2	496.5	31	1[b]	22
29R-4, 128–130	502.2	97	4[b]	28

Note: nd = not detected; tr = trace.
[a] vac = vacutainer sample.
[b] Indicates trace of C_3 also present.

sandstone, and siltstone) and Unit IV (in which dark gray and greenish claystones, believed to reflect a nonmarine environment, were observed) (see "Lithostratigraphy," this chapter). Below this depth the decrease in Mg^{2+} concentration is less pronounced, and several other small concentration reversals were observed down to 268.8 mbsf. Between 268.8 and 322.4 mbsf a very sharp (greater than twofold) decrease in Mg^{2+} was observed. This decrease is also associated with a lithological change. Although the drop in concentration is real, it may actually occur over a slightly different depth interval than represented here because the data correspond to a changeover from Hole 760A to Hole 760B. The Mg^{2+} gradient in the lower section of Hole 760B is much smaller than that above 300 mbsf.

Figure 26 also shows the depth concentration profile for Ca^{2+} wherein variations are less pronounced and generally the reverse of Mg^{2+}. A steady increase in Ca^{2+}, which mirrors the trend of Mg^{2+} (although not the molar Mg^{2+} concentration change), is observed from 11.2 mM at 5.9 mbsf (10% enrichment relative to seawater) to 16.0 mM at 70.6 mbsf. The sympathetic variations exhibited by these two elements in this interval suggest that a different process controls their pore-water concentration. Between 70.6 and 268.8 mbsf, the Ca^{2+} concentration remains unchanged or increases slightly within a narrow range except for a large increase at 166.6 mbsf that also corresponds to the increase noted for Mg^{2+} (Fig. 26). From 268.8 mbsf downward, Ca^{2+} decreases, and near 450.0 mbsf reaches concentrations (9.8–10.1 mM) below normal seawater. The sharp decrease in concentration observed in the lower section of Site 760, which parallels that exhibited by Mg^{2+}, again reflects processes other than carbonate diagenesis. The coincidence of the sympathetic concentration drops with a return to a siliciclastic marginal-marine lithology below 210 mbsf (see "Lithostratigraphy," this chapter) suggests another change in the mechanisms affecting the concentration of these two elements.

Figure 26 also shows the downhole variations in the Mg^{2+}/Ca^{2+} ratio and reveals three major zones in which the Mg^{2+}/Ca^{2+} ratio exhibits relatively consistent trends. These are: (1) from the surface to 81.6 mbsf, (2) between 86.6 and 239.8 mbsf, and (3) from 322.4 to 439.4 mbsf. Each of these zones corresponds to intervals throughout which the lithology is somewhat uniform. In the first section the Mg^{2+}/Ca^{2+} ratio decreases abruptly due to decreases in Mg^{2+} and increases in Ca^{2+}. This is also observed in Hole 759B and probably reflects diagenesis of carbonate-rich sediments. The second zone shows a more gradual decrease in the Mg^{2+}/Ca^{2+} ratio controlled primarily by changes in the Mg^{2+} concentration and corresponds to a nonmarine environment

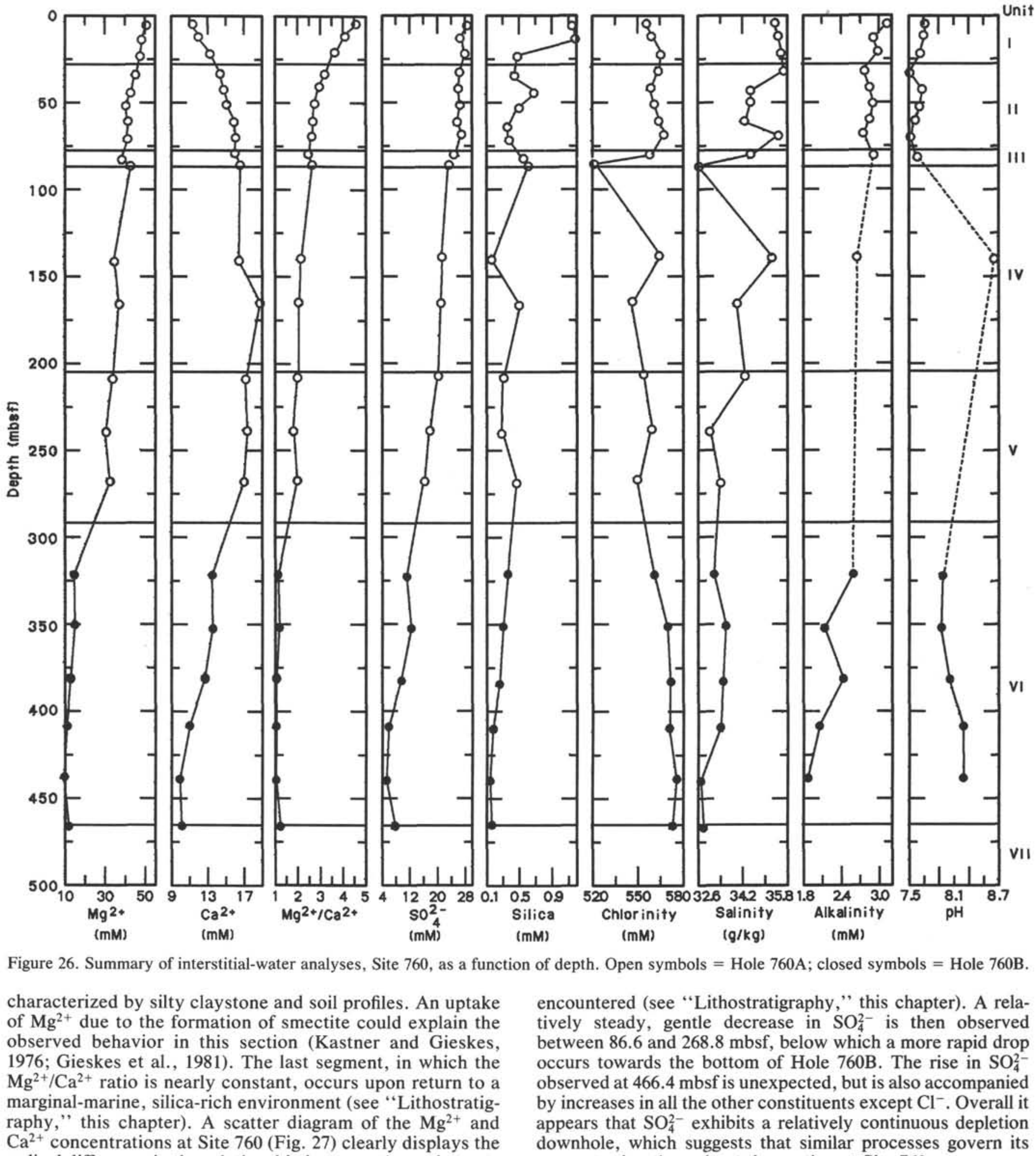

Figure 26. Summary of interstitial-water analyses, Site 760, as a function of depth. Open symbols = Hole 760A; closed symbols = Hole 760B.

characterized by silty claystone and soil profiles. An uptake of Mg^{2+} due to the formation of smectite could explain the observed behavior in this section (Kastner and Gieskes, 1976; Gieskes et al., 1981). The last segment, in which the Mg^{2+}/Ca^{2+} ratio is nearly constant, occurs upon return to a marginal-marine, silica-rich environment (see "Lithostratigraphy," this chapter). A scatter diagram of the Mg^{2+} and Ca^{2+} concentrations at Site 760 (Fig. 27) clearly displays the radical difference in the relationship between these elements in the upper portion of Hole 760A and lower part of Hole 760B.

Sulfate (SO_4^{2-})

Variations in interstitial water SO_4^{2-} concentrations at Site 760 are presented in Figure 26. Concentrations remain within 10% of seawater levels (28.9 mM) between 5.9 and 70.6 mbsf. A relatively sharp drop is then observed in the short interval from 70.6 to 86.6 mbsf, as Fe-rich and Mn-rich sediments are encountered (see "Lithostratigraphy," this chapter). A relatively steady, gentle decrease in SO_4^{2-} is then observed between 86.6 and 268.8 mbsf, below which a more rapid drop occurs towards the bottom of Hole 760B. The rise in SO_4^{2-} observed at 466.4 mbsf is unexpected, but is also accompanied by increases in all the other constituents except Cl^-. Overall it appears that SO_4^{2-} exhibits a relatively continuous depletion downhole, which suggests that similar processes govern its concentration throughout the section at Site 760.

Silica (SiO_2)

The concentration of silica generally decreases downhole at Site 760 (Fig. 26). In the first 14 m of Hole 760A, the concentration of SiO_2 lies between 1.1 and 1.2 mM. It then decreases abruptly to less than half this value by 23.1 mbsf, and exhibits considerable scatter between 0.164 and 0.688 mM down to 268.8 mbsf. The vastly differing concentrations of SiO_2 in the interstitial waters throughout this interval may

Table 7. Composition of interstitial water, Site 760.

Core, section, interval, (cm)	Depth (mbsf)	Vol. (cm^3)	pH	Alk. (mM)	Sal. (g/kg)	Mg^{2+} (mM)	Ca^{2+} (mM)	Mg^{2+}/Ca^{2+}	Cl^- (mM)	SO_4^{2-} (mM)	SiO_2 (mM)
122-760A-											
1H-4, 140–145	5.9	45	7.72	3.114	35.4	51.6	11.2	4.58	557	28.5	1.444
2H-4, 140–145	13.6	35	7.70	2.909	35.5	49.1	12.0	4.1	560	26.5	1.194
3H-4, 140–145	23.1	50	7.65	2.984	35.6	48.4	13.2	3.66	566	27.8	0.476
4H-5, 140–145	34.1	40	7.50	2.777	35.7	46.0	14.4	3.19	565	26.3	0.446
5H-5, 140–145	43.6	50	7.68	2.855	34.5	43.7	14.8	2.96	560	26.1	0.688
6H-5, 140–145	53.1	30	7.64	2.893	34.5	41.4	15.1	2.74	562	26.4	0.494
7H-5, 140–145	62.6	20	7.59	2.861	34.3	42.2	15.9	2.66	565	25.8	0.347
8H-4, 140–145	70.6	25	7.52	2.750	35.5	41.8	16.0	2.61	568	27.0	0.373
9H-5, 140–145	81.6	20	7.60	2.909	34.5	39.3	16.0	2.46	559	24.6	0.547
10X-2, 140–145	86.6	3			32.6	43.4	16.6	2.62	522	23.2	0.616
16X-4, 140–150	141.1	34	8.65	2.659	35.3	35.1	16.4	2.14	565	21.3	0.164
19X-2, 140–150	166.6	5			34.0	37.7	18.7	2.02	547	21.1	0.494
25X-4, 140–150	208.8	5			34.3	34.0	17.2	1.98	554	20.2	0.302
30X-5, 140–150	239.8	4			33.0	30.7	17.3	1.78	560	17.7	0.284
35X-3, 140–150	268.8	5			33.4	33.0	17.0	1.94	550	16.3	0.463
122-760B-											
10R-1, 140–150	322.4	10	7.95	2.583	33.2	15.0	13.4	1.11	561	11.1	0.358
13R-2, 140–150	352.4	30	7.92	2.150	33.6	15.5	13.5	1.14	570	12.4	0.295
16R-3, 140–150	382.4	14	8.04	2.446	33.5	13.2	12.7	1.04	572	9.5	0.261
19R-2, 140–150	409.4	10	8.22	2.065	33.4	11.3	11.0	1.03	572	5.9	0.168
22R-3, 140–150	439.4	10	8.22	1.886	32.7	10.0	9.8	1.02	576	5.2	0.136
25R-2, 140–150	466.4	3			32.8	12.4	10.1	1.23	574	7.8	0.159

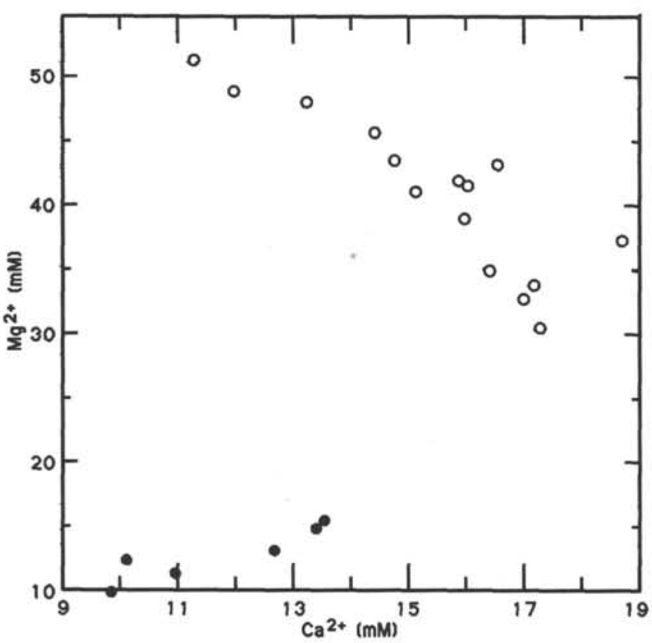

Figure 27. Scatter diagram showing the concentration (in mM) of Mg^{2+} versus Ca^{2+}, Site 760. Open symbols = Hole 760A; closed symbols = Hole 760B.

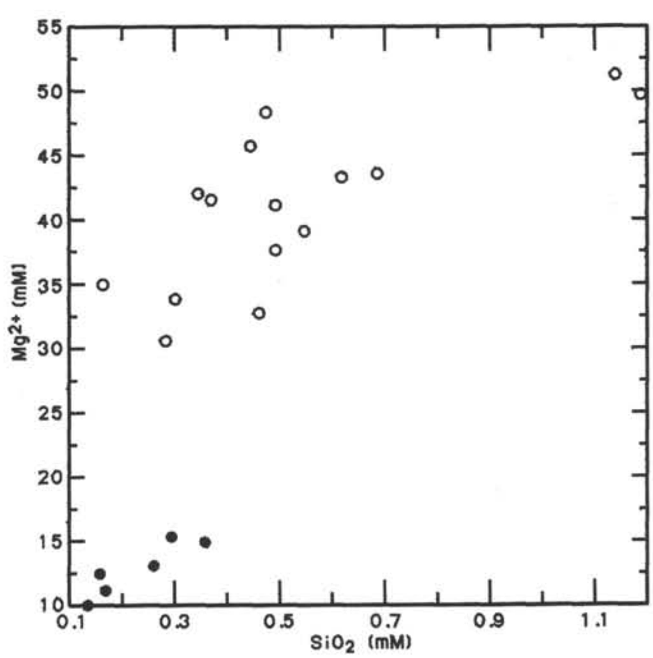

Figure 28. Scatter diagram showing the concentration (in mM) of Mg^{2+} versus SiO_2, Site 760. Open symbols = Hole 760A; closed symbols = Hole 760B.

reflect changes in the amount of amorphous SiO_2 present in the sediments of Hole 760A. No simple inverse relationship between SiO_2 and Ca^{2+} or alkalinity, which would reflect silica diagenesis (Gieskes, 1981), exists in the sediments drilled at Site 760. The weak inverse relationship between SiO_2 and Ca^{2+} observed in Hole 760A and their covariance in Hole 760B again suggest that different processes control the pore water chemistry in the shallow and deep sediments of Site 760. A scatter diagram of Mg^{2+} versus SiO_2 (Fig. 28) reveals two distinct correlations between these pore water constituents. Both relationships are consistent with the uptake of Mg^{2+} and silica during the formation of smectites (Kastner and Gieskes, 1976), but the slopes of the two lines indicate that different reactions may control the dissolved content of these constituents in the fluids.

Salinity and Chlorinity

The variability exhibited by the chlorinity and salinity at Site 760 is greater than that observed in Hole 759B (Fig. 26). The large decrease exhibited by both parameters at 86.6 mbsf occurs below an unconformity that is characterized by a lithological change, from a Mn-rich environment (Unit III) to a restricted marginal-marine silty claystone with soil-profile zone (Unit IV) (see "Lithostratigraphy," this chapter). This

Table 8. Physical-property measurements, Hole 760A (APC cores).

Core, section, interval (cm)	Depth (mbsf)	V_{ph} (km/s)	V_{pv} (km/s)	Anisotropy (%)	Bulk density (g/cm^3)	Porosity (%)	Water content (%)	Grain density (g/cm^3)	Formation Factor horizontal	Formation Factor vertical	Shear strength (kPa)
122-760A-											
1H-2, 20	1.70	1.504			1.49	74.1	50.9	2.68	1.870	2.250	3.100
1H-4, 56	5.06				1.56	72.5	47.7	2.68	1.850	1.910	13.500
2H-2, 72	9.92	1.456			1.55	70.6	46.8	2.58	3.380	2.120	9.900
2H-4, 54	12.92	1.475			1.56	68.5	44.9	2.53	2.560	2.040	11.000
2H-6, 94	16.14	1.510			1.66	68.7	42.5	2.72	3.560	3.620	14.600
3H-1, 78	17.98	1.526									12.500
3H-3, 95	21.15	1.687			1.67	66.6	40.8	2.59	2.920	2.920	
3H-5, 62	23.82	1.537							2.280	2.070	
3H-6, 68	25.38				1.56	68.9	45.2	2.57			
4H-1, 27	26.97	1.569							2.100	1.910	
4H-1, 80	29.00				1.71	68.5	41.0	2.76			
4H-3, 75	30.45	1.552							2.120	2.330	
4H-4, 80	32.00				1.69	64.5	39.2	2.61			
4H-5, 75	33.45	1.558							2.380	2.260	
4H-6, 80	35.00				1.64	66.6	41.6	2.63			
4H-7, 20	35.90	1.557							2.520	1.990	
5H-2, 88	38.58	1.530			1.72	63.4	37.8	2.73	2.730	2.420	11.700
5H-4, 86	41.56	1.546			1.70	63.7	38.4	2.64	2.870	2.630	16.800
5H-6, 86	44.56	1.606			1.81	56.4	32.0	2.61	3.370	2.810	16.400
6H-2, 86	48.06	1.559			1.71	52.3	37.3	2.66	3.420	3.040	18.900
6H-4, 86	51.06	1.600			1.75	57.9	33.9	2.63	4.250	3.740	37.900
6H-6, 91	54.11	1.603			1.80	56.6	32.2	2.67	3.690	3.420	41.800
7H-2, 86	57.56	1.598			1.83	54.2	30.3	2.66	3.950	3.350	26.900
7H-4, 86	60.56	1.531			1.77	57.5	33.2	2.65	2.330	2.540	5.600
7H-6, 74	63.44	1.549			1.77	58.3	33.7	2.72	2.150		7.300
8H-2, 86	67.66	1.537			1.74	59.2	34.8	2.64	2.070	2.090	6.700
8H-4, 86	70.06	1.551			1.82	54.2	30.4	2.68	2.200	2.170	3.700
8H-6, 86	73.06	1.527			1.74	59.7	35.2	2.70	1.730	1.790	5.400
9H-2, 86	76.56	1.525			1.58	68.5	44.4	2.63	1.460	1.840	4.500
9H-4, 86	79.56	1.545			1.55	70.5	46.6	2.67	1.319	1.651	3.800
9H-6, 26	81.96				1.86	56.7	31.9	2.70			

sharp Cl^- concentration drop and salinity decrease are also accompanied by significant increases in dissolved Ca^{2+}, Mg^{2+}, and SiO_2 contrary to the normal trends exhibited by these species above and below this depth. The subsequent return to higher salinity and chlorinity at 141.1 mbsf in sediments interpreted to be of restricted marginal marine origin is puzzling but is consistent with the trends observed earlier. At 166.6 mbsf another drop in salinity and chlorinity is accompanied by increases in the three aforementioned species. Unusual concentration changes are observed in the lower segments of Holes 760A and 760B (Fig. 26). Between 5.9 and 239.8 mbsf a general covariance between salinity and chlorinity is observed, although the salinity changes also reflect the influence of changes in Mg^{2+} and Ca^{2+} concentrations. Below this interval, further slight decreases in salinity are accompanied by increases in the Cl^- concentration. These become particularly noticeable below 268.8 mbsf and correspond to Unit VI (see "Lithostratigraphy," this chapter). This behavior is somewhat intriguing, but the decreased salinity probably results in part from decreased Ca^{2+}, Mg^{2+}, and SO_4^{2-} concentrations. Further shore-based analyses will help elucidate the processes responsible for the observed differences in the salinities and chlorinities.

Alkalinity and pH

A generally decreasing trend in alkalinity (Fig. 26) is observed throughout Site 760. However, the paucity of data in Hole 760A below 141.1 mbsf and at the bottom of Hole 760B makes the interpretation of the alkalinity trend difficult, and does not allow predictions of mechanisms/processes to be made. The upper 86.6 m of Hole 760A is characterized by a gradual but irregular decrease in alkalinity, upon which are superimposed small increases and decreases. The pH of the interstitial waters (Fig. 26) also oscillates in a narrow range between 7.50 and 7.72 in the upper 86.6 m of this hole. At 141.1 mbsf an unexplained radical increase to pH 8.65 was observed. This value was rechecked several hours later, and a slightly decreased value of pH 8.5 indicates that the first observation was correct. No other measured pore-water constituent displayed such an anomalous change at this depth. In Hole 760B the pH gradually increases from 7.95 to 8.22 between 322.4 and 439.4 mbsf. The higher pH exhibited in this section of Site 760 further suggests that different chemical processes control the composition of the interstitial waters at the bottom of Hole 760B.

PHYSICAL PROPERTIES

Introduction

Site 760 consists of two holes 20 m apart, so the results of the physical-property measurements from both holes are presented together. Use of the APC at Hole 760A (in contrast to the previous site) allowed continuous and undisturbed core recovery down to 83.7 mbsf (Core 122-760A-9H). This permitted GRAPE (gamma ray attenuation porosity evaluator) and *P*-wave velocity measurements to be made. Below this depth, drilling continued with the XCB. Because XCB drilling breaks the cored sediment into discontinuous "biscuits" of smaller diameter than the liner, use of the GRAPE and *P*-wave logger was halted. Resistivity measurements were taken for Hole 760A until the sediment became so resistive that no reading was registered by the equipment. Hole 760B was rotary drilled with the RCB, so only velocity, index properties, and a few thermal conductivity values were measured. The values of the various physical properties are listed in Tables 8–10 and their downhole trends are illustrated in Figures 29 to 32.

Other routine physical-property measurements from both holes include compressional wave velocity, velocity anisotropy, thermal conductivity, and the index properties (wet-

Table 9. Physical-property measurements, Holes 760A (XCB cores) and 760B (RCB cores).

Core, section, interval (cm)	Depth (mbsf)	V_{ph} (km/s)	V_{pv} (km/s)	Anisotropy (%)	Bulk density (g/cm^3)	Porosity (%)	Water content (%)	Grain density (g/cm^3)
122-760A-								
10X-2, 84	86.04	1.685	1.673	0.715	1.95	49.9	26.3	2.70
10X-4, 18	88.38				1.90	50.3	27.1	2.64
11X-1, 70	93.90	1.651			1.82	56.2	31.7	2.61
12X-1, 88	103.51				1.97	45.3	23.5	2.58
12X-2, 58	104.78	1.671			1.96	49.1	25.6	2.66
13X-1, 87	113.07	1.681	1.719	−2.235	2.01	44.7	22.7	2.65
14X-1, 19	116.39	1.728	1.767	−2.232	2.05	41.1	20.5	2.67
16X-2, 120	137.90	1.742	1.819	−4.325	2.07	42.5	21.0	2.72
16X-4, 89	140.59	1.769	1.827	−3.226	2.05	40.1	20.0	2.61
17X-1, 65	145.35	1.918	1.899	0.996	2.17	28.9	13.6	2.57
18X-10, 4	163.74	1.602						
19X-1, 55	164.25				1.94	41.8	19.8	2.71
19X-2, 88	166.08				2.02	46.6	23.6	2.69
20X-2, 11	174.81				1.94	43.7	23.3	2.60
20X-2, 134	176.04				2.00	44.2	22.6	2.63
21X-1, 27	182.97	1.807			1.98	41.4	21.4	2.54
21X-1, 74	183.44				2.00	42.8	21.9	2.62
22X-2, 57	188.97	1.841			2.12	35.9	17.4	2.63
22X-3, 31	191.21				2.07	47.0	23.2	2.78
23X-1, 18	193.08	1.732	1.724	0.463	2.05	43.3	21.6	2.77
24X-1, 75	198.65				2.07	44.0	21.8	2.72
25X-3, 31	206.21	1.839			2.01	46.3	23.7	2.70
26X-1, 106	208.96	1.974	2.056	−4.069	2.14	36.3	17.4	2.64
26X-3, 21	211.11	1.934			2.16	36.3	17.2	2.67
27X-1, 145	213.35		1.674		1.88	50.2	27.3	2.63
27X-3, 21	216.11		4.041			12.3	3.8	
28X-3, 103	221.93	1.743			2.13	39.5	19.7	2.70
28X-1, 106	218.96	1.847						
29X-4, 50	227.90	1.842			2.06	42.4	22.0	2.65
30X-1, 32	232.72	1.681			1.95	46.8	24.9	2.69
30X-7, 10	241.50	1.857			2.09	41.4	21.0	2.70
31X-1, 54	242.44	1.705			1.85	52.8	30.4	2.59
31X-3, 142	246.32	6.699			2.65	2.3	0.9	2.67
31X-3, 54	245.44	1.842			2.19	36.3	17.5	2.72
33X-1, 34	254.74	1.737			2.19	37.8	18.7	2.68
33X-4, 80	259.70	1.718			1.96	45.2	24.2	2.62
34X-1, 91	260.31	1.830			2.15	39.6	19.6	2.73
35X-4, 87	269.77	1.845			1.97	40.2	21.7	2.46
35X-2, 76	266.66	1.790			1.97	40.2	21.7	2.46
36X-2, 2	270.92	1.778			2.12	26.7	11.3	2.66
37X-2, 14	280.54	1.924			2.08	34.9	17.2	2.62
37X-5, 12	284.02	1.874			2.14	35.6	17.4	2.66
38X-1, 18	284.08	5.134			2.86	28.5	13.4	2.63
122-760B-								
2R-1, 57	90.47	1.721	1.729	−0.464	1.95	45.0	23.8	2.66
3R-1, 114	100.54	1.715	1.678	2.181	1.94	50.3	27.8	2.67
4R-1, 68	109.58	1.828	1.931	−5.480	2.07	40.4	20.6	2.66
6R-1, 16	283.16	4.663	3.906	17.668	2.76	13.3	5.1	2.92
6R-2, 99	285.49	2.005			2.07	41.1	21.0	2.67
7R-1, 148	293.98	1.959			2.08	39.5	20.0	2.64
7R-3, 28	295.78	3.878			2.67	13.0	5.2	2.80
8R-1, 63	302.63	1.864	1.888	−1.279	2.09	37.5	19.0	2.60
8R-3, 63	305.63	5.760	5.609	2.656	2.79	1.9	0.7	2.70
9R-2, 14	313.14	1.918	1.927	−0.468	2.11	41.1	20.9	2.69
10-1, 103	322.03	1.985	1.889	4.956	2.08	37.6	18.8	2.63
11R-1, 27	330.77	1.873	1.812	3.311	1.97	49.5	26.7	2.73
11R-2, 88	332.88	2.064	2.027	1.809	2.11	41.5	20.9	2.73
12-1, 119	341.19	2.114			2.14	38.2	18.5	2.76
12R-3, 81	343.81	2.054	1.836	11.208	2.33	35.4	17.9	2.55
13R-1, 122	350.72	2.057	1.941	5.803	2.10	35.5	17.9	2.57
13R-2, 41	351.41	2.206	2.137	3.178	2.21	30.3	14.4	2.62
14R-2, 29	360.79	3.873	3.956	−2.120	2.63	12.0	4.8	2.76
15R-1, 17	336.99	2.144	1.968	8.560	2.26	36.8	18.5	2.61
15R-1, 49	368.99	4.545	4.803	−5.520	2.58	9.5	3.8	2.71
16R-1, 134	379.34	4.900	4.813	1.791	2.64	8.0	3.1	2.76
16R-4, 69	383.19	2.088			2.28	33.8	16.3	2.67
17R-1, 8	387.58	2.665	4.685	−0.428	2.73	4.3	1.6	2.72
17R-2, 58	389.58	5.484	5.467	0.310	2.69	1.8	0.7	2.68
17R-3, 84	391.34	2.043	1.969	3.689	2.15	32.4	15.7	2.63
18R-2, 33	398.83	4.181	4.130	1.227	2.57	6.4	2.6	2.66
19R-1, 72	407.22	1.988	2.004	−0.802	2.20	34.0	16.3	2.69
19R-3, 98	410.48	1.996	2.113	−5.695	2.16	34.6	16.8	2.66
20R-1, 127	417.27	2.003	2.004		2.16	35.2	16.7	2.66
20R-3, 142	420.42	2.112	2.031	3.910	2.16	36.8	18.0	2.69

Table 9 (continued).

Core, section, interval (cm)	Depth (mbsf)	V_{ph} (km/s)	V_{pv} (km/s)	Anisotropy (%)	Bulk density (g/cm^3)	Porosity (%)	Water content (%)	Grain density (g/cm^3)
21R-4, 57	430.57	2.249	2.064	8.579	2.31	30.8	13.7	2.85
21R-3, 50	429.00	4.722	4.608	2.444	2.61	4.7	1.8	2.68
22R-1, 26	435.26	5.558	5.560	−0.036	2.78	1.4	0.5	2.77
22R-4, 127	440.77	2.255	2.216	1.745	2.17	33.0	15.8	2.66
23R-1, 145	445.95	2.235	2.091	6.657	2.21	29.2	13.8	2.61
23R-3, 50	448.00	2.276	2.298	−0.962	2.23	27.0	12.5	2.61
25R-1, 17	463.67	4.833	4.523	6.627	2.70	4.7	1.8	2.71
25R-2, 23	465.23	2.165			2.37	23.2	10.4	2.65
26R-3, 17	471.17	2.132	2.032	4.803	2.22	29.4	14.1	2.59
27R-3, 74	481.24	2.240	2.140	4.566	2.29	30.7	13.7	2.65
28R-2, 76	489.26	2.226	2.201	1.129	2.23	27.3	12.5	2.61
28R-4, 64	492.14	2.305	2.169	6.080	2.24	25.9	11.9	2.59
29R-1, 8	496.58	2.120	2.013	5.178	2.13	34.9	16.8	2.59
29R-3, 116	500.68	2.188	2.226	−1.722	2.16	35.8	17.0	2.68

bulk density, grain density, porosity, and water content; see "Explanatory Notes," this volume).

Velocity

The velocity data from Site 760, determined with the Hamilton Frame (Fig. 29), show a range from 1.46 km/s (oozes) to 6.7 km/s (carbonate-cemented sandstone). As at the previous site, the range of sediment velocity values is very large. There appears to be a distinct bimodal distribution of the velocities (Fig. 30) between: (1) limestones and carbonate-cemented sandstones and claystones (fast), and (2) the less-lithified claystones and oozes (slow). The velocity gradient for the slower group is about 1 m/s per meter and is linear. Alternating fast and slow lithologies provide a uniquely contrasting set of physical properties. Claystone velocities at the bottom of Hole 760B are similar to those of Hole 759B (about 2.1–2.2 km/s).

The first occurrence of a high-velocity layer is at about 216 mbsf (Section 122-760A-27X-3) in a thin carbonate-cemented claystone (siderite, V_{pv} = 4.04 km/s). There is a minor velocity increase at about 80 mbsf below a manganese crust layer encountered in Section 122-760A-9H-5. The change is from an average of about 1.55 km/s to about 1.65 km/s. Velocity anisotropy data (Fig. 29) show almost no scatter and no consistent trend with depth.

Index Properties

From the seafloor to about 120 mbsf there is a general increase of the bulk density with depth (Fig. 29). Between 120 mbsf and the bottom of the hole the finer-grained components (i.e., oozes, claystones, and siltstones) increase in bulk density with depth, although with a much smaller average gradient than in the shallower portion. Near an unconformity marked by a manganese crust (at approximately 80 mbsf) the density values are perturbed. There is a local minimum in the densities above the crust and a local maximum below the crust.

Wet-bulk densities vary from as little as 1.5 g/cm^3 (oozes in the upper part of the section) to as much as 2.86 g/cm^3 (bioclastic limestone). The oozes do not exceed 1.82 g/cm^3 and the uncemented claystones and siltstones can range up to 2.02 g/cm^3. Values are lower than for similar lithologies measured at Hole 759B. The high-velocity rocks also have the highest wet-bulk density (2.6–2.8 g/cm^3) reflecting the high carbonate content (see "Organic Geochemistry," this chapter). Low values in wet-bulk density (Fig. 29) reflect the high porosity and water content of the oozes above about 80 mbsf, as well as the low grain density of the claystones and/or siltstones below 80 mbsf (2.1–2.3 g/cm^3).

Reduction in water content (51%–21%) and porosity (74%–41%) with depth is greatest between the seafloor and about 120 mbsf. Below this depth, the carbonate-rich sediments show consistently low values of porosity (1%–12%); the claystones and siltstones show a gradually decreasing trend in the porosity (41%–36%), paralleled by a drop in the water content (21%–17%). These two trends are analogous to the trends seen in the wet-bulk density. Quaternary carbonate oozes near the top of the hole contain high porosities of 60%–75% and water contents of around 45%. Clastic sediments display a gradual downhole decrease from water contents of 25%–30% and porosities of 45%–50% at 41 mbsf, to water contents of 10%–15% and porosities of 25%–35% at 305 mbsf. Grain densities throughout the section vary between 2.46–2.92 g/cm^3, with no consistent trend.

A few meters above the manganese crust (80 mbsf) there are local highs in water content (46.6%) and porosity (70.5%). Below this depth the reverse is true, with local lows in water content (26.3%) and porosity (49.9%).

Thermal Conductivity

Thermal conductivity (Fig. 29) ranges from 0.829 to 3.117 W/m·K between 2 and 467 mbsf. Values for the last four samples are from bioclastic limestones from Hole 760B and are widely spaced. The other measurements were made on APC cores from Hole 760A (0.0–83.7 mbsf); in general, every other core was measured. Below this depth, deployment of the XCB tended to break the cores within the liner, and measurements are less reliable. In general, thermal conductivity tends to increase with depth and the more compact materials (carbonates) are two to three times more conductive than the oozes.

Shear Strength and Formation Factor

Shear strength (Fig. 31A) and formation factor (Fig. 31B) both attain maximum values between 51 and 57 mbsf (Sections 122-760A-6H-4 to -7H-2). Shear strength increases from about 13 kPa near 40 mbsf to 41.8 kPa at 54 mbsf. It then decreases rapidly to about 6 kPa near 60 mbsf. The horizontal formation factor increases from 2.7 kPa near 40 mbsf to 4.3 kPa at 51 mbsf. It then decreases to 2.3 kPa near 60 mbsf. Both properties show a minor decrease from 60 to 80 mbsf, at which point data collection was halted. Similar smaller-scale local maxima appear between 0 and 20 mbsf. The remaining index properties are relatively insensitive to these trends. Correlation of the shear strength and resistivity maxima with porosity suggests that the oozes show varying

Table 10. Thermal conductivity measurements, Holes 760A and 760B.

Core, section, interval (cm)	Depth (mbsf)	Thermal conductivity (W/m·K)
122-760A-		
1H-2, 70	2.20	1.067
1H-3, 70	3.70	0.829
1H-4, 70	5.20	1.112
1H-5, 70	6.70	1.158
3H-2, 70	19.40	1.319
3H-3, 70	20.90	1.460
3H-4, 70	22.40	1.257
3H-5, 70	23.90	1.325
5H-3, 70	39.90	1.423
5H-4, 70	41.40	1.350
5H-5, 70	42.90	1.411
5H-6, 70	44.40	1.559
7H-2, 66	57.36	1.579
7H-3, 66	58.90	1.491
9H-5, 66	61.90	1.532
9H-2, 111	76.80	1.232
9H-3, 107	78.30	1.223
9H-4, 85	79.60	1.234
9H-5, 62	80.80	1.391
10X-2, 65	85.90	1.514
10X-3, 65	87.40	2.081
11X-1, 65	93.30	1.160
13X-1, 65	112.90	2.202
13X-10, 15	116.40	1.698
16X-1, 90	136.10	1.642
16X-2, 90	137.60	1.762
19X-1, 117	164.90	2.025
19X-2, 66	165.90	1.575
19X-3, 26	166.90	2.330
22X-1, 117	188.60	1.697
22X-2, 66	190.10	2.064
22X-3, 26	191.42	1.757
23X-2, 41	194.80	1.819
24X-1, 41	198.30	1.772
26X-1, 41	208.30	1.692
26X-2, 41	209.80	2.361
27X-1, 41	213.30	1.296
27X-2, 41	214.80	1.636
28X-2, 61	220.60	1.874
28X-3, 39	221.30	1.543
28X-4, 65	223.10	2.256
29X-2, 30	224.70	1.972
29X-3, 65	226.60	2.061
29X-4, 30	227.70	2.453
31X-1, 57	242.50	1.227
31X-2, 52	243.90	1.582
31X-3, 51	245.40	1.901
31X-4, 47	246.90	1.454
33X-1, 66	255.10	1.630
33X-2, 66	256.60	1.898
33X-3, 66	258.10	2.423
33X-4, 66	259.60	2.344
35X-2, 36	267.80	1.552
35X-3, 38	269.40	1.701
35X-4, 36	270.70	1.677
37X-1, 75	279.70	1.600
37X-2, 75	281.10	1.970
37X-3, 75	282.60	1.746
122-760B-		
8R-2, 70	304.20	2.218
13R-1, 46	349.96	3.117
14R-2, 34	360.84	2.303
25R-1, 39	463.89	1.745

degrees of stiffness and electrical conductivity, perhaps in response to differences in the state of diagenesis.

GRAPE and *P*-wave Logger

P-wave logging was stopped with the last APC core at about 80 mbsf (Core 122-760A-9H) (Fig. 32A). However, GRAPE density measurements (Fig. 32B) were continued down to approximately 113 mbsf (Core 122-760A-13X) as they were less affected by XCB drilling disturbance. GRAPE bulk-density measurements agree well with gravimetric bulk densities, as do the *P*-wave logger compressional wave velocities with the Hamilton Frame *P*-wave velocity measurements. A slight departure between the two velocity data sets is seen in Figure 32A between 2 and 16 mbsf (Section 122-760A-2H-6). Coincidence between velocities and densities attests to real small-scale variability in the sediments (on the order of a few meters). Just as the drop in density is related to the unconformity at about 80 mbsf, so may the other variations be related to changes in sediment rates or diagenesis.

Heat Flow

A single temperature-probe measurement (at 74.2 mbsf) was made in Hole 760A to check the equipment in preparation for the holes to be drilled on the Wombat and Exmouth plateaus, and to provide information for a comparison of the thermal properties of the two plateaus. The sea state was calm, and the probe stayed at the mudline for 5 min on both the ascent and descent, remaining on the bottom for 10 min. Although the temperature record shows a normal profile of initial heating after insertion, followed by gradual decay toward equilibrium, the mudline temperature of 10.7°C and the bottom temperature of 12.7°C (Fig. 33) are regarded as too high and indicative of incorrect insertion of the probe. No temperature gradient or heat flow data were calculated at Site 760.

Summary

Physical properties show a wide range of values and clearly distinguish the major rock types at Site 760 (limestone, siltstone/claystone, and nannofossil ooze). Contrasting lithologies create a bimodal distribution between slow and fast (denser) rocks. Carbonate cement can affect the physical properties of claystones by increasing their measured velocities and densities. Shear strength and formation factors are easily affected by subtle changes in compaction otherwise undetected by physical-property measurements. The observed increase in velocities below the manganese crust could be a result of the removal of lower-velocity material through erosion. A higher porosity above the manganese crust may indicate an accelerated sedimentation rate. The change in both the velocity and sedimentation rate could be related to the detected unconformity (see "Biostratigraphy," this chapter).

SEISMIC STRATIGRAPHY

See "Seismic Stratigraphy," Site 764 chapter, for a combined report of Sites 759, 760, 761, and 764.

DOWNHOLE MEASUREMENTS

Operations

Logging operations at Hole 760B began at 1200 hr (all times given in local time) on 17 July 1988 with hole conditioning and bit release. At 1910 hr, the seismic stratigraphic tool combination was rigged up. At this site the tool string consisted of long spaced sonic (LSS), phasor induction (DIT-E), natural gamma spectroscopy (NGT), caliper (MCD), and accelerometer (GPIT). Telemetry problems forced the change out or removal of the telemetry cartridge, GPIT, and cable head (in that order). At 2350 hr, the tool string was lowered into the pipe. A bridge was encountered at 178.2 mbsf and the decision was made to log up to the pipe.

The time remaining allowed for only one or two runs with the same tool combination. To obtain the maximum amount of

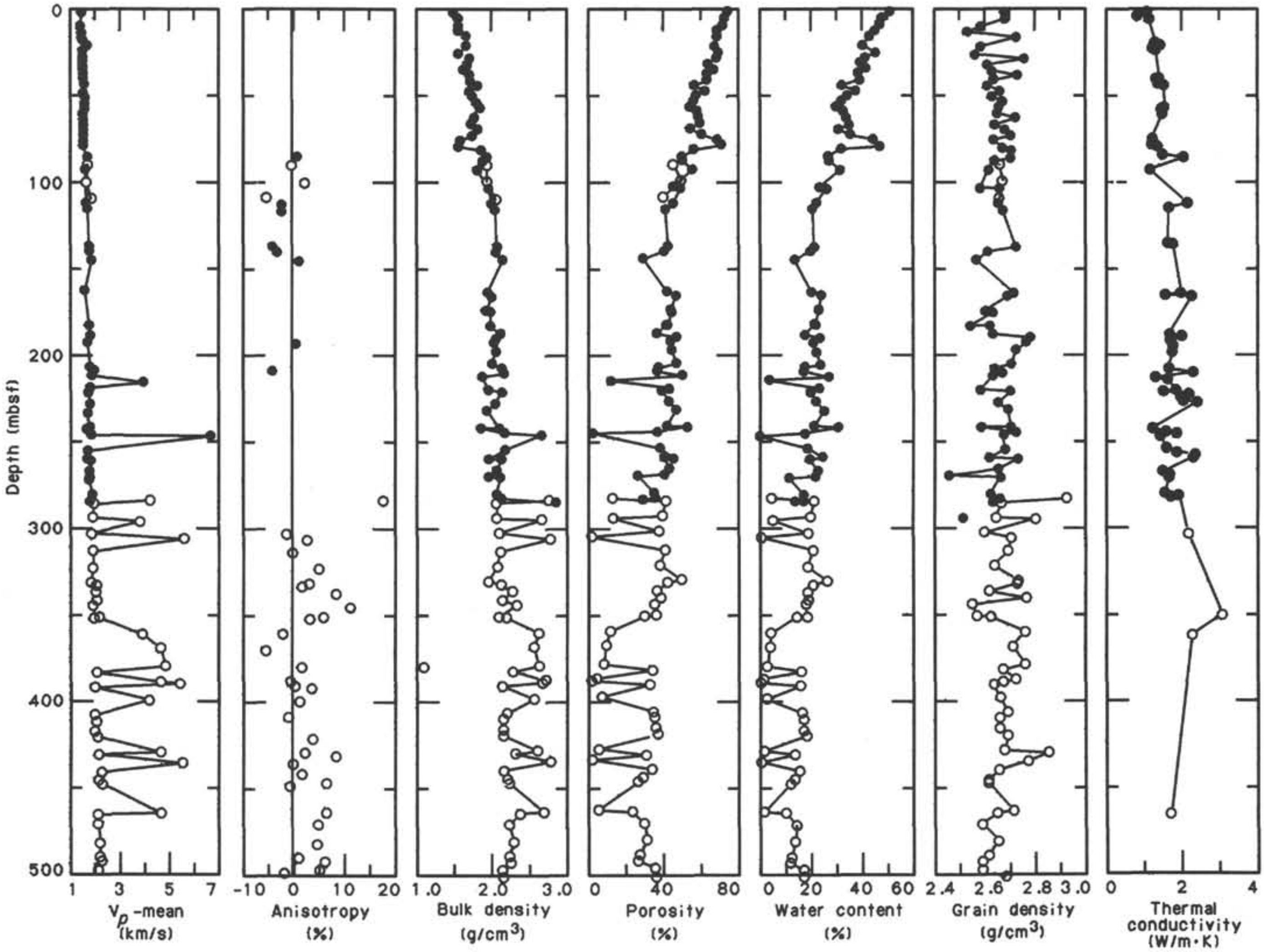

Figure 29. Physical-property data from Site 760 (mean compressional velocity from Hamilton Frame measurements, velocity anisotropy, wet-bulk density, porosity, water content, grain density, and thermal conductivity). Closed symbols = Hole 760A; open symbols = Hole 760B.

data from the logging run, the neutron porosity tool (CNL) was added to the tool string. After a wiper trip, the tool string was lowered into the pipe. A bridge was encountered at 184 mbsf, 9 m lower than before. The open hole was logged from 184 mbsf to the base of the pipe (63 mbsf), and from 63 to 50 mbsf through the pipe. The drill pipe was lowered to 208 mbsf. At 1505 hr, the tool string was run into the hole; a bridge was encountered at 217 mbsf. The hole was logged through the pipe to 90 mbsf. Logs were obtained from 151 m of open hole out of a possible 506 m of hole.

Rig-down of the logging tools was completed at 1830 hr on 18 July. In all, 12.5 hr were used for hole conditioning and 18 hr were used for logging. The heave compensator was not used because seas were flat.

Log Quality

Logs obtained with the seismic stratigraphic tool string included interval transit times, shallow, medium, and deep formation resistivity, total gamma radiation plus potassium, thorium, and uranium concentrations, neutron porosity, and hole diameter. Operating principles and details of the measurements are discussed in the "Explanatory Notes" (this volume).

All logs except long-spaced traveltimes (DTLF) were of good quality. Replicability of results was generally very good, as indicated by agreement between repeat sections from the first (63–176 mbsf) and second (63–184 mbsf) passes with the tool string.

The tool string was also run in the drill pipe from 85 to 206 mbsf. The total gamma-ray signal measured through the pipe was attenuated, but follows the trends observed in the open-hole log (Fig. 34). Attenuation of the gamma-ray signal was approximately 74% in the bottom hole assembly (2-in.-thick pipe) from 206 to 123 mbsf, and approximately 40% in the 5.5-in. pipe (0.5 in. thick, from 123 to 85 mbsf). The neutron porosity log reads higher porosities in the pipe than in the open hole by approximately 5%, but exhibits the same pattern in the pipe as in the open hole.

Log Responses of Lithologic Units

Open-hole logging began at 63 mbsf in nannofossil ooze (Unit II, 21–80 mbsf). Low gamma-ray values and high porosities characterize this interval. The high porosities are evident on the three logs that respond primarily to porosity: resistivity, neutron porosity, and velocity logs. The base of the nannofossil ooze (80 mbsf) is marked by an unconformity

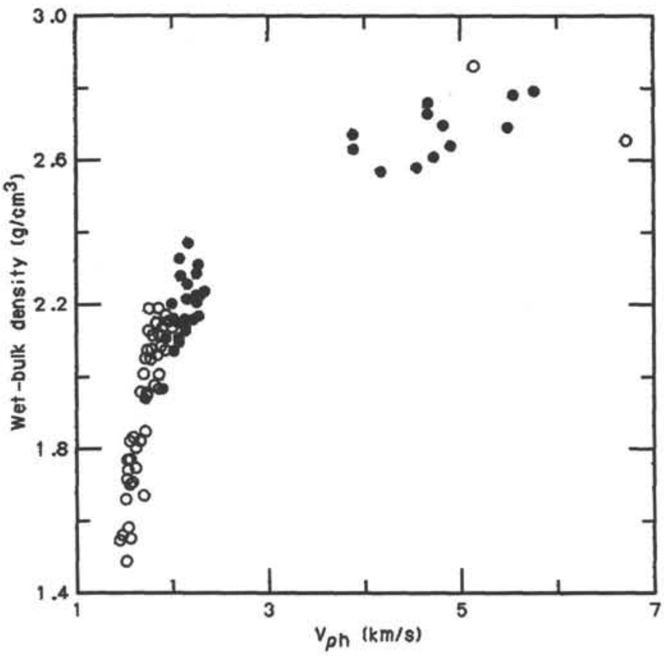

Figure 30. Wet-bulk density (g/cm^3) versus horizontal compressional velocity (km/s) for samples from Site 760. Open symbols = Hole 760A; closed symbols = Hole 760B.

and is underlain by a sequence of sandstones and siltstones (Unit III). The unconformity is visible on the logs as a sudden baseline shift in the resistivity and gamma-ray signal at 81 mbsf. Velocity and porosity remain essentially unchanged across the boundary. Instead, both velocity and porosity decrease gradually with depth, reflecting the effect of compaction. The alternating sandstones and siltstones observed in the cores (e.g., Cores 122-760A-8H and -9H) are characterized by alternating high and low gamma-ray values and variable porosity.

The hardground observed at 81.2 mbsf (see "Lithostratigraphy," this chapter) cannot be identified on the logs, probably because the 40-cm-thick interval is beyond the limits of the vertical resolution of the logging tools. An unconformity at the base of Unit III (80–87 mbsf) is marked by a sharp increase in gamma-ray values, an increase in resistivity and velocity, and a decrease in porosity.

Unit IV (87–210 mbsf) consists of silty claystone, clayey siltstone, and silty sandstone. Typically, the claystone sections exhibit a relatively high gamma-ray signal (80–100 API units), increased thorium and uranium levels, and velocities between 1.7 and 2.0 km/s. The silty sandstones are identified by low gamma-ray values, with corresponding low resistivity and velocity readings for unconsolidated sandstone, and high resistivity and velocity and low porosity for cemented sandstone.

On the basis of log responses alone, Unit IV is subdivided into three subunits or cycles: (1) from the top of Unit IV (87 mbsf) to 127 mbsf, (2) 127–151 mbsf, and (3) from 151 mbsf to the bottom of the logged interval (170 mbsf).

The bottom of each subunit is marked by high (65%–70%) porosities and very low gamma-ray values (18–30 API units), resistivity, and velocity values (Figs. 35 and 36). The log responses suggest a relatively clean, unconsolidated sand at this interval. The sand is overlain by alternating sand and clay, as indicated by the shifts in the gamma-ray and velocity logs. The porosity alternates from high (65%) in the sands to low (45%) in the clays in the lower section of each subunit, and

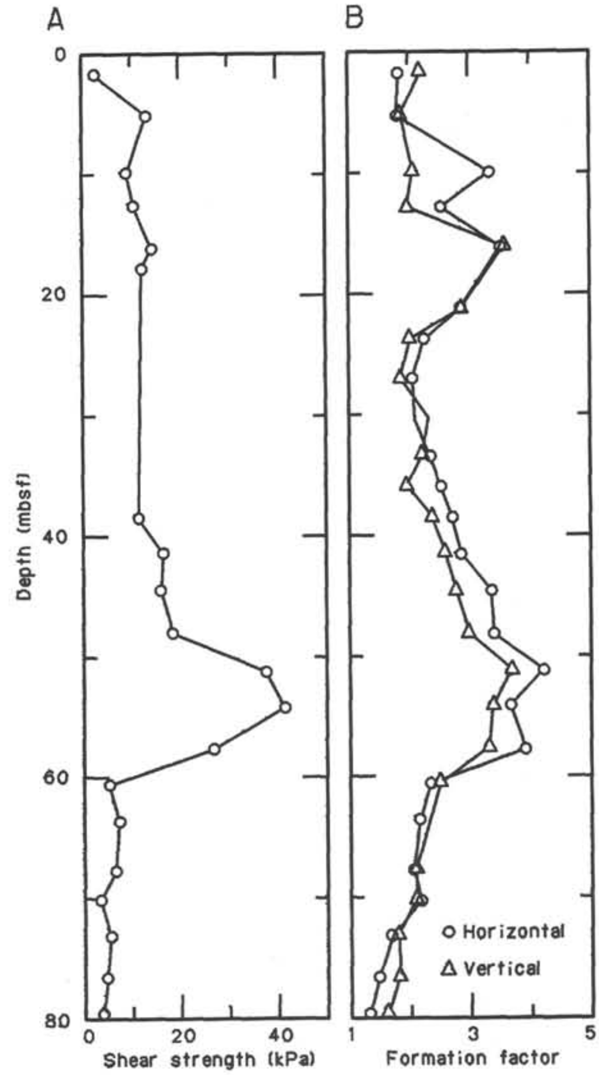

Figure 31. Physical-property data from Hole 760A. **A.** Shear strength. **B.** Formation factor (circles = horizontal; triangles = vertical).

remains low (40%) in the upper section, independent of the lithology (Fig. 35). The top of each subunit is punctuated by a pronounced increase in gamma-ray values (105–130 API units) and increased thorium count. Velocity and resistivity exhibit significant increases as well. All but the top of the first subunit (87 mbsf) were poorly recovered. The lithology of the sediments recovered from this interval was silty clay with root mottling and oxidized pebbles. Sand and silty sandstones were recovered above the soil horizon at 87 mbsf. The log responses suggest that the sand overlies a hard surface with high clay content, low porosity, and high radioactivity. The log response is essentially similar to that in Hole 759B at 139 mbsf, which was also marked by high gamma-ray and thorium counts. Because core recovery at Site 759 was poor in this interval, this horizon was interpreted from the logs as a siltstone or placer deposit containing thorium-bearing heavy minerals (e.g., zircon, tourmaline, and/or rutile).

Two other subunits or cycles are indicated by neutron porosity and gamma-ray responses. The lower boundaries of these cycles occur at 169 and 195 mbsf. The log response at these intervals exhibits a sharp decrease in neutron porosity and gamma-ray signal, as was observed at the base of the

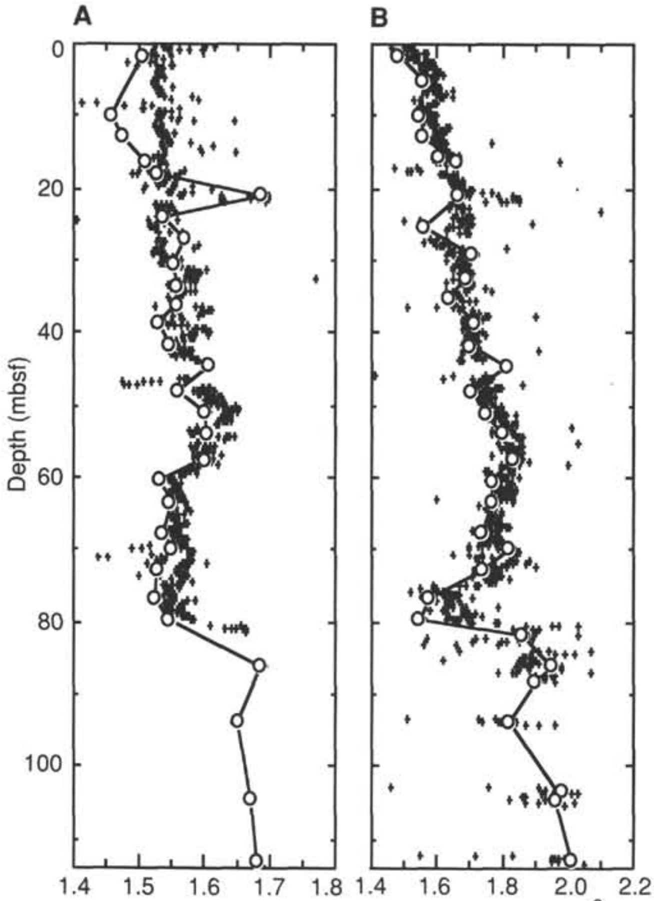

Figure 32. **A.** *P*-wave logger velocity measurements from Hole 760A (crosses) plotted versus depth, together with the Hamilton-Frame-derived velocities (open circles connected by lines). **B.** GRAPE wet-bulk density estimates (crosses) plotted versus depth, together with the gravimetric wet-bulk density index property values (open circles connected by lines).

other subunits. Sonic and resistivity logs do not extend deep enough to confirm the interpretation of the lower two cycles.

Summary

The logged section can essentially be divided into two facies associations. Above 80 m, a deep-water carbonate environment is prevalent, separated from the underlying association by a 40-cm-thick manganese crust (not apparent on the logs). High gamma-ray values and low velocities below 80 mbsf suggest that the sediments are fine-grained and were deposited in a restricted, low-energy environment (Serra, 1986). This is supported by rootlets in the cored mudstone intervals and a lack of marine fauna.

Log interpretation allows the sequence below 80 m to be divided into upward-shoaling sandstone to mudstone cycles, succeeded by a subaerial or swamp environment (see "Lithostratigraphy," this chapter). Each cycle therefore results in an upward facies transition from lagoonal to tidal-flat type sediments, capped by marsh deposits or soil horizons.

SUMMARY AND CONCLUSIONS

Introduction

Site 760 (proposed Site EP10A′) is located at the top of Wombat Plateau, near its southeast edge and close to the steep escarpment facing Montebello Canyon. It lies about 5 km north northwest (and downdip) of Site 759, at 16°55.32′S, 115°32.48′E, and at a water depth of 1969.7 m. Hole 760A was continuously cored by APC to a depth of 83.9 mbsf, and by XCB to a depth of 284.9 mbsf. Hole 760B was rotary-cored between 89.9 m and 118.4 mbsf, washed between 118.4 and 283.0 mbsf, and cored from 283.0 mbsf to a total depth of 506 mbsf. The total recovery of both holes was about 320 m. Both holes were drilled and logged in about 5.5 days. The average recovery rate of Hole 760A was 69% (196.56 m), whereas that of Hole 760B only 48.9% (123.02 m). This low recovery underscores the pressing need to solve the technological problem of improved recovery in alternating hard (e.g., limestone) and soft (e.g., sand and mud) lithologies. Unfortunately, several attempts to log the hole (which would have helped to reconstruct the lithologic column in low-recovery intervals) failed because of severe bridging at possibly sandy horizons between 80 and 100 mbsf and below 150 mbsf. Only the seismic stratigraphic tool was run. Open-hole logs were obtained between 63 and 184 mbsf. Logs were obtained through the pipe from 50–63 mbsf and 90–206 mbsf.

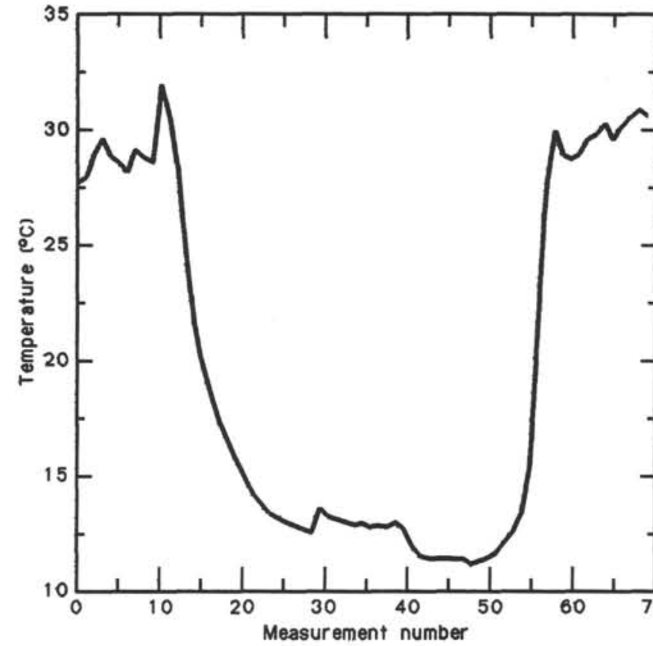

Figure 33. Temperature-versus-time record obtained with the temperature probe at 74.2 mbsf in Hole 760A.

The objectives of Site 760 were to retrieve the post-Norian Triassic (and possibly Jurassic) section that was missed at Site 759 owing to the deep truncation of the uplifted, tilted, southeastern part of the Wombat Plateau horst. In general, the background and objectives are the same as for Site 759 (see "Background and Objectives," Site 759 chapter, this volume). The discovery that the main unconformity at Site 760 was underlain by late Triassic sediments (although younger than those at Site 759) and not by Jurassic sediments was a surprise for the seismic interpreters and proponents of this site. This changed our original objectives, and prompted us to ask for permission to drill Site 761 (EP9E) 20 km north of Site 760 in order to recover the missing Jurassic record.

Site 760, nevertheless, recovered a valuable 506-m-thick record of late Carnian to Pleistocene age that was subdivided into seven lithologic units (see "Lithostratigraphy," this chapter). Here we only include the salient points of the stratigraphy and paleoenvironmental evolution as summarized

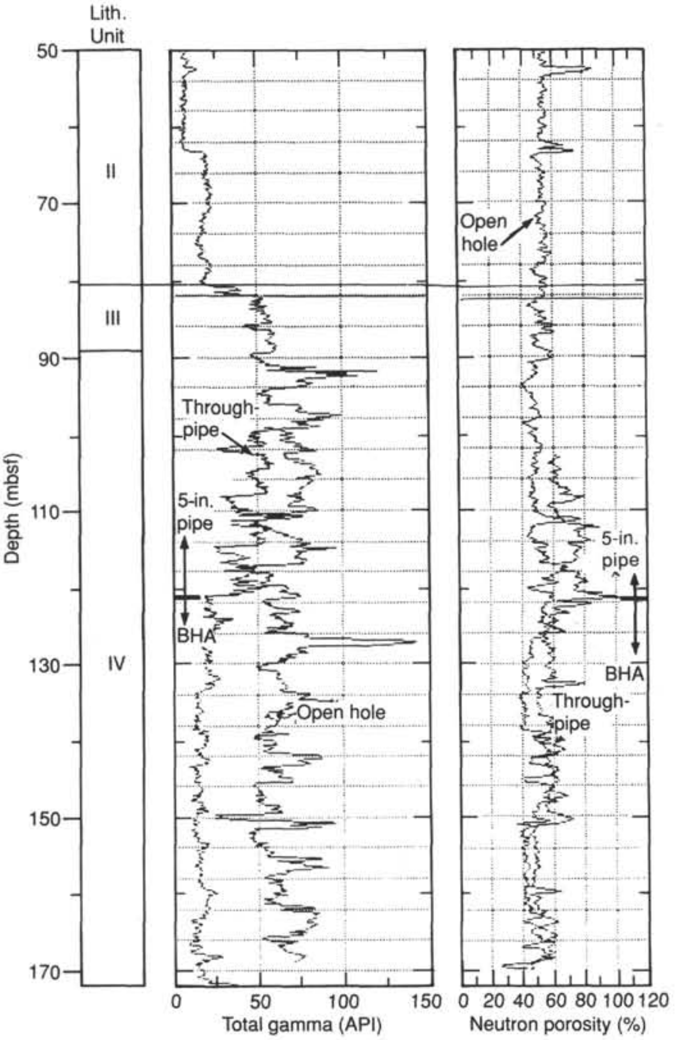

Figure 34. Neutron porosity and total gamma-ray spectrum logs from open-hole and through-pipe recordings at Hole 760B. Open-hole logs were obtained from 63–175 mbsf. Through-pipe logs were recorded from 50–63 mbsf and 90–206 mbsf. The gamma-ray log trend through the pipe and in the open hole is similar, but the signal from through-pipe measurements is attenuated. Neutron porosity readings are higher through the pipe than in the open hole, but follow the same trends.

in Figure 2B of the "Summary and Highlights" chapter, this volume (in back pocket). Obviously, the lack of downhole logging results for most of the hole makes the interpretation of the Triassic record (with its poor recovery) more ambiguous than that of Site 759.

Stratigraphy and Paleoenvironmental Evolution

Carnian Siliciclastic Deposition (Unit VII, 506.0–464.05 mbsf)

The oldest sediments recorded at Site 760 consist of black to dark-gray, mostly parallel-laminated silty claystones with minor silty sandstone intercalations, siderite beds, lenses and nodules, pyrite, and a few occurrences of mollusk-rich layers. The presence of coccoliths suggests an open-marine environment, and fine laminations (i.e., the absence of bioturbation and benthic life) indicate oxygen-depleted conditions in the rapidly deposited, organic-matter-rich near-surface sediments.

Two preliminary interpretations are offered for this paleoenvironment: (1) a protected, low-energy tidal flat or back-bay (lagoonal) setting (see "Lithostratigraphy," this chapter), or (2) an open-marine, deeper (>50–100 m?) prodelta setting. Soft-sediment deformation, slump structures, and siderite beds in Unit VII of Site 760 resemble the same features observed in Unit V of Site 759 (see "Summary and Conclusions," Site 759 chapter, this volume); the latter unit was interpreted to have been deposited in a distal prodelta environment. However, the mollusk horizons and the sandier sediment at the base of Unit VII of Site 760 differ from the characteristics of the correlative interval of Site 759. The final paleoenvironmental interpretation of this unit awaits detailed shore-based facies studies.

Carnian to Norian Deposition of Shallow-Water Carbonates and Siliciclastic Material (Unit VI, 464.05–284.9 mbsf)

The purely siliciclastic sedimentation (described above) was succeeded by the deposition of a very variable sequence of alternating shallow-water carbonates and paralic clayey, silty, and sandy sediments. In general, an upward-shallowing trend is observed between 506 mbsf (distal prodelta muds?) and 408 mbsf (lowermost coal occurrence), although this trend depends on the interpretation of the paleodepth of Unit VII. The lower part of this unit (from 460 to about 408 mbsf) contains calcite-cemented quartz sandstones, redeposited mollusk coquinas, algal limestones rich in red algae and dasycladaceans, and oncolitic/oolitic pelsparites rich in mollusks, corals, and other bioclasts. Only a detailed microfacies analysis will help to decipher the environmental significance of these limestones, which include mainly mud-dominated packstones, wackestones, carbonate mudstones, and minor grainstones.

In general, we infer a fluctuating shallow-marine, quiet, intertidal (lagoonal) carbonate-bank environment for these limestones. Of special significance is a conglomeratic limestone (rudstone) found at the top of Core 122-760B-19R (at 408 mbsf) near the Carnian/Norian boundary. This material might be downhole contamination from between 305 and 400 mbsf. This conglomerate contains 20% rounded pebbles (<5 mm long) of altered intermediate volcanic rocks and altered volcanic glass, as well as mollusks and algal limestone fragments, all of which are surrounded by algal (oncolitic) coatings. The conglomerate suggests the erosion of preexisting volcanic and carbonate rocks and their deposition in a high-energy shallow carbonate-bank environment. Rhaetian early-rift volcanics of trachytic to rhyolitic composition have been dredged from the northern Wombat Plateau (von Rad and Exon, 1983; von Rad et al., in press), and the described volcanic fragments might indicate an earlier (Norian) phase of early-rift volcanism in the area.

The sequence between 405 and 283 mbsf is characterized by the fluctuation between shallow-water (subtidal) carbonate environments (e.g., grainstones and wackestones with corals, ooids, peloids, thick-shelled species such as *Ostrea* sp. and *Gervillia* sp., etc.) and intertidal (lagoonal to back bay) settings, characterized by dolomites, algal mats, and mudstones containing mollusks and solitary corals. The carbonate facies is dominated by oyster-type mollusks and by foraminifers, with few red algae or solitary corals; this is a typical "foramol" (foraminiferal-mollusk) assemblage, characteristic of more temperate Tethyan associations. This shallow-water carbonate facies is interbedded in an acyclic manner with dark gray to black silty claystones with minor cross- to parallel-laminated siltstones and sandstones, documenting a fluviodeltaic (delta front to alluvial plain) setting. Commonly, an emergent to subaerial environment is indicated by (su-

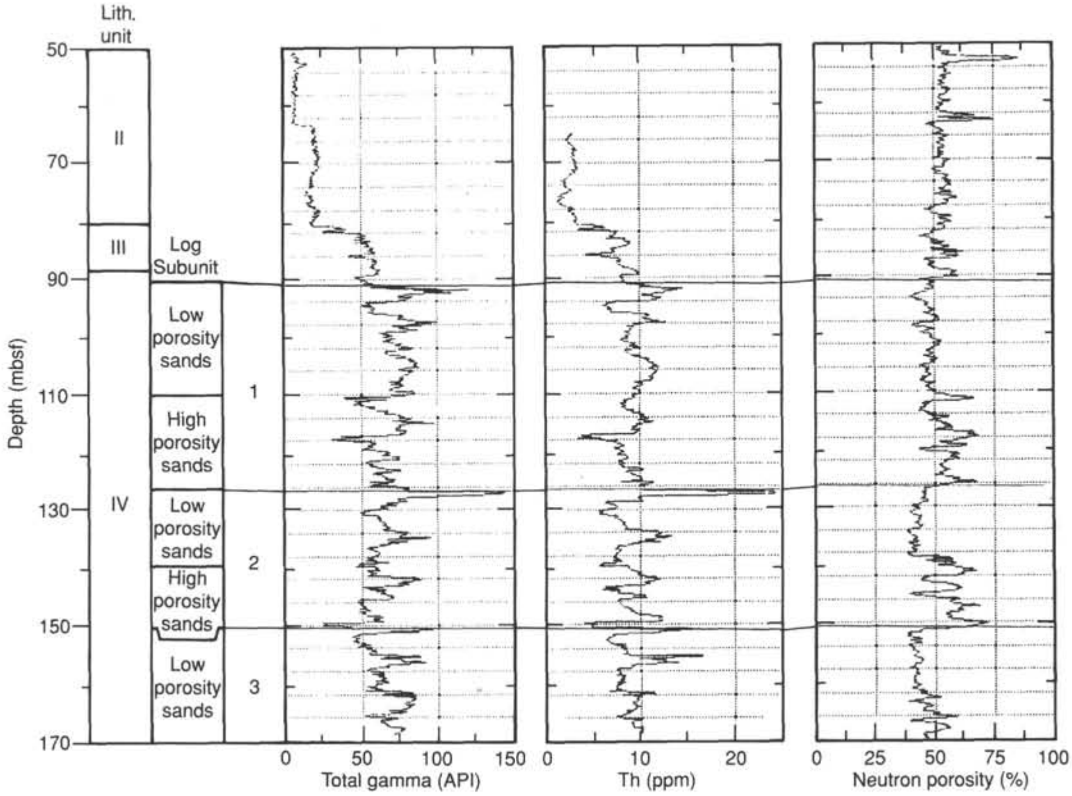

Figure 35. Correlation of lithologic units to open hole logs of total gamma ray, thorium count, and neutron porosity at Hole 760B. Subunits identified on the basis of log data are also shown.

pratidal?) algal mats, claystones with rootlets, and local coal seams.

The alternation of shallow-water carbonate to deltaic siliciclastic facies can be explained by the lateral migration of delta lobes over a preexisting carbonate shelf. This was apparently covered at a later time by another carbonate bank, after the depocenter of the active delta lobe had switched laterally from a "delta abandonment facies" to a new position. This "Mississippi-type" migrating delta-lobe model does not require a fluctuating sea level to explain the frequent alternation of the two facies in space and time (see "Lithostratigraphy," this chapter; also, Figs. 18 and 19).

Norian Siliciclastic Sedimentation (Units V and IV, 284.9–84.9 mbsf)

A redepositional (transgressive?) event (marked by a calcite-cemented sandstone and coquina at about 128.5 mbsf) indicates the transition to another sequence of carbonate-free siliciclastic sediments. In general, Units V and IV show an upward-shallowing (regressive) trend from marine, glauconite-bearing mudstone (inner shelf to lagoon) to marginal-marine, sandier and siltier deltaic sediments. The sediments of the lower siliciclastic Unit V were deposited in a shallow- to marginal-marine environment, probably in an estuarine, distributary bay, or tidal flat/channel setting, with a few excursions into a subaerial delta plain to coal swamp milieu. However, fish debris, glauconite, and mollusks generally indicate a marine setting. The upper siliciclastic interval (Unit IV) has an even smaller marine component. This unit is characterized by black silty claystone, interbedded with clayey siltstones to silty sands. Several horizons with thin coal seams, root mottling, caliche, and soil profiles indicate a restricted marginal marine (estuary or distributary bay), flood plain, delta channel, and coal swamp environment.

The Major Post-Norian Unconformity and the Mid- to Late Cretaceous(?) Manganese Hardground (Unit III, 84.9–80.1 mbsf)

The major angular unconformity between upper Norian and overlying upper(?) Cretaceous sediments spans a period of about 110 m.y. As the top of the late(?) Norian sequence below the unconformity is a soil horizon with rootlets, we infer that the post-Norian erosion of Wombat Plateau started under subaerial conditions. From regional geophysical data and the preliminary results of Site 761, we infer that this erosional event followed a major block-faulting phase that isolated and tilted the Wombat Plateau horst, either during the late Norian/early Rhaetian or the mid-Jurassic (see "Summary and Conclusions," Site 761 chapter, this volume). We do not know when the Wombat horst began to subside below sea level, but the results of Site 761 (where a condensed ferruginous sandstone overlying the unconformity is dated as late Berriasian to early Valanginian) suggests an early Neocomian age.

During the first 60 m.y. of subsidence in paralic to neritic environments, only a few meters of variegated claystones to silty sandstones were deposited in a setting where erosion and reworking prevailed. Later, the Wombat Plateau sank to bathyal water depths, but remained in a predominantly nondepositional realm (similar to the present-day Blake Plateau), evidenced by several layers of manganese nodules with nuclei of yellowish carbonate to siliciclastic material. The uppermost layer of soft manganese nodules is 40 cm thick, and shore-based work on the age of the nuclei and subsequent laminae of

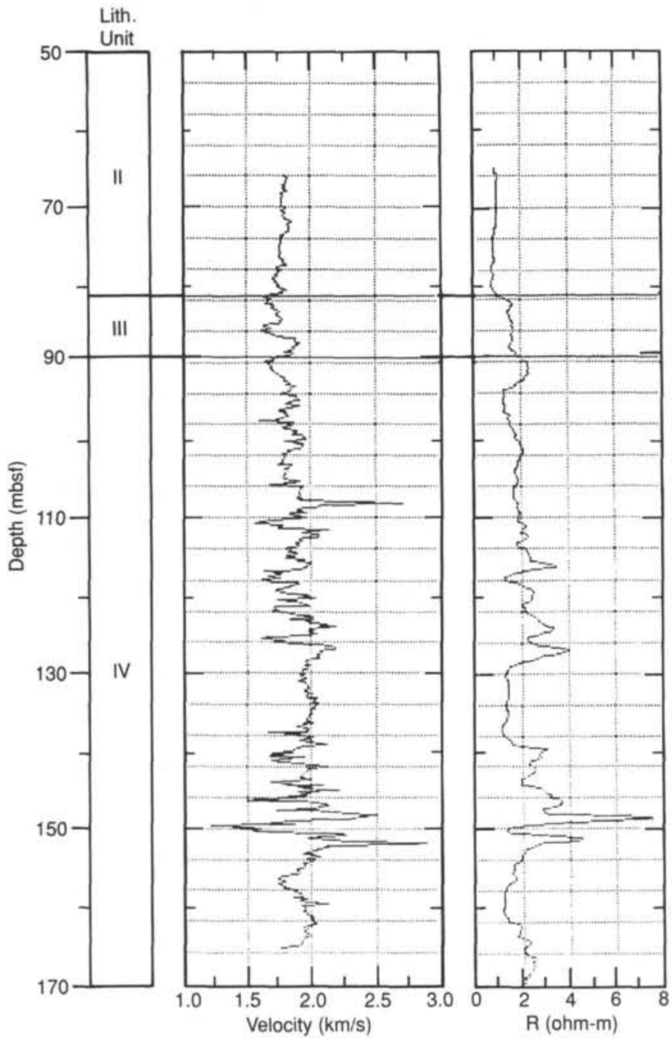

Figure 36. Correlation of lithologic units to velocity data, calculated from interval transit times, and the deep-formation-resistivity log (R) at Hole 760B.

these nodules might document important events in the history of this subsiding plateau between 90 and 50 Ma.

Eocene to Quaternary Evolution (Units II and I, 80.1–0.0 mbsf)

During the past 50 m.y., the Wombat Plateau subsided slowly to the present water depth. During this time, eupelagic nannofossil ooze (becoming more foraminifer-rich between late Pliocene and Pleistocene time) was deposited. Several hiatuses were noted from the biostratigraphic determinations: one 2–4-m.y.-long hiatus between upper Eocene and lower Oligocene sediments, and one 3-m.y.-long hiatus separating the upper Miocene from the upper Pliocene to Pleistocene sequence. Other hiatuses might be identified with more detailed shore-based biostratigraphic work. Color bands in the upper Oligocene to upper Miocene section (15–30 cm thick) and the upper Pliocene to Pleistocene section (5–50 cm thick) might document Milankovitch-type cycles, on the order of 10^3–10^5 years.

Biostratigraphy and Magnetostratigraphy

Biostratigraphy

Holes 760A and 760B recovered fossiliferous sediments ranging from Carnian to Quaternary in age. Calcareous nannofossils and planktonic foraminifers provided accurate ages for the upper 80 m of the pelagic carbonate part of the section, which ranges in age from late Paleocene to Quaternary. Rare radiolarians were also recorded, especially in the upper Eocene, Miocene, and Quaternary part of the section. Nannofossil biostratigraphy indicates hiatuses in the lower Oligocene and upper Pliocene.

The predominantly noncarbonate, paralic to marginal marine section below the angular unconformity (at 80 mbsf) was dated as late Triassic on the basis of spores and pollen. Some intervals in the lower part of the section (e.g., 265–283 mbsf and 464–496 mbsf) also yielded Triassic calcareous nannofossils. In the lower of these two occurrences, however, the calcite in the nannofossils is probably replaced by siderite. Some intervals also yielded rare Triassic foraminifers and traces of late Triassic radiolarians.

Magnetostratigraphy

Magnetostratigraphy yielded promising results that, owing to the absence of VAX computing, have not been fully evaluated. In the Quaternary (Subunit IA) the Brunhes/Matuyama, Jaramillo, and J1 reversals were detected. In Subunit IB many reversals were detected, including a long reversed interval in the upper Oligocene. The Triassic rocks are strongly magnetized, but more shore-based work is necessary to resolve magnetic reversals.

Inorganic and Organic Geochemistry

Detailed depth profiles of the geochemistry of interstitial water samples from the upper 100 m showed a strong downhole decrease of Mg^{2+}. The Mg^{2+}/Ca^{2+} ratio decreases sharply from the seafloor to 81.6 mbsf as a result of the diagenesis of carbonate-rich sediments, and more gradually from 86.6 to 239 mbsf, probably owing to the marginal-marine to nonmarine environment of the upper Triassic sediments. The Triassic is characterized by a sharp drop in Cl^--concentrations (salinity decrease), as well as by a Ca^{2+}, Mg^{2+}, and SiO_2 increase.

Carbonate contents range from 0.1 to 97%. Total organic carbon (TOC) is normally <3%, and reaches up to 18% in coaly material. The organic matter originated from the destruction of higher land plant material (as evidenced by large hydrogen index values).

Headspace hydrocarbon analyses indicated low methane contents (42 ppm, maximum 10–20 ppm) with <1 ppm ethane. At the bottom of Hole 760B, however, C_1 and C_2 values rose dramatically to 97 ppm and 4 ppm, respectively (C_1/C_2 = about 25). This indicates that the gas observed below the Tertiary oozes is thermogenic. Since this gas is migrating updip and out of the rocks at the seafloor in an open system, it did not represent a safety hazard.

Physical Properties and Seismic Stratigraphy

Use of the APC system allowed continuous and undisturbed core recovery and GRAPE and *P*-wave logging for the upper 83.7 m of the section. Sonic velocity values range from 1.46 km/s (ooze) to 6.7 km/s (calcite-cemented sandstone). Alternating (bimodal) high-velocity (limestones and carbonate-cemented sandstones and claystones) and low-velocity lithologies (less lithified claystones and oozes) dominate the interval between 216 and 470 mbsf. Average claystone velocities at the bottom of Hole 760B are about 2.1–2.2 km/s, similar to those at Site 759. Bulk density increases with depth from 1.5 (soft ooze) to 1.82 g/cm^3 (compacted ooze); density values are up to 2.02 g/cm^3 for uncemented claystones, and up to 2.86 g/cm^3 for bioclastic limestones. The smallest measured porosities (at 305 mbsf) were 25%–35% (10%–15% water content). Thermal conductivity ranges from 0.83 to 3.12 W/m·K between 2 and 467 mbsf.

Low sedimentation rates at the Mn-nodule hardground around 80 mbsf are indicated by lower porosities. An explanation for the sharp increase of bulk density and the jump in sonic velocity observed at the hardground is removal of lower-velocity material by erosion and exposure of older, harder (i.e., "faster") material below the hardground.

The seismic stratigraphy of Site 760 is discussed in a combined report of Sites 759, 760, and 761 (see "Seismic Stratigraphy," Site 764 chapter, this volume). For a discussion of the limited downhole logging results, see "Downhole Measurements" (this chapter).

REFERENCES

Blome, C. D., 1984. Upper Triassic Radiolaria and Radiolarian Zonation from Western North America. *Bull. Amer. Paleontol.*, 85:88.

Claypool, G. E., and Kvenvolden, K. A., 1983. Methane and other hydrocarbon gases in marine sediment. *Ann. Rev. Earth Planet. Sci.*, 11:299–327.

Coleman, J. M., and Gagliano, S. M., 1964. Cyclic sedimentation in the Mississippi river deltaic plain. *Trans. Gulf Coast Assoc. Geol. Soc.*, 14:67–80.

Cook, A. C., Smyth, M., and Vos, R. G., 1985. Source potential of Upper Triassic fluvio-deltaic systems of the Exmouth Plateau. *APEA J.*, 25:204–215.

Dolby, J., and Balme, B. E., 1976. Triassic palynology of the Carnarvon Basin, Western Australia. *Rev. Palaeobot. Palynol.*, 22:105–168.

Emeis, K.-C., and Kvenvolden, K. A., 1986. Shipboard Organic Geochemistry on *JOIDES Resolution*. *ODP. Tech. Note*, 7.

Fisher, W. L., Brown, L. F., Scott, A. J., and McGowen, J. H., 1969. *Delta Systems in the Exploration for Oil and Gas:* Austin (Bur. Econ. Geol. Univ. Texas).

Frazier, D. E., 1967. Recent deltaic deposits of the Mississippi delta: their development and chronology. *Trans. Gulf Coast Assoc. Geol. Soc.*, 17:287–315.

Gieskes, J. M., 1981. Deep-sea drilling interstitial waters: implications for chemical alteration of the oceanic crust, Layer I and II. *Spec. Publ. Soc. Econ. Mineral. Paleontol.*, 31:149–167.

Gieskes, J. M., Elderfield, H., Lawrence, J. R., Johnson, J., Meyers, B., and Campbell, A., 1981. Geochemistry of interstitial waters and sediments, Leg 64, Gulf of California. *In* Curray, J. R., Moore, D. G., et al., *Init. Repts. DSDP*, 64, pt. 2: Washington (U.S. Govt. Printing Office), 675–694.

Haq, B. U., Hardenbol, J., and Vail, P. R., 1987. Chronology of fluctuating sea levels since the Triassic. *Science*, 235:1156–1167.

Helby, R., Morgan, R., and Partridge, A. D., 1987. A palynological zonation of the Australian Mesozoic. *Mem. Assoc. Australas. Palaeontol.*, 4:1–94.

Kastner, M., and Gieskes, J. M., 1976. Interstitial water profiles and sites of diagenetic reactions, Leg 35, DSDP, Bellingshausen Abyssal Plain. *Earth Planet. Sci. Lett.*, 33:11–20.

Leythaeuser, D., Schaefer, R. G., and Yukler, A., 1982. Role of diffusion in primary migration of hydrocarbons. *AAPG Bull.*, 66:408-429.

Leythaeuser, D., Schaefer, R. G., and Pooch, H., 1983. Diffusion of light hydrocarbons in subsurface sedimentary rocks. *AAPG Bull.*, 67:889-895.

Martini, E., 1971. Standard Tertiary and Quaternary calcareous nannoplankton zonation. *In* Farinacci, A. (Ed.), *Proc. 2nd Plankt. Conf.*: Rome (Ed. Tecnoscienza), 739–785.

Perch-Nielsen, K., 1985. Cenozoic calcareous nannofossils. *In* Bolli, H. M., Saunders, J. B., and Perch-Nielsen, K. (Eds.), *Plankton Stratigraphy:* Cambridge (Cambridge University Press), 427–554.

Sanfilippo, A., Westberg-Smith, M. J., and Riedel, W. R., 1985. Cenozoic Radiolaria. *In* Bolli, H. M., Saunders, J. B., and Perch-Nielsen, K. (Eds.), *Plankton Stratigraphy:* Cambridge (Cambridge University Press), 631–712.

Serra, O., 1986. *Fundamentals of Well-log Interpretation,* Vol. 2: Amsterdam (Elsevier).

von Rad, U., and Exon, N. F., 1983. Mesozoic-Cenozoic sedimentary and volcanic evolution of the starved passive margin off northwest Australia. *AAPG Mem.*, 34:253–281.

von Rad, U., Schott, M., Exon, N. F., Mutterlose, J., Quilty, P., and Thurow, J., in press. Mesozoic sedimentary and volcanic rocks dredged from the northern Exmouth Plateau: petrography and microfacies. *BMR J. Aust. Geol. Geophys.*

Zaninetti, L., 1976. Les Foraminiferes du Trias. *Riv. Ital. Paleon.*, 82:1–258.

Ms 122A-106

NOTE: All core description forms ("barrel sheets") and core photographs have been printed on coated paper and bound as Section 3, near the back of the book, beginning on page 387.